# THE ROLES OF POSTSYNAPTIC DENSITY-95 INTERACTORS IN DENDRITE DEVELOPMENT AND RECOVERY AFTER TRAUMATIC BRAIN INJURY

by

MIHIR V. PATEL

A dissertation submitted to the

School of Graduate Studies

Rutgers, The State University of New Jersey

In partial fulfillment of the requirements

For the degree of

Doctor of Philosophy

Graduate Program in Neuroscience

Written under the direction of

Bonnie L. Firestein

And approved by

_____

_____

_____

_____

_____

New Brunswick, New Jersey

October 2018

# ABSTRACT OF THE DISSERTATION

THE ROLES OF POSTSYNAPTIC DENSITY-95 INTERACTORS IN DENDRITE DEVELOPMENT AND RECOVERY AFTER TRAUMATIC BRAIN INJURY

By MIHIR V. PATEL

Dissertation Director:

Bonnie L. Firestein

Postsynaptic density 95 (PSD-95) is the major scaffolding protein at excitatory synapses, and it plays a major role in synaptic plasticity. Furthermore, PSD-95 and its interactor, cytosolic PSD-95 interactor (cypin), regulate dendrite branching by altering microtubule dynamics. Additionally, other PSD-95 binding proteins, end-binding protein 3 (EB3) and *adenomatous polyposis coli* (APC), promote microtubule bundling and stabilization. Thus, PSD-95 and binding partners may regulate the dendritic arbor during development and after injury.

I first addressed the role of cypin in the brain *in* vivo. While generating cypin knockout mice, I identified a novel short isoform of cypin, termed cypinS, which also binds to PSD-95 and regulates dendrite branching, although an increase in dendrites occur more distal from the soma when cypinS is overexpressed compared to when cypin is overexpressed. In addition, unlike cypin, cypinS does not have guanine deaminase activity. Overexpression of cypin, but not cypinS, decreases spine density, suggesting

that the regulation of spine density but not dendrite branching by cypin is dependent on guanine deaminase activity. Furthermore, I have uncovered novel presynaptic roles for both isoforms as overexpression of either isoform leads to increases in miniature excitatory postsynaptic current (mEPSC) frequency. Thus, cypin and cypinS, play distinct roles in neuronal development.

I then chose to study the roles of PSD-95 and interactors in recovery after traumatic brain injury (TBI). We previously identified cypin as a novel target for TBI, and thus, here I studied the role of PSD-95 and its interaction with APC or EB3 in after injury induced by *in vitro* and *in vivo* models of TBI. I show that our *in vitro* model of mechanical stretch injury mimics moderate injury induced by controlled cortical impact (CCI) in mice. During the early stage (1-7 days) post-moderate CCI, the interaction of PSD-95 with APC and EB3 increases. Furthermore, downregulation of PSD-95 prevents stretch-injury mediated decreases in secondary dendrite number and total dendrite length, suggesting a required role of PSD-95 in injury-mediated insults to dendrites. Thus, PSD-95 may sequester APC and EB3 from microtubules to cause decreases in dendrite branching after TBI, and PSD-95 can be targeted as a novel approach for the treatment of patients with TBI.

# ACKNOWLEDGEMENTS

First, I would like to express my greatest gratitude to my advisor, Dr. Bonnie Firestein, for her advice and who has been very supportive of my research ideas, experimental approaches and the most difficult times to finish this dissertation. I would also like to thank my committee members, Dr. Gleb Shumyatsky, Dr. Janet Alder, Dr. Gabriella D'Arcangelo and Dr. Loren Runnels for their valuable guidance throughout this dissertation.

I would also like to thank the Firestein lab members, especially Dr. Przemyslaw Swiatkowski (Peter), Dr. Harita Menon, Dr. Ana Rodriguez, Dr. Frank Kung, Anton Omelchenko, Dr. Chen Liang and Dr. Kate O'Neill for all thoughtful discussions on science.

My sincere thanks also goes to my family, Brijesha Patel (Wife), Vijay Patel (Father) and Mita Patel (Mother) for their support and prayers.

Last but not the least, my Guru Pramukh Swami Maharaj and Mahant Swami Maharaj for their divine blessings, without it this dissertation would not be possible.

# Table of Contents

# Chapter 1: Introduction

## 1.1 The Neuron

Neurons are highly polarized cells.[1] The neuron consists of a cell body and two types of processes, the dendrites and axon. Dendrites receive signals from other neurons and transmit the signal to the cell body. Efficient neuronal communication highly depends on the complexity of the dendritic arbor. Learning and memory depend on extension and retraction of dendrites, which represent dendrite dynamics.[2, 3] Efficient synaptic connections are also required for precise neuronal networking. Synaptic activity regulates dendritic arborization. Early synaptic activity induces elongation of dendritic branches, while later, it stabilizes branches and the development and maturation of synapses.[4] Abnormal dendritic patterning correlates to different neurocognitive disorders and neurodegenerative diseases, such as autism spectrum disorder (ASD), Rett syndrome, schizophrenia, Fragile X syndrome (FXS), Down syndrome (DS), Alzheimer's disease (AD), stress, and anxiety.[5, 6] Thus, it is necessary to explore the detailed molecular mechanisms of dendritogenesis to understand how to treat patients with these disorders.

## 1.2 Morphology of Dendrites

The structure of dendrites and axons is different in terms of microtubule spacing and alignment. Dendrites have widely spaced microtubules, which are not aligned, while

axons have tightly spaced microtubules, which are aligned.[2] The dendritic cytoskeleton is composed of microtubules (tubulin), microfilaments (actin), and intermediate filaments. Dendrite branching depends on polymerization of microtubules and actin filaments. Microtubules are composed of polymerized tubulin, are capped with microtubule-associated proteins (MAPs), and are transported into growing dendrites. The depolymerization and polymerization of microtubules is in an equilibrium state at stable dendrite branch points.[7] Thus, microtubules are dynamic and regulate dendritic branching. Similarly, actin can either promote or disrupt dendrite initiation by serving as a track for microtubule invasion in neurites or by retrograde flow, respectively.[8] The interaction between microtubules and F-actin mediates dendrite elongation during cell migration.[9] Actin has a rapid turnover rate and is present in dendritic synapses, and thus, it is highly involved in dendritic and synaptic plasticity. The actin cytoskeleton in dendritic synapses regulates the trafficking of receptors and distinct proteins in spines.[10]

## 1.3 Factors that Regulate Dendrite Branching

Many intracellular and extracellular proteins regulate dendritic morphology. Specifically, intracellular proteins involved in shaping dendrites affect microtubule or actin dynamics. The following proteins have been shown to regulate dendrite branching and are studied in this dissertation.

*1.3.1 Adenomatous Polyposis Coli (APC) and microtubule +TIP end-binding (EB) family proteins*

*Adenomatous Polyposis Coli* (APC) binds to cytoskeletal proteins and stimulates microtubule assembly, bundling, and stabilization.[11] APC is involved in the regulation of bundling of actin filaments and microtubules as both are in competition for binding to APC in a concentration-dependent manner.[12] APC interacts with the end-binding (EB) family proteins of +TIPs (plus end-tracking proteins). EB1 is involved in the regulation of microtubule dynamics.[13] EB1 binds to APC and antagonizes the actin binding ability of APC.[12] Thus, the regulation of EB1 and APC binding is a key factor for the regulation of dendrite branching.

The APC homologue APC2 (APCL) is specifically expressed in the central nervous system (CNS) and has high homology to APC.[14] Similarly, the EB1 homologue EB3 is also specifically expressed in the CNS and binds to APC2. This CNS-specific APC2-EB3 interaction may be involved in the stabilization of the neuronal microtubule network.[14, 15] In mouse brain, APC2 expression is highest from E14 to P10 and decreases from P12 to adulthood. It is in highest amounts in the developing cerebellum. As APC2 is expressed in neurons throughout the entire brain during development, APC2 has been implicated in playing a role in the development of neurons and dendritic arborization.[15] Moreover, APC is required for the differentiation and maintenance of adult neuronal stem cells in the adult neurogenic niche.[16] Lack of APC2 causes disrupted neuronal migration and severe laminary defects in multiple regions of brain.[17] Thus, APC and EB proteins are involved in microtubule stabilization and regulation of dendritic arborization.

*1.3.2 Postsynaptic density 95 (PSD-95)*

Postsynaptic density 95 (PSD-95/SAP90) is the major scaffolding protein in the postsynaptic density of excitatory synapses. It is part of the membrane-associated guanylate kinase (MAGUK)[18, 19] family of proteins as it has three PDZ domains, an SH3 domain, and a guanylate kinase homology domain.[20, 21] PSD-95 is indirectly associated with microtubules and the actin cytoskeleton. It is associated with F-actin via additional scaffolding proteins, GKAP, Shank, and Cortactin.[22, 23] Through its association with the cytoskeleton, PSD-95 is involved in the regulation of dendritic spine density and maturity,[24, 25] PSD-95 is expressed prior to neuronal maturation and synaptogenesis. Moreover, a large portion of PSD-95 clusters are non-synaptic, which implicates a non-synaptic role for PSD-95.[26-28] Overexpression of PSD-95 results in a decrease in the branching of primary dendrites, resulting in a decrease in secondary dendrites.[28] Knockdown of PSD-95 increases dendritic arborization close to the cell body.[28] Thus, PSD-95 is a stop signal for dendrite branching and arborization.[28] Cypin, cytosolic PSD-95 interactor,[29] is also involved in the regulation of dendrite branching,[30] PSD-95-mediated decreases in dendrite branching are activity-independent and are regulated by cypin.[28] In addition, PSD-95 decreases EB3 comet lifetime in dendrites by binding EB3 via the PSD-95 SH3 domain, and this mechanism underlies decreased dendritic arborization.[31] Overexpression of PSD-95 also causes disorganization of microtubules at branch points and increases microtubule spacing in the dendritic shaft.[32] As PSD-95 binds to APC[33] and affects microtubule assembly, bundling, and stabilization,[28, 34] PSD-95 and its interaction with APC and EB3 may play vital roles in the regulation of dendrite branching.

*1.3.3 Cypin (Cytosolic PSD-95 Interactor)*

Cytosolic PSD-95 interactor (cypin) is the major PSD-95 interactor in the brain.[29, 35] Cypin binds to PSD-95 via its C-terminal PDZ-binding motif and perturbs PSD-95 localization at the postsynaptic density.[29] Cypin is mainly localized in dendrites and spine necks.[29] As cypin binds to tubulin heterodimers and promotes microtubules assembly, overexpression of cypin in hippocampal neurons increases dendrite branching and arborization.[30] SNARE-associated protein (snapin) binds to cypin and disrupts the cypin-tubulin interaction, negatively regulating cypin activity.[36] Activated RhoA, a small GTPase, decreases the expression of cypin, and thus, acts as a negative regulator of dendrite branching and arborization.[37] Brain-derived neurotrophic factor (BDNF) increases dendritic arborization via CREB-dependent transcription of cypin.[38] Thus, cypin acts downstream of RhoA -and BDNF-mediated regulation of dendrite branching.

Cypin plays a role in normal brain function. It has been reported that autoantibodies with increased reactivity for cypin and/or the related protein collapsin response mediator protein 1 have been found in 23% of mothers of children with maternal autoantibody-related autism (MAR).[39] Moreover, oxidative stress increases the levels of cypin in the hippocampus,[40] and cypin expression is increased in the striatum in a rat model of Parkinson's disease.[41] Overexpression of cypin protects neurons from glutamate-induced toxicity,[42, 43] and thus, cypin may play a vital role in neuroprotection in injured or disease conditions.

## 1.4 Traumatic Brain Injury (TBI): Involvement of PSD-95, a Protein that Regulates Dendrite Morphology

Traumatic brain injury (TBI) is caused by the rapid movement of the brain within the skull, leading to neuronal damage and injury to the brain. TBI results in primary and secondary insults to brain. Primary brain insult includes mechanical damage to blood vessels, neurons, and glial cells, occurring immediately after trauma. Secondary insult, activated by primary insult, includes glutamate-induced excitotoxicity and intracellular calcium overload,[44, 45] causing deficits to dendrite morphology.[44, 46] These insults result in short-term cognitive deficits in mild TBI[47] and long-term or permanent cognitive deficits and disabilities[48] in moderate to severe TBI. In addition, less attention has been given to the study of the effects of TBI on dendrite morphology.[49] Detailed molecular mechanisms regulating dendrite morphology after TBI can identify new therapeutic targets to repair neuronal processes after TBI.

Glutamate-induced excitotoxicity causes formation of varicosities (focal swellings) in dendrites[50] and loss of dendritic spines.[51] Varicosity formation is due to the disruption of microtubules.[50, 52, 53] PSD-95 is involved in the regulation of microtubule dynamics[30-32, 54] and regulates varicosity formation in response to glutamate-induced excitotoxicity.[43] NMDA-induced excitotoxicity and subsequent recovery cause changes to the expression of PSD-95.[43] Furthermore, PSD-95 knockdown increases the percentage neurons with varicosities and decreases the size of varicosities after sublethal NMDA treatment, correlating with neuronal survival.[43] Changes in PSD-95 levels post-trauma have been

reported in multiple studies using the *in vivo* TBI model of controlled-cortical impact (CCI) in rodents.[55-58]

As discussed above, PSD-95 regulates dendrite branching by binding to APC and EB3 at +TIPs of microtubules. The role of PSD-95 in dendrite development and NMDA-induced excitotoxicity motivates the study of molecular mechanisms by which PSD-95 and its interaction with APC and EB3 alter neuronal survival, morphology, and function after TBI.

## 1.5 Current Study On The Role Of PSD-95 Interactors In Development And Injury

### *1.5.1 Identification of a short isoform of cypin that regulates neuronal development*

To study the detailed role of cypin in the brain, we generated cypin knockout mice. Surprisingly, these knockout mice are hypomorphic as they retain 20% of total cypin protein expression. It appears that this level of cypin expression compensates and partially mimics full function of cypin, suggesting further investigation of tissue-specific cypin knockout using cre-mice lines. While studying the cypin hypomorphic mice, we identified a novel short isoform of cypin, termed cypinS, which also binds to PSD-95, and we studied its role in the regulation of neuronal development. In brief, cypinS lacks guanine deaminase activity (GDA) and regulates dendrite branching, but it does so in a different manner than does cypin. Overexpression of cypin results in decreased spine density, while overexpression of cypinS does not. In addition, overexpression of cypin or

cypinS distinctly increases mEPSC frequency but not in amplitude. Thus, cypin and cypinS may play different roles in neuronal development.

### 1.5.2 The Role of PSD-95, APC, and EB3, and their Interaction in Remodeling the Dendritic Arbor after Injury

Using an *in vitro* model of mechanical stretch-induced injury and an *in vivo* TBI model of controlled cortical impact (CCI), we show that PSD-95 may sequester APC and EB3 from the +TIPs of microtubules after injury to mediate the effects of trauma on dendrite branching. Furthermore, downregulation of PSD-95 protein prevents stretch-induced injury-mediated decreases in secondary dendrite number and total dendrite length. Thus, PSD-95 is required to mediate the effects of injury on dendrite branching.

In summary, this dissertation work shows that 1) cypinS plays a vital but distinct role from cypin in neuronal development and 2) PSD-95 is required for trauma-mediated changes to dendrite morphology after TBI.

# Chapter 2: A Novel Short Isoform of Cytosolic PSD-95 Interactor (Cypin) Regulates Neuronal Development

This work was previously published in Patel, M.V., Swiatkowski, P., Kwon, M., Rodriguez, A.R., Campagno, K., and Firestein, B.L. (2018) A novel short isoform of cytosolic PSD-95 interactor (cypin) regulates neuronal development. Molecular Neurobiology, 55, 6269-6281. [**Copyright:** License# 4366060356916. Print and electronic permission from Springer Nature]

## 2.1 Abstract

The guanine deaminase cypin (cytosolic PSD-95 interactor) binds to PSD-95 (postsynaptic density protein 95) and regulates dendrite branching by promoting microtubule polymerization. Here, we identify a novel short isoform of cypin, which we term cypinS, which is expressed in mouse and human, but not rat, tissues. Cypin and cypinS mRNA and protein levels peak at P7 and P14 in the mouse brain, suggesting a role for these isoforms during development. Interestingly, although cypinS lacks guanine deaminase activity, overexpression of cypinS increases dendrite branching. This increase occurs further away from soma than increases resulting from overexpression of cypin. In contrast, overexpression of cypin, but not cypinS, decreases dendritic spine density and maturity. This suggests that changes to spines, but not to dendrites, may be dependent on

guanine deaminase activity. Furthermore, overexpression of either cypin or cypinS increases miniature excitatory postsynaptic current (mEPSC) frequency, pointing to a presynaptic role for both isoforms. Interestingly, overexpression of cypinS results in a significantly greater increase in frequency than does overexpression of cypin. Thus, cypin and cypinS play distinct roles in neuronal development.

## 2.2 Introduction

Cypin (cytosolic PSD-95 interactor), also known as nedasin [35], is guanine deaminase (GDA; guanase) [29] and the major interactor of the scaffolding protein postsynaptic density 95 (PSD-95) in the brain. The carboxy terminus of cypin binds to the first two PDZ domains of PSD-95 and decreases PSD-95 localization at postsynaptic sites [29]. Cypin binds to tubulin heterodimers via its collapsin-response mediator protein (CRMP) homology domain and promotes microtubule assembly. Overexpression of cypin in hippocampal neurons increases dendrite numbers, and knockdown of cypin decreases dendrites [30]. This action of cypin correlates with GDA activity [30] and zinc binding [59]. Our group has identified signaling molecules that act in concert with cypin to regulate dendritic morphology. For example, we reported that the SNARE-associated protein snapin binds to cypin and disrupts the cypin-tubulin interaction, acting as a negative regulator of cypin-mediated microtubule assembly [36]. Similarly, overexpression of PSD-95 blocks cypin-mediated increases in dendritic branching; however, the binding of cypin to PSD-95 is necessary for stabilization of dendrite growth promoted by cypin [28]. Upstream regulators of cypin include RhoA, a small GTPase, and brain-derived

neurotrophic factor (BDNF). Activated RhoA acts as a negative regulator of dendrite branching by decreasing cypin expression in a translation-dependent manner [37]. In contrast, BDNF increases dendritic arborization via CREB-dependent transcriptional activation of cypin [38]. Thus, multiple regulators of dendrite morphology act via cypin, which then regulates microtubule assembly, shaping the dendritic arbor.

Recent evidence suggests a required role for cypin in normal brain function. Genome-wide transcriptome profiling revealed increased expression of cypin in the CA1 region of the hippocampus after oxidative stress [40]. Additionally, nigro-striatal degeneration in a rat model of Parkinson's disease results in increased expression of cypin in the striatum [41]. Furthermore, overexpression of cypin protects cultured somatic motor neurons from glutamate-induced toxicity [42] and cultured hippocampal neurons from *N*-methyl-D-aspartate (NMDA) glutamate receptor-induced toxicity by increasing the number of small varicosities on dendrites [60]. Thus, cypin may act in a neuroprotective manner in the injured or diseased brain. Intriguingly, it was recently reported that 23% of mothers of children with maternal autoantibody-related autism (MAR) have autoantibodies with increased reactivity for cypin and/or the related protein collapsin response mediator protein 1 [39]. Taken together, these data suggest that further investigation of cypin function in the brain is warranted to increase our understanding of its role in neuronal development and disease.

In the current study, we identify a short isoform of cypin (cypinS) that lacks guanine deaminase (GDA) activity. Surprisingly, this isoform is expressed in tissue from mouse and human but not rat. Cypin and cypinS mRNA and protein levels peak at P7 and P14 in the mouse brain, suggesting a role for these isoforms during development when maximal

changes to neuronal morphology occur. Our data suggest that the two isoforms play similar but distinct roles in neuronal development. Overexpression of cypinS increases dendrite branching further away from the soma than does overexpression of cypin, and overexpression of cypin significantly decreases spine density and maturity while overexpression of cypinS does not affect spines. Overexpression of cypin or cypinS results in increased mEPSC frequency but not amplitude. Thus, our current data suggest distinct roles for cypin and cypinS in neuronal development.

## 2.3 Results

### *2.3.1 Analysis of the GDA gene predicts expression of a short isoform of cypin*

The *GDA* gene consists of 14 exons, resulting in a protein product of the 454 amino acid (aa) cypin. An alternative exon 1a exists in *GDA*, yielding an additional isoform of cypin, which we term cypinS for cypin short. CypinS is encoded by 14 exons with only part of the last exon present, resulting in a shorter 3' UTR in cypinS mRNA compared to the 3' UTR in cypin mRNA (Fig. 2.1a). This isoform is predicted to be expressed only in mouse and human, but not rat, tissues. In fact, we have not observed the presence of this isoform in rat tissue in any of our past studies [29, 30, 37, 38]. As we previously reported [29, 30], cypin protein contains a zinc-binding domain (76-84 amino acids (aa)), a collapsin response mediator protein (CRMP) homology domain (350-403 aa), and carboxy terminal PDZ-binding motif (451-454 aa). CypinS consists of the carboxy terminal 380 aa (75-454 aa)

of cypin, thus lacking the amino terminal 74 aa of cypin. Both cypin and cypinS contain His240, His279, and Asp330, three aa that we have reported to be involved in zinc binding ([59]; Fig. 2.1b).

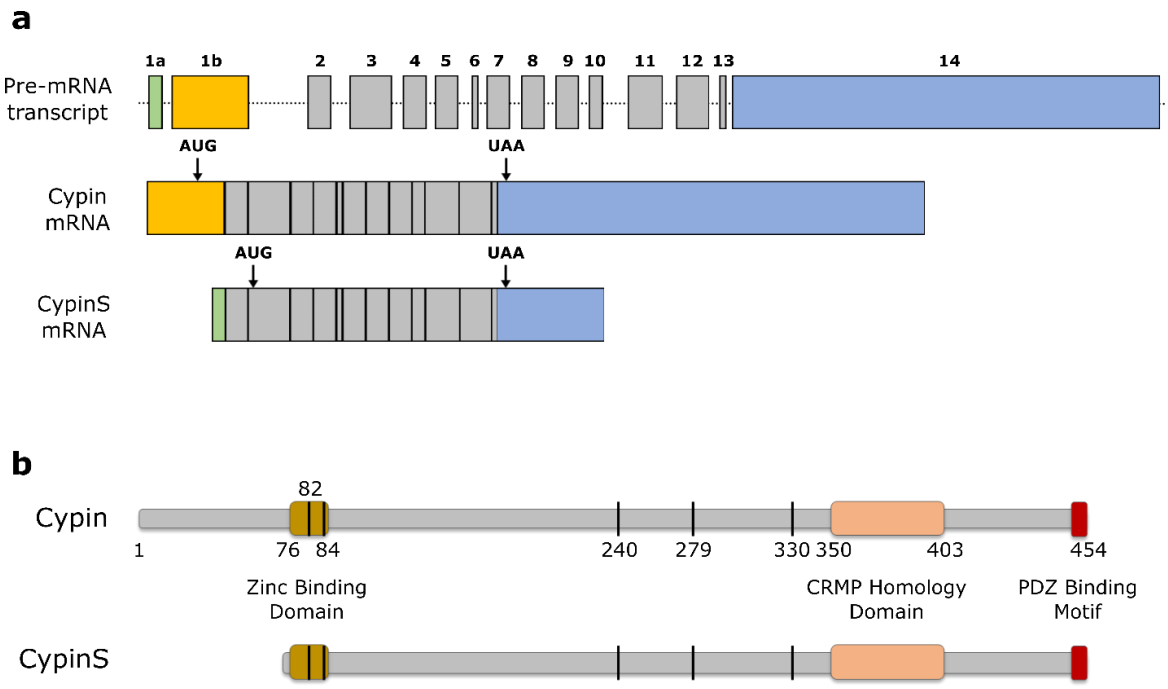


**Fig. 1.** Schematic of the *GDA* gene and resulting cypin proteins. **a.** Alternative splicing of *GDA*, resulting in two isoforms of cypin. Alternative exon 1 for short isoform of cypin (cypinS - Ensembl: ENSMUST00000121725; cypin - Ensembl: ENSMUST00000087600) is indicated in green. This alternative exon is present in mouse and human, but not rat. **b.** Schematic of cypin proteins. The zinc-binding domain (brown) binds zinc [59], the collapsin response mediator protein (CRMP) homology domain (peach) binds tubulin heterodimers [30], and the PDZ-binding motif (red) binds to PSD-95 family members [29]. Additional residues involved in zinc binding, His240, His279, and Asp330, are highlighted (black lines; [59]).

*2.3.2 Cypin and cypinS mRNA and protein are expressed in multiple mouse brain regions and tissues*

Cypin and cypinS mRNA differ only in their exon 1 sequences (Fig 2.1a). Thus, we constructed primers targeted to the junction of exons 1 and 2 to specifically amplify cypin or cypinS mRNA. Using these primers, we identified unique RT-PCR products for cypin and cypinS mRNA, suggesting the presence of both transcripts in mouse brain (Fig. 2.2a). To assay for protein expression, we validated the detection of cypinS protein by our polyclonal rabbit cypin antibody (BF6; [38, 60]) by overexpressing cypin and cypinS in HEK293 cells and subjecting lysates from these cells to Western blot analysis (Fig. 2.2b). Results of this analysis reveal that both isoforms are easily resolved by SDS-polyacrylamide gel electrophoresis and detected by Western blotting. Our data show that cypinS is present in multiple mouse brain regions, including cerebellum, which has low expression of cypin [29, 61], and organs, such as lung, heart, liver, spleen, kidney, and skeletal muscle, which also show expression of cypin (Fig. 2.2c and 2.2d). Similar to what is observed in mouse tissue, cypinS is expressed in human cortical tissue (Fig. 2.2e).

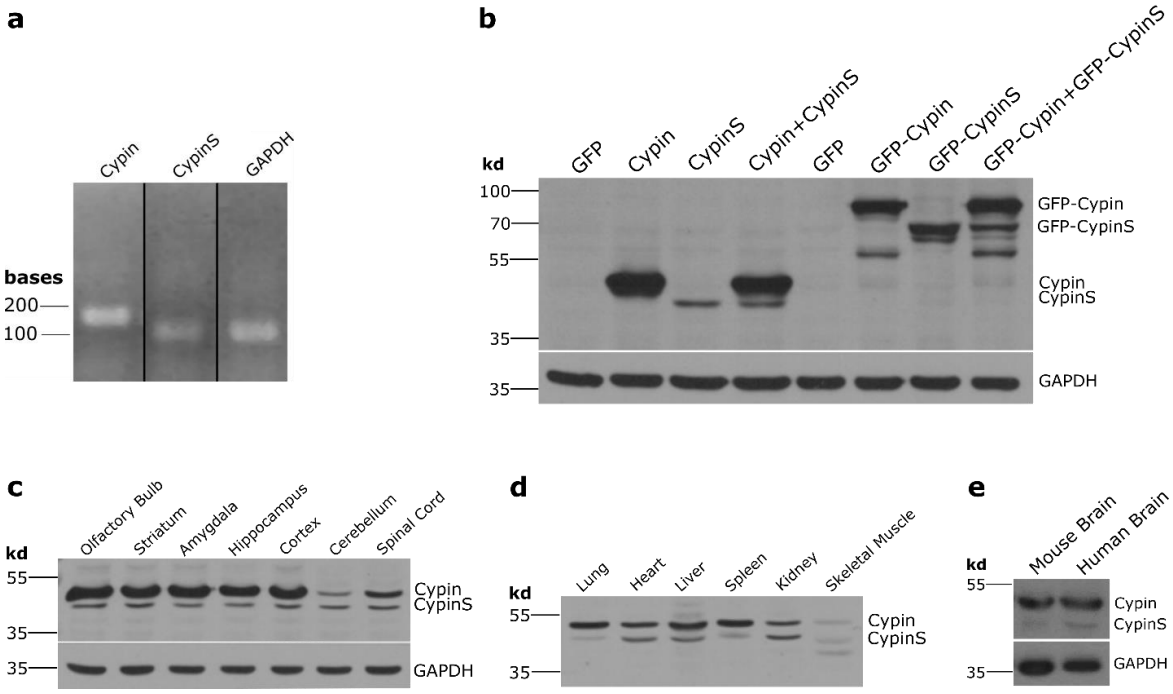


**Fig. 2.2.** Expression of cypinS mRNA and protein. **a.** Detection of cypinS mRNA transcripts in mouse brain by qRT-PCR reaction. **b.** Detection of cypin protein isoforms with polyclonal rabbit anti-cypin antibody (BF6, raised against full length cypin; [38, 60]). Overexpression of indicated proteins in HEK293 cells demonstrates that our polyclonal antibody recognizes both cypin and cypinS protein and that the two isoforms are easily resolved by Western blotting. GAPDH is shown as a control for equal protein loading. **c.** Expression of cypin and cypinS proteins in different brain regions. **d.** Expression of cypin and cypinS proteins in different mouse organs. **e.** CypinS is expressed in human brain.

*2.3.3 Cypin and cypinS mRNA and protein levels peak at postnatal day 7 in mouse brain*

To identify how cypinS may play a developmental role in brain function, relative mRNA and protein levels were determined in brain from mice at postnatal day (P) 0, 7, 14, 30,

and 100 (adult). qRT-PCR results show that cypinS transcript is present at significantly higher levels at P0, P7 and P14 compared to that expressed in adult brain (Fig. 2.3A). In addition, cypin transcript is highest at P7 (Fig. 2.3a). Consistent with these results, brain cypin and cypinS protein levels peak at P7 and P14 (Fig. 2.3b). We determined brain region-specific expression and enrichment in the adult and found that expression of cypinS occurs at similar levels across all regions while cypin is expressed at 20% of these levels in cerebellum (Fig. 2.3c), consistent with previous reports and by our group and others [29, 61].

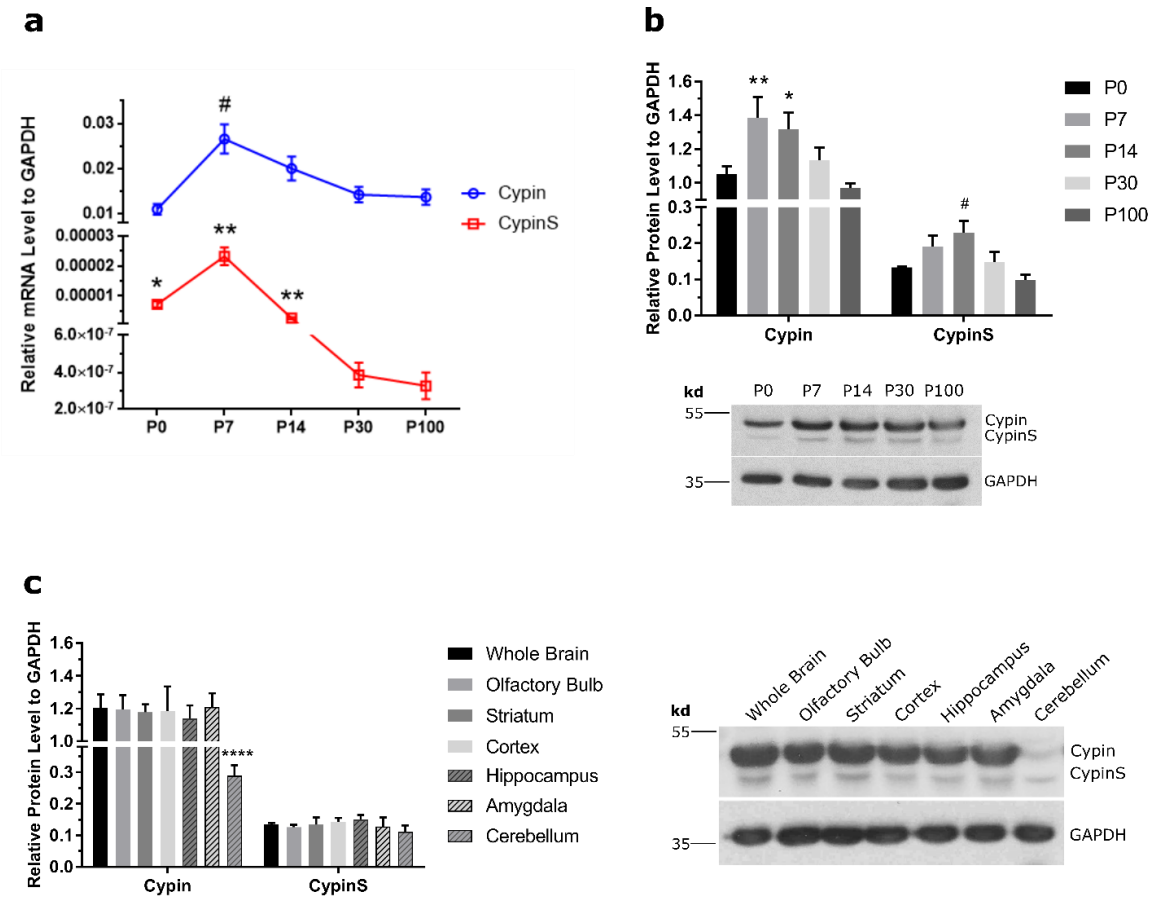


**Fig. 2.3.** Expression profile of cypin and cypinS proteins in mouse brain. **a.** Relative mRNA levels (normalized to GAPDH) of cypin and cypinS at developmental time points P0, P7, P14, P30 and P100. mRNA was isolated from four different mouse brains and

subjected to qRT-PCR to determine the fold change in mRNA levels compared to adult brain (P100). *p<0.05, **p<0.01 compared to P100 for cypinS. #p<0.05, P100 vs P7 for cypin. p values were determined by two-tailed Student's t-test comparing the $2^{(-\Delta Ct)}$ values of the two groups. The p value is adjusted using Benjamini-Hochberg False Discovery Rate. n=4 biological replicates (male mice), each with three technical replicates. Internal control=GAPDH; Calibrator or reference group=P100 (adult mouse brain). DataAssist Software automatically excluded outliers of technical replicates. **b.** Quantification and representative images of blots for relative protein levels of cypin and cypinS at various developmental time points. Cypin and cypinS levels peak at developmental time points P7 and P14. **p<0.01, P100 vs P7; *p<0.05, P100 vs P14 (cypin). p=0.07, P100 vs P7; #p<0.05, P0 vs P14 (cypinS). **c.** Relative protein levels of cypin and cypinS in different mouse brain regions, demonstrating significantly low levels of cypin in cerebellum compared to whole brain. ****p<0.0001, whole brain vs cerebellum (cypin). All statistics determined by one-way ANOVA followed by Dunnett's multiple comparisons test. n=3-4. Error bars= ± SEM.

### *2.3.4 CypinS does not function as a guanine deaminase*

Cypin is guanine deaminase (GDA; guanase), an enzyme that converts guanine to xanthine [30, 61]. As we previously reported using colorimetric assay, cypin has GDA activity [30, 61]. Since cypinS lacks the amino terminal 74 aa of cypin but has all aa responsible for zinc binding, a GDA assay was performed to determine whether cypinS

has this activity. We transfected COS-7 cells with plasmids encoding GFP, GFP-Cypin or GFP-CypinS and subjected the cells to the colorimetric GDA assay. Interestingly, unlike cells expressing GFP-Cypin, cells expressing GFP-CypinS do not show GDA activity (Fig. 2.4a). In addition, we performed Amplex Red GDA assay, which demonstrates kinetics of the GDA reaction rather than activity at a fixed time point (Fig 2.4b,c). Amplex Red assay shows a gradual increase in absorbance with time in extracts from samples cells expressing cypin, while extracts from cells expressing GFP and cypinS do not show increases in absorbance. Taken together, these data suggest that cypin acts as guanine deaminase while cypinS does not. Thus, cypinS may not play a role in guanine metabolism.

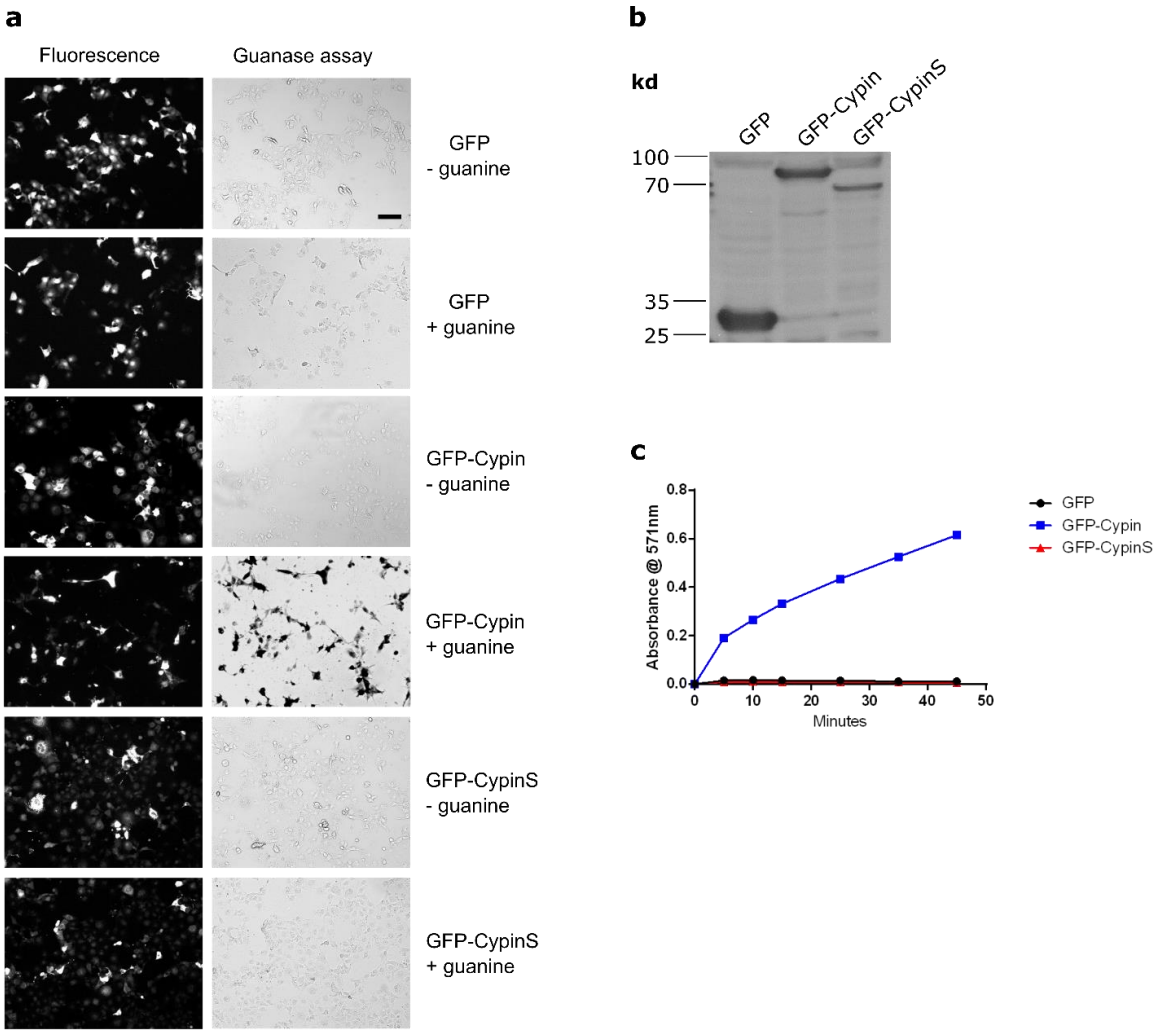


**Fig. 2.4.** CypinS does not function as a guanine deaminase. **a.** COS-7 cells were transfected with pEGFP-C1, pEFGP-C1-Cypin or pEGFP-C1-CypinS, fixed, and subjected to guanine deaminase assay. -guanine is negative control lacking guanine substrate in the reaction. Cypin has guanine deaminase activity while cypinS lacks guanine deaminase activity. Scale bar=100µm. **b** Western blot analysis for detection of protein expression of GFP, cypin-GFP, and cypinS-GFP in transfected HEK293 cells. **c.** Amplex Red colorimetric assay to analyze guanine deaminase activity [59, 62]. HEK293 cell lysate (50µg) was subjected to the assay. Lysate from HEK293 cells expressing GFP and cypin were used as negative and positive controls, respectively. Lysate from cells

expressing cypinS does not demonstrate guanine deaminase activity (n=3). Error bars=± SEM.

*2.3.5 Overexpression of cypinS increases dendrite branching in hippocampal neurons*

Overexpression of cypin increases primary and secondary dendrite numbers in cultured hippocampal neurons, and GDA activity correlates with this increase [30]. Since cypinS lacks GDA activity (Fig. 2.4), we asked whether cypinS regulates dendrite branching. Cypin and cypinS were overexpressed on DIV7 in cultured rat hippocampal neurons, and dendrite branching was analyzed at DIV12 using Sholl analysis [63-65]. It is important to note that cypinS is not expressed in rat neurons [29, 30, 37, 38], and thus, we used these neurons to determine the role for cypinS in a null background. Overexpression of cypinS results in increased dendrite branching more distal from the cell body than the resulting increase in dendrites resulting from overexpression of cypin (Fig. 2.5a-c). Overexpression of either cypin or cypinS results in increased tertiary and higher order dendrites, total dendrites, branch points, and terminal points (Fig. 2.5d-i). Thus, cypinS overexpression results in increases in overall dendrite arborization that is similar to the increase promoted by cypin. Importantly, our data suggest that the GDA activity of cypin is not required for increases in dendrites.

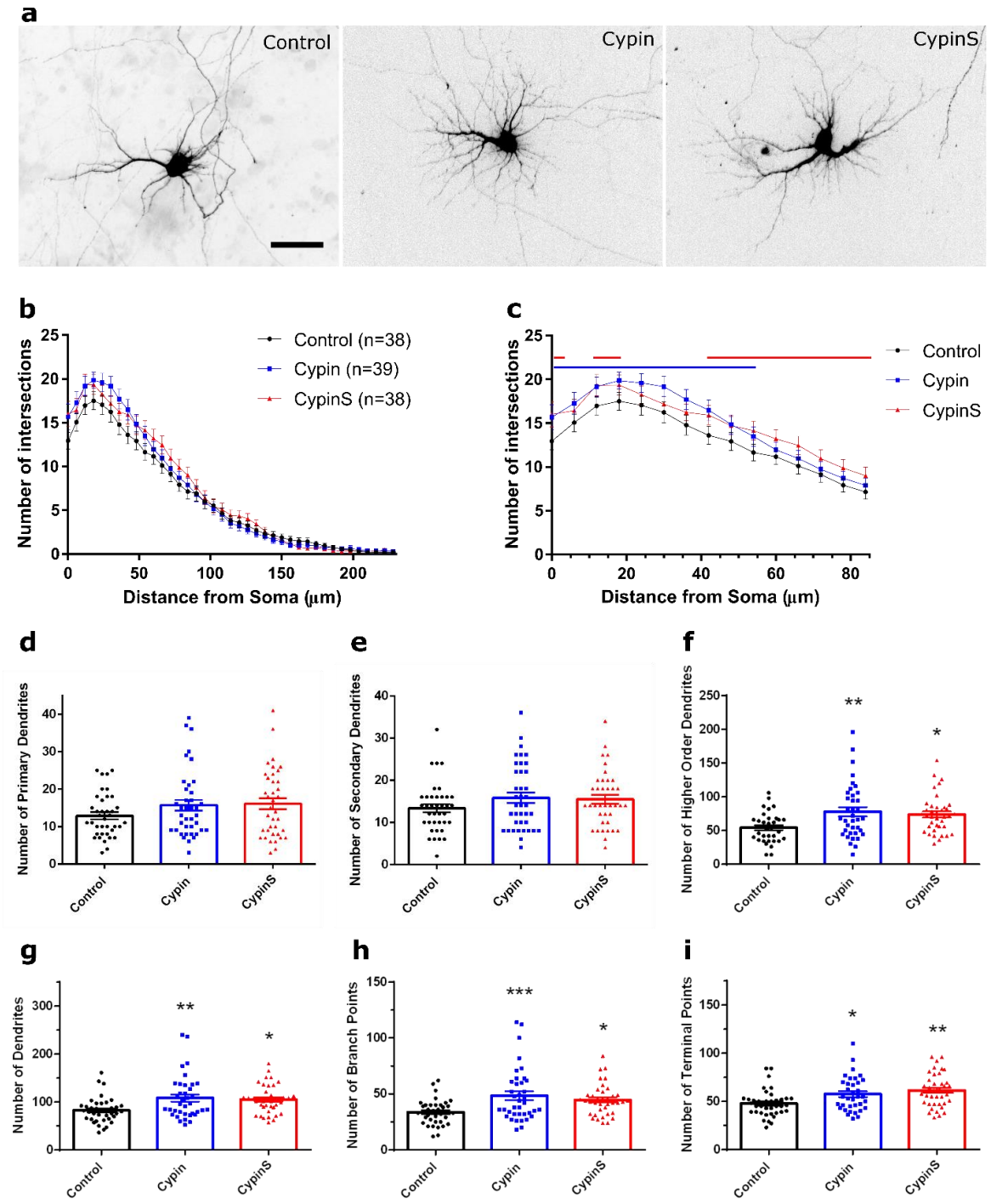


**Fig. 2.5.** Overexpression of cypin or cypinS results in increased dendrite branching in rat hippocampal neurons. Hippocampal neurons were cultured from rat embryos at 18 days gestation. Neurons were transfected on DIV7 with pEGFP-C1-Cypin or pEGFP-C1-CypinS, co-transfected with cDNA encoding mRFP (to fill the dendritic arbor), and fixed

at DIV12. **a.** Representative inverted mRFP images. **b.** Sholl analysis of neurons expressing indicated proteins. **c.** Overexpression of cypin or cypinS results in increased proximal dendritic arborization compared to control neurons expressing GFP. Blue solid line: $p<0.05$, control vs cypin; red solid line: $p<0.05$, control vs cypinS, determined by two-way ANOVA followed by Tukey's multiple comparisons test. **d-i**. Overexpression of cypin or cypinS increases tertiary and higher order dendrites, total number of dendrites, branch points, and terminal points. *$p<0.05$ (terminal points), **$p<0.01$ (tertiary and higher order dendrites, total number of dendrites), ***$p<0.001$ (branch points), control vs cypin. *$p<0.05$ (tertiary and higher order dendrites, total dendrites, and branch points), **$p<0.01$ (terminal points), control vs cypinS. Determined by one-way ANOVA followed by Tukey's multiple comparisons test. Error bar=±SEM. n=38 (control), n=39 (cypin), and n=38 (cypinS). Scale bar= 50 µm.

*2.3.6 Overexpression of cypin, but not cypinS, alters spine density and morphology*

To determine whether the subcellular localization of cypinS differs from that of cypin, we performed synaptosomal fractionation. Cypin is present in all fractions, including cellular cytosol, crude synaptosomes, synaptic cytosol, and synaptic membranes. In contrast, although cypinS is also present in crude synaptosomes and synaptic cytosol, it is present in synaptic membranes where cypin is present at a lower level than in other fractions (Fig. 2.6a). Furthermore, since PSD-95 is enriched in the synaptic membrane fraction [29], and cypinS contains a carboxy terminal PDZ-binding motif, we performed co-

immunoprecipitation in mouse brain lysate. As expected, cypin and cypinS co-immunoprecipitate with PSD-95 (Fig. 2.6b). Thus, based on these results, we hypothesize that cypinS plays a role in spine development due to its interaction with both PSD-95 and its localization at synaptic membranes. To test our hypothesis, we overexpressed cypin or cypinS in rat hippocampal neurons at DIV14, and spine number and morphology were assessed at DIV17. Overexpression of cypin results in a significant decrease in spine density and the number of mature spines. In contrast, cypinS had a marginal but non-significant effect on spine density ($p=0.077$; Fig. 2.6c-f). Overexpression of either cypin or cypinS had no effect on spine length or width (Fig. 2.6g,h). Our results suggest that cypinS may not play a major role in spinogenesis, especially since rat neurons do not express cypinS.

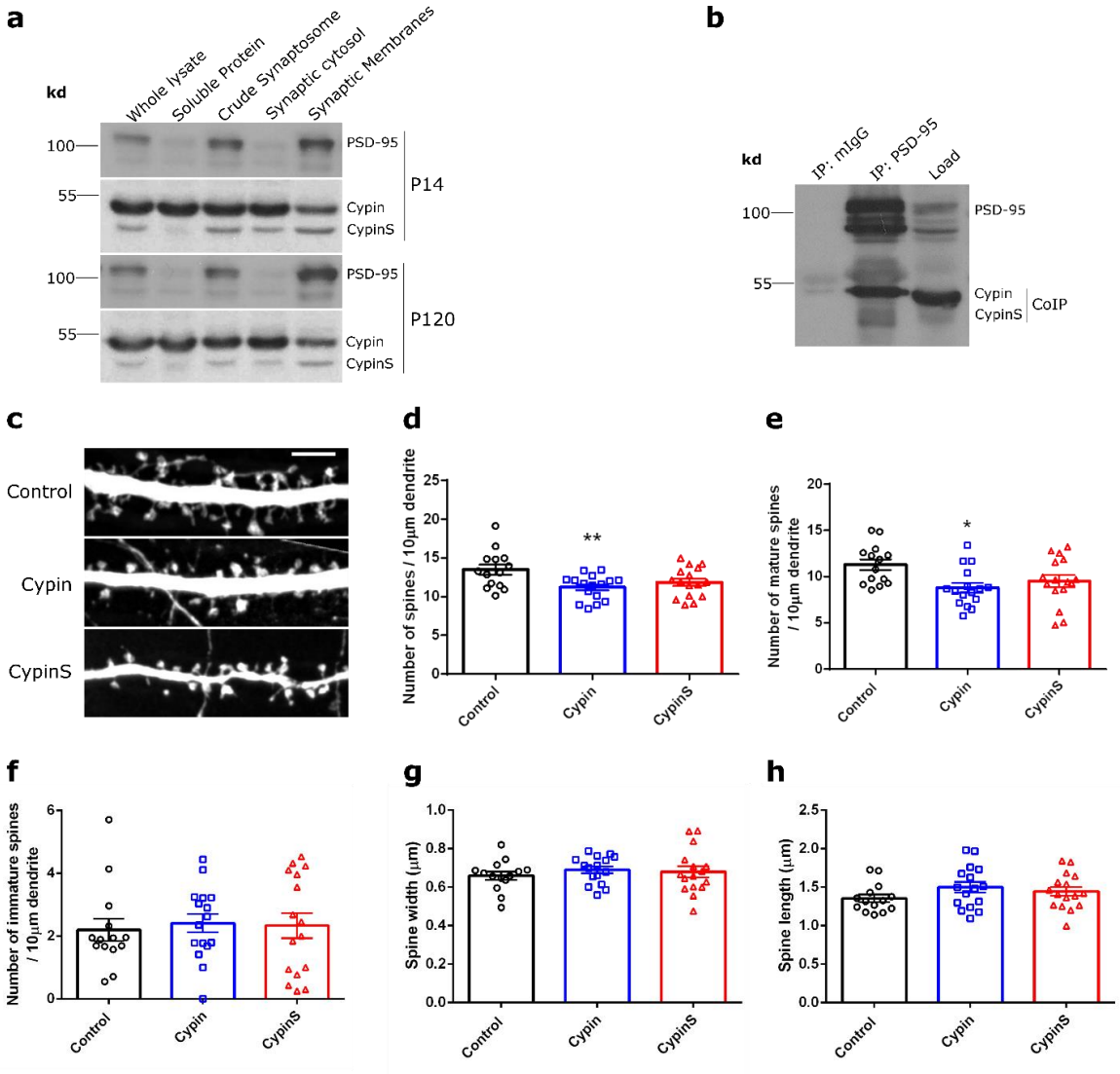


**Fig. 2.6.** Overexpression of cypin, but not cypinS, alters spine density and morphology. **a.** Western blot analysis demonstrating the presence of cypin and cypinS in synaptosomal fractions from brains of young (P14) and adult (P120) mice. **b.** Co-immunoprecipitation of cypin and cypinS with PSD-95 from whole brain lysate. PSD-95 is detected as multiple bands, consistent with previous reports. Cypin and cypinS are detected in PSD-95 immunoprecipitates with a smaller molecular weight band below where cypinS is detected, representing a modified cypinS or possible degradation product. **c.** Representative images of dendritic spines at DIV17 from neurons transfected with

pEGFP-C1 (control), pEGFP-C1-Cypin, or pEGFP-C1-CypinS. **d.** Total spines/10 µm within a 60 µm segment away from the soma in neurons expressing indicated proteins. **p<0.01, control vs cypin; p=0.077, control vs cypinS (total spines) determined by one-way ANOVA followed by Tukey's multiple comparisons test. **e.** Mature spines/10 µm within a 60 µm segment away from the soma in neurons expressing indicated proteins. *p<0.05, control vs cypin; p=0.096, control vs cypinS (number of mature spines) determined by one-way ANOVA followed by Tukey's multiple comparisons test. **f**-**h**. Overexpression of cypin or cypinS has no effect on immature spine density, spine width, or spine length. n=14 (control), n=16 (cypin), n=16 (cypinS) from three independent rat cultures. Error bar= ± SEM. Scale bar= 5 µm.

*2.3.7 Overexpression of cypin and cypinS increase mEPSC frequency*

Since both cypin and cypinS are present in synaptic cytosol fractions where synaptic vesicles are present, we asked whether overexpression of either isoform affects neuronal electrophysiology. Rat hippocampal neurons were transduced at DIV 14 with lentivirus encoding GFP, GFP-Cypin, or GFP-CypinS, and patch clamp analysis was performed at DIV 21. Interestingly, overexpression of cypin or cypinS resulted in a significant increase in the frequency of mEPSCs with no effect on amplitude (Fig. 2.7a-c). In addition, the effect of overexpression of cypinS on frequency is significantly higher than that of overexpression of cypin. Taken together with dendrite branching and spine morphology

data, our results suggest that cypin and cypinS regulate both postsynaptic and presynaptic sites in hippocampal neurons in distinct manners.

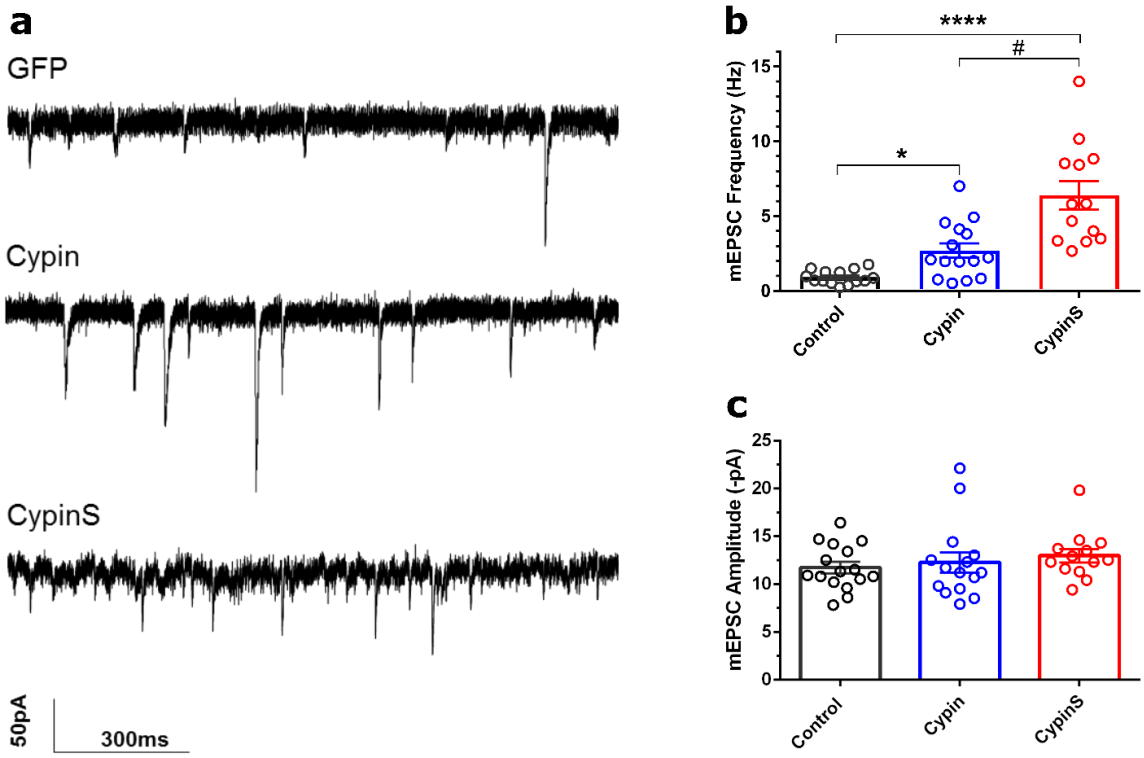


**Fig. 2.7**. Overexpression of cypin or cypinS results in increased frequency of miniature excitatory postsynaptic currents (mEPSCs). mEPSCs were recorded on DIV21 from rat hippocampal neurons overexpressing GFP (n=16), cypin (n=15), or cypinS (n=13). **a.** Representative trace recordings. **b-c**. Bar graph analysis of mEPSC frequency and amplitude. *p<0.05, control vs cypin; ****p<0.0001, control vs cypinS; #p<0.05, cypin vs cypinS. p values determined by Kruskal-Wallis test followed by Dunn's multiple comparisons test. Error bars= ± SEM.

## 2.4 Discussion

In the current work, we report the identification of a novel isoform of cypin, which we term cypinS. Interestingly, cypinS is expressed in human and mouse tissues, but not in rat tissues. CypinS is expressed at lower levels than cypin in mouse brain tissues except in the cerebellum, where cypin is expressed at very low levels [29, 61]. Cypin functions as a guanine deaminase [30, 61]; however, cypinS lacks this activity. We found that mRNA and protein levels of cypin and cypinS peak at P7-P14 in mouse brain, suggesting an important role for these proteins during neuronal development when maximum changes in morphology occur. Expression of either cypin or cypinS increases dendrite branching, which we previously reported to be dependent on the CRMP homology region [30] that binds to tubulin heterodimers and promotes microtubule assembly [66, 67]. In contrast, only overexpression of cypin results in changes to dendritic spines. Overexpression of either isoform results in increases in frequency of mEPSCs; however, overexpression of cypinS promotes a significantly higher increase in mEPSC frequency. Taken together, these data suggest different pre- and postsynaptic roles for cypin and cypinS.

Until now, we proposed that the guanine deaminase activity of cypin is important for its effects on dendritogenesis. Previous results from our laboratory suggest that mutation of residues that bind zinc eliminate the GDA activity and the dendrite promoting activity of cypin [30, 59], leading us to conclude that the two activities are related. However, based on our work presented here, it appears that zinc binding, but not GDA activity, is necessary for cypin-promoted changes to dendrites. Evolutionary analysis performed by our laboratory led to a model by which an ancestral cytidine deaminase-like protein evolved

by gene duplication followed by acquisition of PDZ-binding motifs and a zinc-binding domain. This model suggests that a new but distinct function was acquired by the mammalian guanine deaminase cypin.

CypinS is present in mouse and human but not rat. Although the human genome shares greater than 97% genes with the mouse and rat genomes [68, 69], maps of conserved synteny between human, mouse, and rat genomes suggest that there are differences in the genome when comparing human to mouse and human to rat [69]. In this same study, 278 orthologous segments were identified between human and rat, with 280 between human and mouse [69]. Thus, while cypin may function as a guanine deaminase and regulator of dendritic morphology in all three species, cypinS may act to further shape neuronal function in the mouse and human. Specifically, cypinS regulates distal dendrite branching away from soma while cypin shapes the proximal arbor, suggesting a GDA-independent role for cypinS in mouse and human.

CypinS has shorter 3'UTR compared to cypin (Fig. 2.1a) and we have shown that protein expression of cypinS is only 6-10 fold lower than that of cypin while mRNA expression is 1000-40,000 fold lower than cypin (Fig. 2.3a). Although a number of studies have reported high correlation between reference mRNA and protein levels [70, 71], other studies have shown poor correlation between mRNA and protein levels, where magnitudes of difference in mRNA exist for the same levels of protein expression and *vice versa* [71, 72]. There are multiple factors, including ribosomal occupancy, half-lives of proteins, and codon adaptation index, that explain the absence of a correlation between mRNA and protein expression [71]. The 3'UTR of mRNA is involved in post-transcriptional regulation of gene expression [73]. Adenosine (A) and uridine (U) rich elements, also called AU rich

elements (AREs), are present in 3'UTRs of mRNA [74]. AREs consist of one or more AUUUA pentamers and are involved in the regulation of mRNA stability and changes to translation [74, 75]. The 3'UTRs of cypin and cypinS differ, and thus, we used the ARESite database to identify AREs in the 3'UTRs of cypin and cypinS transcripts [76]. There are ten AUUUA pentamer motifs in the 3'UTR of cypin and five AUUUA pentamer motifs in the 3'UTR of cypinS (Fig. 2.8). This difference in the number of AUUUA pentamers in the AREs of the 3'UTRs of cypin and cypinS mRNAs may be responsible for different stabilities of both mRNAs, and thus may explain the lack of correlation between mRNA and protein expression. Since this is one of many mechanisms that may be responsible for our observation, why cypin and cypinS protein levels do not correlate with transcript levels will be a focus of future studies.

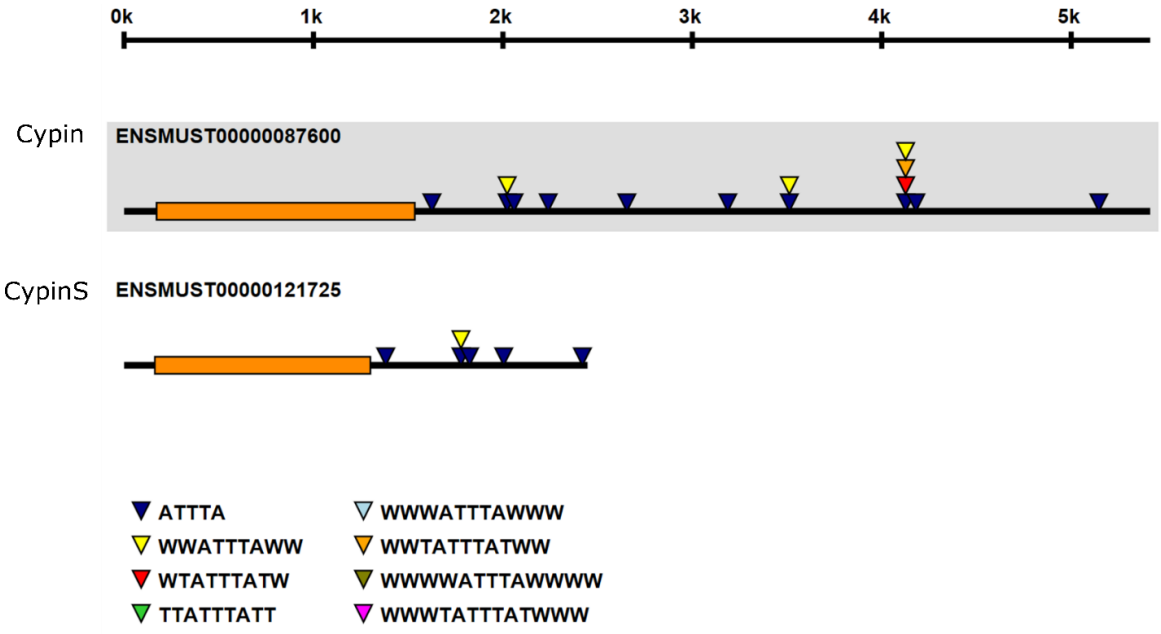


**Fig. 2.8.** AUUUA pentamers present in the AREs of the 3'UTRs of cypin and cypinS mRNAs. Results generated by ARESite show ten AUUUA pentamer motifs in the 3'UTR of cypin and five AUUUA pentamer motifs in the 3'UTR of cypinS as coded by genomic

DNA for these proteins. Colored arrowheads represent AUUUA pentamers present in mRNA.

Zinc is involved in the regulation of dendrite branching by promoting stability of microtubules [77]. In fact, in a rat model of zinc deficiency, there is impaired dendritic differentiation of basket and stellar cells [78]. Zinc also regulates multiple zinc finger proteins and transcriptional factors that shape the dendritic arbor [79-83]. CypinS may bind to zinc as does cypin [59] since the two isoforms share all residues that coordinate for zinc binding. We posit that cypin and cypinS may act as zinc sensors to increase dendrites. Zinc not only plays an important role in normal synaptic function, but when altered, it plays a role in a host of brain disorders, such as Alzheimer's disease, depression, Parkinson's disease, Huntington's disease, amyotrophic lateral sclerosis, and prion disease (reviewed in [84]). Furthermore, excess zinc mediates toxicity due to brain injury or stroke (reviewed in [84]). In line with these data, we previously reported that overexpression of cypin in cultured hippocampal neurons protects them from *N*-methyl-D-aspartate-mediated death [60]. It is possible that in this scenario, cypin acts to sense zinc and mediate protective changes to dendrites [60].

Cypin also binds to PSD-95 through its PDZ-binding motif and regulates PSD-95 synaptic targeting [29]. Moreover, overexpression of cypin decreases spine density (Fig. 2.6d and [60]). We have now demonstrated that cypinS is present in crude synaptosomes, synaptic cytosol, and synaptic membranes (Fig. 2.6a). Like cypin, cypinS contains a PDZ-binding motif on its carboxy terminus, and our data suggest that cypinS binds to

PSD-95 (Fig. 2.6b). Surprisingly, we found that overexpression of cypinS has no significant effect on spine density (Fig. 2.6d), suggesting that cypinS functions distinctly from cypin in the regulation of spine density and morphology.

All previous work in our laboratory focused on cypin function in dendrites; however, cypin is also present in the axon [29], and histochemical assays for GDA activity in rat brain reveals the presence of cypin in the mossy fibers in the CA3 region of hippocampus [61], consistent with our data in mouse brain (Patel and Firestein, unpublished data). For the first time, we report the effects of cypin and cypinS overexpression on neuronal electrophysiology. Overexpression of either cypin or cypinS increases the frequency of mEPSCs with no effect on amplitude. This lack of effect on amplitude despite decreased spine density mediated by cypin overexpression may reflect homeostatic compensatory activities. Although cypinS alters mEPSC frequency without having an effect on spine density, this discrepancy may reflect a cell autonomous function for cypinS. However, since we used lentivirus to transduce neurons to overexpress cypinS, our transduction efficiency was 100%. Thus, we cannot rule out whether changes in mEPSC frequency include a cell non-autonomous component. Moreover, overexpression of cypinS results in a significantly greater increase in frequency of mEPSCs than does overexpression of cypin. The higher frequency of mEPSCs is caused by increased release of neurotransmitters [85]. We previously reported that cypin binds to snapin, a SNARE-associated protein involved in modulating neurotransmitter release by regulating vesicle docking and fusion [86], via the CRMP homology domain of cypin [36]. Thus, the increases in mEPSC frequency observed when cypin or cypinS is overexpressed may be due, in part, to binding of snapin. Furthermore, release of vesicular pools of neurotransmitter is zinc-

dependent (i.e. [87-91]). As cypin binds to zinc and cypinS retains all zinc binding sites, cypin and cypinS may act as zinc sensors to regulate the vesicular pool and neuronal electrophysiology. Thus, cypin and cypinS may play roles in zinc-dependent pathways.

Taken together, we not only have identified a novel cypin isoform, but we have also uncovered new presynaptic roles for both isoforms. As summarized in Figure 2.9, our data suggest that the two isoforms of cypin play similar but distinct roles in neuronal development. Cypin is a guanine deaminase, but cypinS does not have this enzymatic activity. Both isoforms regulate dendrite branching; however, cypin regulates proximal dendrite branching while cypinS regulates distal dendrite branching. Cypin regulates spine number while overexpression of cypinS has no effect on spines. Both isoforms regulate presynaptic release of neurotransmitters, but overexpression of cypinS promotes a greater release than does overexpression of cypin. Although both isoforms of cypin are predicted to bind snapin, the lack of the 74 amino terminal amino acids in cypinS may contribute to different effects on snapin-mediated synaptic vesicle release. For example, cypin may have additional binding partners and regulators at its amino terminus than does cypinS, resulting in distinct regulation of function or three-dimensional folding, conferring unique functions to each cypin isoform.

| | Guanine Deaminase | Dendrite Branching | Spine Density | mEPSC Frequency |
|---|---|---|---|---|
| Cypin | ✓ | ↑ Proximal | ↓ | ↑ |
| CypinS | ✗ | ↑ Distal | - | ↑↑ |

**Fig. 2.9.** Summary of the specific effects of overexpression of cypin or cypinS on dendrites, spines and electrophysiology. Cypin is guanine deaminase while cypinS does not have this enzymatic activity. Cypin overexpression increases proximal dendrite branching, and overexpression of cypinS increases distal dendrite branching. Cypin overexpression decreases spine density, while overexpression of cypinS has no effect on spine density. Overexpression of cypin or cypinS increases mEPSC frequency, with cypinS overexpression showing significantly greater mEPSC frequency than that observed with cypin overexpression.

## 2.5 Methods and Materials

### *2.5.1 Ethical Approval*

All studies using animals were approved by the Rutgers Institutional Animal Care and Use Committee.

### *2.5.2 Western Blot and quantification*

Mouse (C57BL/6J; #000664; Jackson Laboratory) brain tissue was homogenized in 0.5 ml TEE (20mM Tris-HCl, pH 7.4, 1mM EDTA, 1mM EGTA, pH 7.4) for each 100mg wet weight of tissue and incubated with an equal volume of 2x RIPA buffer (100 mM Tris-HCl, pH 7.4, 300 mM NaCl, 1% deoxycholate, 2% NP-40, 0.2% SDS, 2 mM EDTA, pH 7.4) containing 1 mM phenylmethylsulfonylfluoride (PMSF) and protease inhibitor cocktail and rocked at $4^{o}$ C for 1hr on a Nutator. Insoluble material was pelleted at 12,000 x *g* at $4^{0}$C for 15 min. All protein extracts were evaluated for protein concentration using the Pierce BCA protein assay kit (Thermo Scientific) following the manufacturer's protocol. Proteins (12-15 µg) were resolved on a 10% SDS-polyacrylamide gel and transferred to polyvinylidene difluoride (PVDF) membrane. The membrane was blocked with 5% bovine serum albumin in TBST (20mM Tris pH 7.5, 150mM NaCl, 0.1% Tween-20) for 1 hr. The blots were probed with the indicated antibodies in TBST containing 3% BSA: polyclonal rabbit anti-cypin (1:500; BF6) [38, 60], monoclonal mouse anti-PSD-95 (1:1000; K28/43, UC Davis/NIH NeuroMab Facility), polyclonal chicken anti-GFP (1:1000, A10262, Invitrogen (Thermo Fisher Sci.)) and monoclonal mouse anti-

GAPDH (1:1000; MAB374, Millipore). Experiments were repeated at least three times. Blots were scanned, and intensities of bands were quantified using ImageJ software from NIH. The number of pixels of absolute intensity of bands was normalized to the intensity of those for GAPDH (internal controls). Human cortical tissue was provided by the Human Brain and Spinal Fluid Resource Center (Los Angeles, CA).

*2.5.3 Analysis of cypin and cypinS mRNA*

mRNA was isolated from different mouse brain tissues using the Trizol reagent (Invitrogen) following the manufacturer's protocol. A reaction of 2µg of RNA in a total volume of 20µl was converted to cDNA using the High Capacity cDNA Reverse Transcription Kit (Applied Biosystems) following the manufacturer's protocol. cDNA (10 µl) was used to perform real-time PCR using SYBR Green Real-Time master mix following the manufacturer's protocol. The following primer pairs (F for forward, R for reverse) were used for real-time PCR reactions: mouse GAPDH: (F) AGGTCGGTGTGAACGGATTTG, (R) TGTAGACCATGTAGTTGAGGTCA; mouse cypin (Ensembl: ENSMUST00000087600): (F) GTCTTCCGAGGGACTTTCGTC, (R) ATGGTTTGAAGCACCACTCCT; mouse cypinS (Ensembl: ENSMUST00000121725): (F) AGAGCAAGCCCATTGCTGTG (R) ATGGTTTGAAGCACCACTCCT. ABI 7900 HT sequence detection system (Applied Biosystems) was used to record the Ct values. SDS 2.4, RQ Manager 1.2.1 and DataAssist V3.01 (Applied Biosystems) software packages were used to generate RQ (relative quantitation or Fold Change) and p-values using two-tailed Student's t-test comparing the $2^{(-\Delta Ct)}$ values of the two groups. The p-value was adjusted using Benjamini-Hochberg False Discovery Rate. Four biological

replicates were performed, with each of them having three technical replicates. GAPDH served as the control for levels of total mRNA analyzed, and mRNAs levels from brain from mice at postnatal day 100 served as the reference group.

*2.5.4 Guanine Deaminase Activity Assay*

COS-7 cells were grown at a density of 15,000 cells/$cm^2$ on glass coverslips. Cells were transfected with cDNA encoding GFP, GFP-Cypin or GFP-CypinS using Lipofectamine 2000 (Invitrogen) following the manufacturer's protocol. Forty-eight hours after transfection, cells were washed with ice-cold phosphate-buffered saline (PBS), and images were taken using a fluorescence microscope. The protocol for the guanine deaminase assay was modified from Paletzki [61] as we have previously reported [30]. Cells were fixed for 1hr in 3% glutaraldehyde in 0.05M sodium cacodylate buffer, pH 7.8. Endogenous xanthine was removed by incubating the coverslips in 2.5U/ml xanthine oxidase (Sigma) in bicine buffer for 15-30 min at $37^0$C followed by two 5min rinses in bicine buffer. Cells were incubated in substrate solution (8mM guanine, 0.625U/ml xanthine oxidase, 0.9% 4-nitro blue tetrazolium chloride (NBT; Sigma) in 0.1M bicine pH 7.8) for 1-3hr at $37^0$C. The reaction was stopped by washing the cells in distilled water twice for 2 min and coverslips were mounted onto slides. Control reactions were performed without guanine.

*2.5.5 Amplex Red Assay*

HEK293 cells were plated at 1 million cells/well of 6 wells plate on DIV0 and transfected with indicated plasmids using Lipofectamine 2000 (Invitrogen) on DIV1. Cells were lysed in GDA lysis buffer (150 mM NaCl, 25 mM Tris–HCl, pH 7.4 and 1 mM PMSF) on DIV3 to prepare lysate. 50 µg of lysate was subjected to guanine deaminase assay using GDA lysis buffer containing 0.025 U/ml xanthine oxidase (Sigma), 0.002 U/ml peroxidase (Sigma), 50 µM Amplex Red reagent (Molecular Probes), and 16 mM guanine (Sigma). Samples were centrifuged at 9500 x *g* for 1 min at to remove insoluble guanine. Negative control without guanine were also used. All samples were incubated at 37$^{o}$ C and absorbance was recorded at 571nm using a single beam Genesys 10 UV/vis Spectrophotometer (Spectronic, UK) at indicated time intervals [59, 62].

*2.5.6 Hippocampal neuronal culture and transfection*

Hippocampal neuronal cultures were prepared from rat embryos at 18 days gestation as previously described [92]. Neurons were cultured in Neurobasal medium (Life Technologies) supplemented with B27, L-glutamine, penicillin, and streptomycin. Neurons were plated on to glass coverslips coated with poly-D-lysine (0.1mg/ml, Sigma) in a 37$^{o}$C incubator with 5 % CO2. Neurons were plated at a density of 105,000 cells/cm$^2$ for dendrite branching experiments and at a density of 50,000 cells/cm$^2$ for spine analysis. Neurons were transfected with pEGFP-C1, pEGFP-C1-Cypin or pEGFP-C1-CypinS using Lipofectamine LTX+PLUS (Invitrogen) following the manufacturer's protocol for dendrite branching and using calcium phosphate transfection for spine analysis [92]. For all conditions, neurons were co-transfected with pGW1-mRFP to

visualize dendrites and axon. For dendrite branching experiments, neurons were transfected at 7 *days in vitro* (DIV7) and fixed with 4% paraformaldehyde (PFA) in PBS at DIV12. For spine analysis, neurons were transfected on DIV14 and fixed on DIV17. Cells were immunostained with chicken anti-GFP (1:250; Thermo Fisher Sci.), rabbit anti-RFP (1:250; Rockland) and mouse anti-MAP2 (1:250; BD PharMingen). Immunostaining was visualized with Cy2-, Cy3-, or Cy5-conjugated secondary antibodies (1:500; Thermo Fisher Sci.).

*2.5.7 Dendrite branching and Sholl analysis*

Imaging was performed using an EVOS-FL fluorescence imaging system (Thermo Fisher Sci.). All images were analyzed using ImageJ software (NIH) and MATLAB (MathWorks). Sholl analysis was performed using the Bonfire program developed by the Firestein laboratory [63-65]. In brief, concentric circles were drawn around the soma every 6 µm and intersections with dendrite branches were counted. All data were exported from MATLAB to Excel for quantification. Statistical differences ($p<0.5$) were determined by two-way or one-way ANOVA followed by Tukey's multiple comparisons test using GraphPad Prism6 software. The experimenter was blinded to conditions during all Sholl and data analyses.

*2.5.8 Synaptosomal Fractionation*

One hemisphere from an adult or P14 male mouse brain was lysed in 1.2 ml sucrose buffer (10 mM HEPES, pH 7.5, 1.5mM MgCl2, 320mM sucrose, 5mM EDTA, 5mM dithiothreitol (DTT), 0.1 mM PMSF, 10 µM MG132, PMSF and 1x protease Inhibitors).

The lysate was centrifugated for 10 min at 1000 x *g* to remove nuclei and cellular debris. The supernatant was centrifuged for 15 min at 10,000 x *g* to pellet crude synaptosomes and a supernatant containing soluble proteins. The pellet was resuspended in sucrose buffer containing 1% Triton X-100 for 1 hr at 4$^{o}$ C followed by centrifugation for 30 min at 40,000 x *g* using a TLA 100.3 fixed angle rotor in a Beckman Coulter Optima LTX centrifuge to isolate a pellet containing synaptic membranes and supernatant containing synaptic cytosol [93].

*2.5.9 Immunoprecipitation*

Mouse whole brain lysate was prepared in 1x RIPA buffer with PMSF and protease inhibitor cocktail at 4$^{o}$ C as mentioned above. Protein (2 mg) was used to immunoprecipitate PSD-95 with 5 µg anti-ms-PSD-95 (K28/43, NeuroMab) and 50 µl Protein G magnetic beads (GE Healthcare). 5 µg of normal mouse IgG was used for control immunoprecipitation. Precipitated protein was eluted from antibody-bead complexes using 2x SDS-PAGE sample buffer (125 mM Tris, pH 6.8, 20% glycerol, 4% sodium dodecyl sulfate, 0.01% bromophenol blue, 5% β-mercaptoethanol) and subjected to Western blot analysis.

*2.5.10 Dendritic Spine Analysis*

Images of dendritic segments were taken with a 60x Plan Apo oil-immersion objective (NA 1.4) using a Yokogawa CSU-10 spinning disk confocal head attached to an inverted fluorescence microscope (Olympus IX50). X-Y and Z-resolution were set as 0.067 µm-

0.067 μm and 0.1 μm, respectively, to define dendritic spines. All images were analyzed using ImageJ software (NIH). The number of protrusions was counted from two randomly chosen secondary or tertiary dendrites per neuron. Spines along dendritic segments were counted at distances 20 μm to 80 μm from the soma. Spines were manually counted from at least 14 neurons for each experimental condition. The following criteria were used in excel to classify spines: mushroom spines have total length $\leq$ 5μm and head width/neck width $\geq$ 1.5; thin spines have total length $\leq$5 μm and head width/neck width >1 but $\leq$ 1.5; stubby spines have total length $\leq$ 1 μm and head width/neck width $\leq$ 1; filopodia have total length > 1 and head width/neck width $\leq$ 1. Mushroom and thin/stubby are mature and immature spines, respectively. Analysis was performed with the experimenter blinded to the condition.

*2.5.11 Lentivirus production*

cDNA encoding cypin or cypinS was cloned into the pHUG lentiviral vector (gift from Dr. Christoph Proschel) at the BsrG1 site using the Infusion HD Cloning kit (Takara Bio USA, Inc.) by following the manufacturer's protocol. In brief, on day 1, HEK293 cells were plated at the density of 6.5 x $10^6$ cells/ T75 flask. On day2, cells were transfected by the calcium phosphate method [92] with lentiviral plasmids for expression of GFP, GFP-cypin, or GFP-cypinS and PAX2 and VSV packaging vectors. On day5, supernatant was collected and centrifuged at 1500 x *g* for 5 min to remove dead cells and debris. The supernatant was transferred into a new tube containing 5x PEG-*it* virus precipitation solution (System Biosciences), thus diluting 1:4, followed by incubation at 4°C for 2 days

to concentrate the virus. On day 7, the mixture was centrifuged at 1500 x *g* for 30 min at 4°C to pellet the virus. The supernatant was carefully removed, and the pellet was resuspended in 150-200 µl sterile PBS and aliquoted into 10µl fractions stored at -80°C [94].

*2.5.12 Electrophysiology*

All electrophysiological recordings were performed as we previously described [95]. In brief, hippocampal neurons were transduced on DIV 14 with lentivirus encoding GFP, GFP-cypin, or GFP-cypinS, and recording was performed on DIV 20-21. Whole cell patch-clamp recordings were made on the soma of hippocampal neurons. For recordings, cells were bathed in artificial cerebrospinal fluid (ACSF) containing (in mM): 140 NaCl, 5 KCl, 2 CaCl2, 2 MgCl2, 10 HEPES, and 10 Glucose (pH 7.4 adjusted with NaOH; 290-310 mOsmol). Recording electrodes (3 –5 MΩ) contained a K-based internal solution composed of (in mM): 126 K-gluconate, 4 KCl, 10 HEPES, 4 ATP-Mg, 0.3 GTP-Na2, 10 Phosphocreatine, and 10 QX-314 bromide (pH 7.2; 280 –300 mOsmol). In order to record miniature excitatory postsynaptic currents (mEPSCs), action potentials were blocked with 1 µM tetrodotoxin (Tocris, R&D Systems), and GABA inhibitory currents with 50 µM picrotoxin (Tocris, R&D Systems). The membrane potential was held at -70mV throughout all experiments. Data were amplified and filtered at 2 kHz by a patch-clamp amplifier (Multiclamp 700B), digitalized (DIGIDATA 1440A), stored, and analyzed by pCLAMP (Molecular Devices, Union City, CA). Data were discarded when the input resistance changed >20% during recording.

## 2.6 Acknowledgements

This research was supported by National Science Foundation grant IOS-1353724 to BLF. MVP was supported in part by a Predoctoral Fellowship from the New Jersey Commission on Brain Injury Research #CBIR15FEL009. PS was supported in part by National Institutes of Health Biotechnology Training Grant T32 GM008339-20 and a Predoctoral Fellowship from the New Jersey Commission on Brain Injury Research #CBIR16FEL013. ARR was supported by the National Institutes of Health Biotechnology Training Grant T32 GM008339-20. KC was supported in part by a Rutgers University Aresty Research Fellowship.

### Author Contributions

MVP and BLF designed experiments and wrote the manuscript with input from PS. MVP performed biochemistry and morphology experiments and analyzed resulting data. MK identified cypinS in mouse and performed preliminary experiments. PS performed electrophysiology experiments and analyzed all resulting data. KC worked with MVP to perform cloning of the plasmids and the biochemistry experiments to validate BF6 antibody against cypinS. ARR provided cultured neurons for morphology experiments and performed imaging of dendrite branching experiments. BLF supervised the project.

# Chapter 3: A Role for Postsynaptic Density 95 and its Binding Partners in Models of Traumatic Brain Injury.

This work is currently under journal review. Patel M.V., Sewell E., Dickson S., Kim H., Meaney D. F., and Firestein B.L. A Role for Postsynaptic Density 95 and its Binding Partners in Models of Traumatic Brain Injury.

## 3.1 Abstract

Postsynaptic density 95 (PSD-95), the major scaffold protein at excitatory synapses, plays a major role in mediating intracellular signaling by synaptic N-methyl-D-aspartate (NMDA) type glutamate receptors. Despite the fact that much is known about the role of PSD-95 in NMDA-mediated toxicity, less is known about its role in mechanical injury, and more specifically, in traumatic brain injury. Given that neural circuitry is disrupted after TBI and that PSD-95 and its interactors *end-binding protein 3* (EB3) and *adenomatous polyposis coli* (APC) shape dendrites, we examined whether changes to these proteins and their interactions occur after stretch-induced injury *in vitro* and controlled cortical impact (CCI) *in vivo*. Here, we report that the interaction of PSD-95 with EB3 increases 1 hour after stretch-induced injury and 1 and 7 days after moderate CCI. In contrast, mild CCI promotes activation of a distinct mechanism whereby the interaction between PSD-95 and EB3 decreases 2 hours post-injury. In addition, using our stretch model to mimic moderate injury, we show that PSD-95 has no role in the

regulation of neuronal survival post-stretch injury, which is in contrast to previous reports in an NMDA-mediated injury system. However, our data support the fact that PSD-95 must be present to disrupt dendritic arborization post-stretch injury. Thus, PSD-95 and its interactors may serve as therapeutic targets for repairing dendrites after TBI.

## 3.2 Introduction

Traumatic brain injury (TBI) is caused by the rapid movement of the brain within the skull, leading to neuronal damage and injury to the brain. A traumatic event can be an impact, such as direct contact to an object, or non-impact, such as an indirect blast or acceleration. In the United States, TBI leads to 56,000 deaths per year.[96] Falls, vehicle accidents, sports-related concussions,[97] and blast injury in military individuals,[98] are the leading causes of TBI in the United States.

Primary brain insult occurs immediately after trauma and includes mechanical damage to blood vessels, neurons, and glia. Secondary insult is the indirect result of the events initiated by the primary brain injury and occurs from hours to weeks after trauma.[44] Secondary insult involves glutamate-mediated excitotoxicity and increased calcium influx, promoting synaptic dysfunction, dendrite and axon degeneration, and ultimately, neuronal death.[44, 45] Downstream signaling cascades activated by increased calcium influx from NMDA receptors cause damage to dendrites,[99] resulting in short-term cognitive deficits after mild TBI,[47] and long-term or permanent cognitive deficits and disabilities after moderate to severe TBI.[48] As of yet, no medication is available to either

prevent or treat secondary insult. Many NMDA receptor antagonist drugs and neuroprotective agents have failed to promote cognitive improvement after TBI in clinical trials.[100, 101] Thus, the unavailability of a promising therapeutic approach motivates the study of detailed molecular mechanisms involved in short- and long-term changes or deficits after TBI.

Possible therapeutic targets for recovery after TBI include pathways involved in the reconnection of neural circuitry. For example, reestablishment of the dendritic network is required for proper neuronal signaling and improvement of cognitive function. Although a number of studies have focused on axonal degeneration following TBI (as reviewed in [102-104]), less attention has been given to the effects of TBI on dendritic arborization.[49] Understanding mechanisms underlying the development and maintenance of dendritic arborization will help to develop new therapeutic approaches for the recovery of cognitive function and identify new molecular targets for the development of novel drugs and therapeutic approaches for the treatment of TBI.

Postsynaptic density-95 (PSD-95), one such molecular target, is the major scaffolding protein in the postsynaptic density (PSD) of dendritic spines[18, 19, 21, 105-107] and is essential for glutamate-mediated excitotoxicity.[108, 109] Overexpression of PSD-95 exacerbates neuronal excitotoxicity mediated by N-methyl-D-aspartate (NMDA) glutamate type receptors, and knockdown attenuates neuronal death.[43] Furthermore, overexpression of PSD-95 in cultured hippocampal neurons promotes maturation of spines.[25] Besides its function in spines, PSD-95 restricts dendritic arborization by binding to a proline-rich region in the +*TIP* microtubule *end-binding protein 3* (EB3) through its SH3 domain.[28, 31]. Additionally, interaction between PSD-95 and another +*TIP* binding protein,

*adenomatous polyposis coli* (APC),[33] results in stimulation of microtubule assembly, bundling, and stabilization.[11, 34] APC regulates microtubules at branch points[110] and mediates neurite outgrowth.[111-113] Thus, targeting PSD-95 levels and interactions with binding partners may be of therapeutic value for repair of neural circuits, and specifically dendrite morphology, after TBI.

In the current study, we used both *in vitro* and *in vivo* models to assess the role of PSD-95 and its interaction with binding partners in TBI. We found that although PSD-95 levels do not change after stretch-mediated (primary) injury in mouse brain slices, the interaction of PSD-95 with EB3 increases as a result of stretch-induced injury. Furthermore, to mimic TBI *in vivo*, we used both mild and moderate controlled cortical impact (CCI) mouse models. Two hours post mild-TBI, EB3 levels increase; however, the interaction between PSD-95 and EB3 decreases. Moderate TBI increases PSD-95 levels and interaction with APC and EB3 at 1 and 7 days post-CCI, and levels return to baseline by 14 days, suggesting that remodeling mechanisms after TBI differ depending on injury severity. Based on the fact that PSD-95 and its interactors may play a role in the remodeling process after injury, we knocked down PSD-95 in cultured rat cortical neurons. We found that this knockdown prevents decreases in secondary dendrite number and total dendrite length after stretch-mediated injury and that PSD-95 must be present for stretch-mediated injury to decrease dendrites. Thus, targeting PSD-95 and its interactions with microtubule-associated proteins may serve as a therapeutic strategy after TBI.

## 3.3 Results

### *3.3.1 The second PDZ domain of PSD-95 is necessary for the regulation of dendritic arborization*

It has been reported that PSD-95 levels change in rat and mouse models of TBI[55, 56] and that excitatory scaffold networks mediate the downstream effects of TBI.[114] Specifically, two PSD-95 interactors, EB3[31, 32] and APC[11, 33, 34], regulate microtubule dynamics, a process involved in dendritic remodeling, an important component of recovery. We previously reported that the interaction between PSD-95 and EB3 regulates dendrite number; however, this interaction does not fully explain PSD-95-mediated decreases in dendrite number.[31] We previously reported that the presence of the SH3 domain is needed for PSD-95-promoted decreases in dendrite branching.[31] To extend these studies and identify potential PSD-95 interactors that may regulate dendrite number after injury, we overexpressed PSD-95 and PSD-95 lacking PDZ 1 (PSD-95ΔPDZ1), PDZ2 (PSD-95ΔPDZ2) or PDZ3 (PSD-95ΔPDZ3) in cultured hippocampal neurons from DIV 7-12. As expected, overexpression of PSD-95 reduced dendrite number (**Fig. 3.1A-C**). When the second PDZ domain of PSD-95 was deleted, PSD-95 overexpression did not decrease dendrite branching to the levels seen with overexpression of intact PSD-95. Thus, in addition to the SH3 domain, and the binding of EB3 to this domain,[31] PDZ2 interactors may play a role in regulating the dendritic arbor.

Since APC interacts with PSD-95 via its second PDZ domain,[33] and this interaction promotes microtubule bundling,[34] we confirmed that this interaction exists in the brain. Interestingly, co-immunoprecipitation experiments show that *adenomatous polyposis coli* (APC) associates with PSD-95 to a greater degree in the developing rat brain (P12) when dendritogenesis is occurring than it does in the adult rat brain when dendritogenesis has stopped (**Fig. 3.1D**). Thus, based on the fact that the second domain of PSD-95 regulates dendrite morphology and that APC binds to this region (and to EB3 independently of PSD-95[115]) and is involved in the regulation of microtubule dynamics, we performed experiments to assess whether interaction of PSD-95 with APC and EB3 is altered after injury.

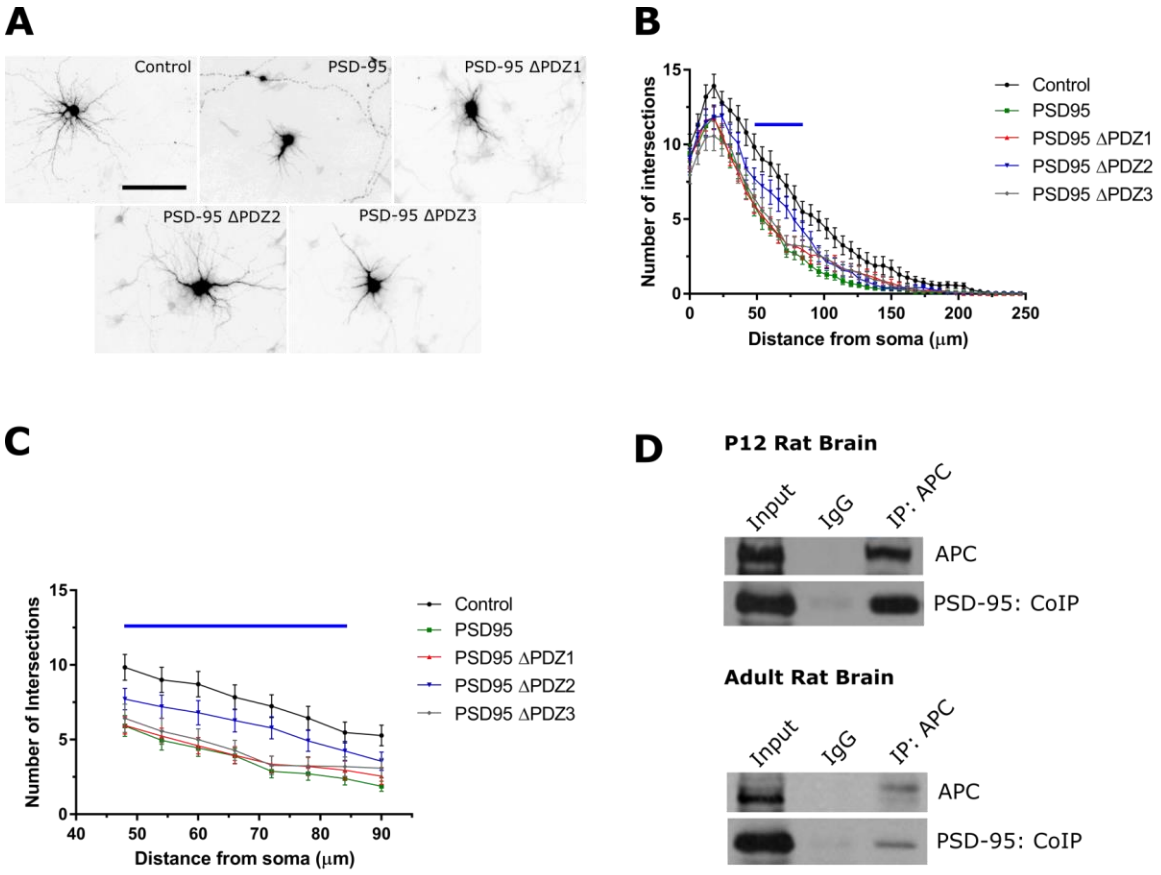


**Fig. 3.1. The second PDZ domain is necessary for PSD-95-mediated decreases in dendritic arborization. (A)** Representative images of neurons expressing mRFP (to elucidate morphology) and co-expressing GFP, GFP-tagged PSD-95, PSD-95ΔPDZ1, PSD-95ΔPDZ2 or PSD-95ΔPDZ3. (**B,C)** Sholl analysis of neurons expressing the indicated proteins. Deletion of PDZ2 (PSD-95ΔPDZ2) attenuates PSD-95-mediated decreases in dendritic arborization for distances of 48-84 μm away from the soma while deletion of PDZ1 and PDZ3 (PSD-95ΔPDZ1 and PSD-95ΔPDZ3) do not. Blue line indicates $p<0.05$ for PSD-95 vs. PSD-95ΔPDZ2 as determined by two-way ANOVA followed by Tukey's multiple comparisons test. n=23-25 neurons for each condition. Error bars = S.E.M. Scale bar = 100 μm. **(D)** APC co-immunoprecipitates with PSD-95 from developing (P12) and adult rat brain. APC was immunoprecipitated from whole

brain lysate from adult or P12 rat. Precipitates were subjected to immunoblotting followed by Western blot analysis with an antibody against PSD-95. Input represents 2% of protein used for immunoprecipitation (IP).

### *3.3.2 Stretch-induced injury increases the interaction of PSD-95 with EB3*

To assess whether changes to PSD-95, APC, and EB3 occur after TBI, we exposed brain slices from mice to stretch-induced injury (**Fig. 3.2A,B**). We chose to use brain slices for these studies as they maintain neuronal circuitry and all brain cell types are present, including oligodendrocytes and other non-neuronal cell types. Stretch had no effect on total PSD-95 levels or the interaction of PSD-95 with APC; however, it increased the interaction between PSD-95 and EB3 (**Fig. 3.2C,D**). Thus, PSD-95 may sequester EB3 immediately after injury (<1 hour), decreasing dendrite branching.

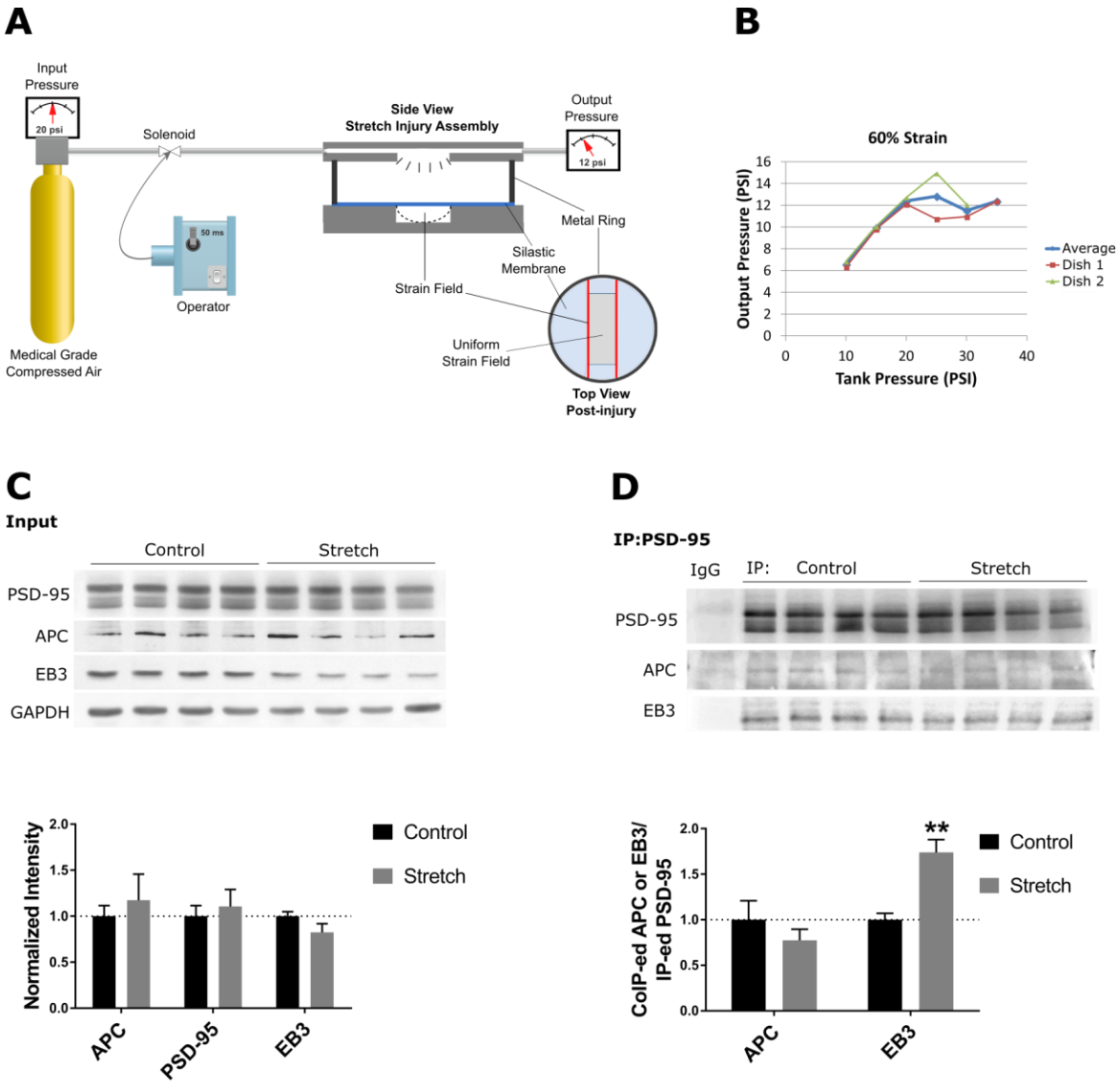


**Fig. 3.2. Stretch-induced injury increases the interaction between PSD-95 and EB3.** **(A)** Schematic of stretch injury device. **(B)** Data collected from the device, showing consistent output pressure of 12 psi for an applied pressure of 20 psi. **(C)** Coronal brain slices from wildtype adult male mice were exposed to stretch-induced injury. *Top panel*, Western blot analysis of total levels of PSD-95, APC, and EB3. *Bottom panel*, All protein levels were normalized to GAPDH and plotted as normalized intensity. Stretch had no effect on total protein levels. **(D)** *Top panel*, Western blot for immunoprecipitated PSD-

95 and co-immunoprecipitated APC and EB3. *Bottom panel*, The ratio of band intensities of APC or EB3 to PSD-95 from stretch conditions was compared to control (unstretched). Stretch-induced injury increases the interaction between PSD-95 and EB3. n=7 mice per condition. *p=0.05; **p<0.01 for control vs. stretch as determined by Student's t-test followed by Welch's correction test. Error bars = S.E.M.

*3.3.3 Mild and moderate CCI result in distinct changes to PSD-95 and EB3*

Since our stretch injury model does not replicate all changes that occur after TBI, we used controlled cortical impact (CCI) as an *in vivo* model of injury to assess changes to PSD-95 and its interactors. At 2 hours post-mild injury, we observed an increase in EB3 levels; however, the interaction with PSD-95 decreased (**Fig. 3.3A; E**(IgG control)). All changes returned to baseline by 1 day post-injury and at later time points (**Fig. 3.3B-D**). Since mild TBI and moderate TBI activate different cellular mechanisms (reviewed in [116]), we assessed changes to protein levels in mice exposed to moderate CCI. We did not analyze the 2 hours post-injury time point for moderate injury as hemorrhage at that time confounds results. We observed that total levels of PSD-95 increased at 1 day and 7 days post-moderate CCI (**Fig. 3.3B,C, left panels**). In addition, the levels of EB3 that co-immunoprecipitate with PSD-95 increased at 1 day and 7 days, and that of APC increased at 1 day post-moderate CCI (**Fig. 3.3B,C, right panels**). Total protein levels of PSD-95 and its interaction with APC and EB3 returned to control levels by 14 days post-CCI. Our results demonstrate that PSD-95 and its interaction with APC and EB3 may be involved in post-injury response and that response mechanisms after mild and moderate TBI differ.

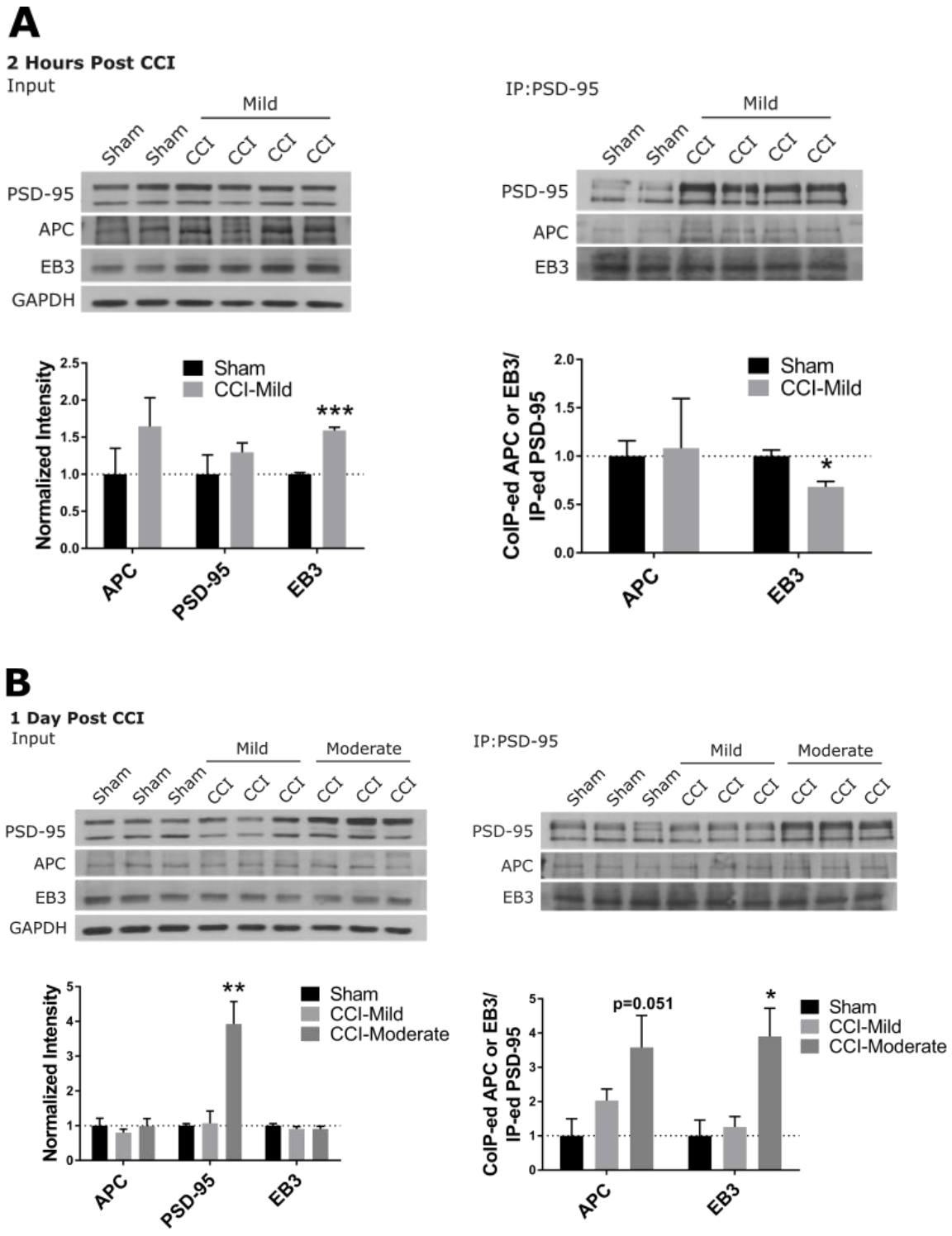
A
2 Hours Post CCI
Input
Mild
Sham
Sham
CCI
CCI
CCI
CCI
PSD-95
APC
EB3
GAPDH
IP:PSD-95
Normalized Intensity
Sham
CCI-Mild
***
APC
PSD-95
EB3
CoIP-ed APC or EB3/ IP-ed PSD-95
*
B
1 Day Post CCI
Moderate
CCI-Moderate
**
p=0.051

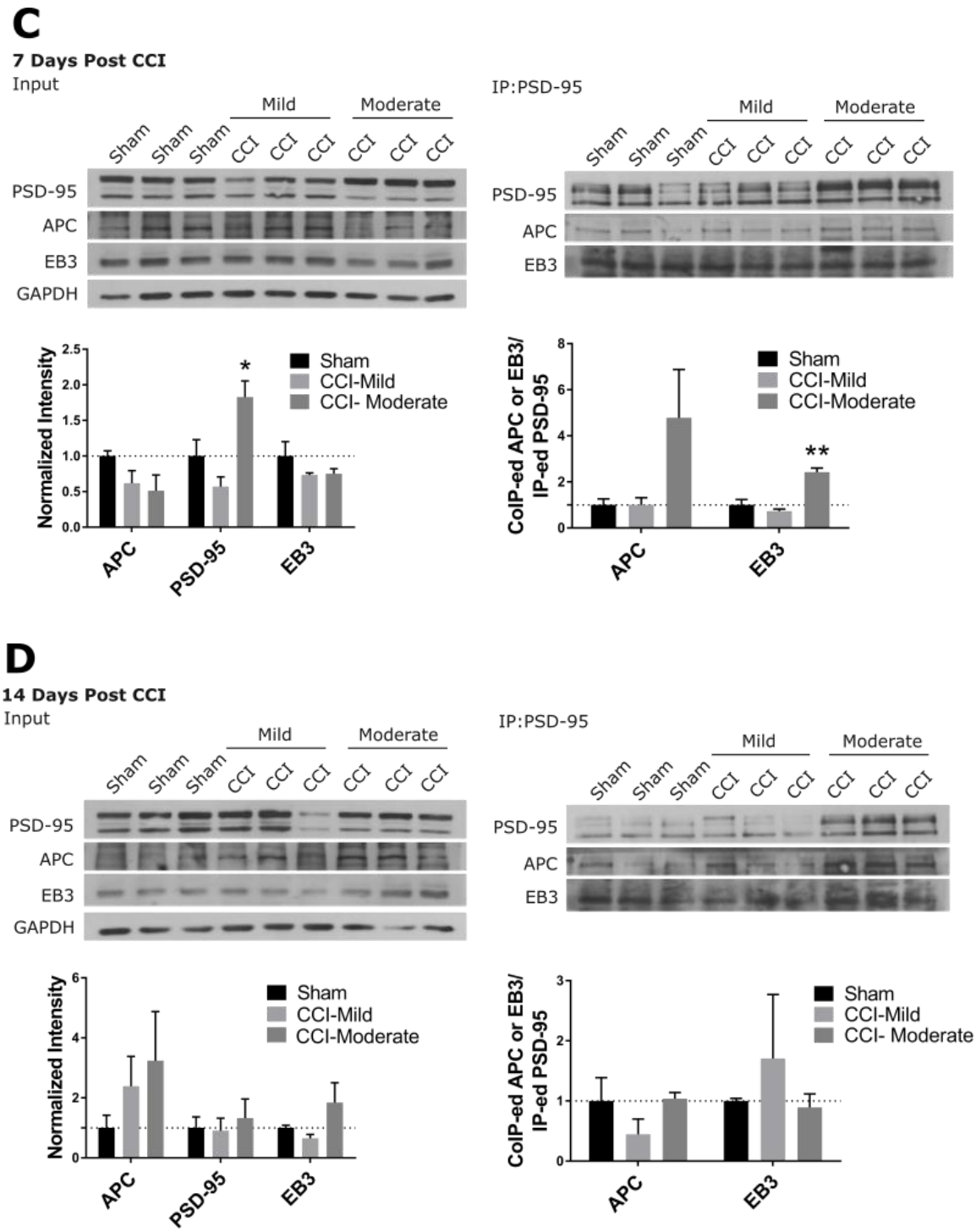
C
7 Days Post CCI
Input
IP:PSD-95
Mild
Moderate
Sham
CCI
PSD-95
APC
EB3
GAPDH
Normalized Intensity
ColP-ed APC or EB3/ IP-ed PSD-95
Sham
CCI-Mild
CCI- Moderate
CCI-Moderate
*
**
APC
PSD-95
EB3
D
14 Days Post CCI

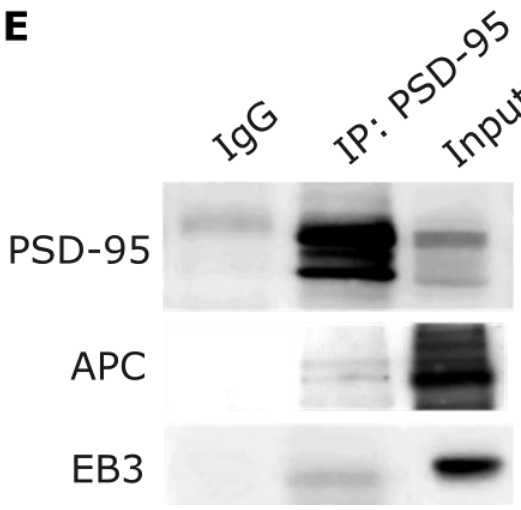


**Fig. 3.3**. **Expression of PSD-95 and interaction with APC and EB3 change differently in mice subjected to mild or moderate CCI.** PSD-95 was immunoprecipitated from extracts from cortices of mice exposed to sham injury or CCI. Lysates and immunoprecipitates were subjected to Western blot analysis. **(A)** Western blots and densitometric analysis for cortices at 2 hours post-mild injury. **(B)** Western blots and densitometric analysis for cortices at 1 day post-mild and moderate injury. **(C)** Western blots and densitometric analysis for cortices at 7 days post-mild and moderate injury. **(D)** Western blots and densitometric analysis for cortices at 14 days post- post-mild and moderate injury. **(E)** Representative Western blot of immunoprecipitation with mouse IgG (negative control) or anti-PSD-95 performed on mouse brain cortical lysate. APC and EB3 co-immunoprecipitate with PSD-95 but are not present in the IgG lane. n=3-4 mice for each time point. *$p<0.05$, **$p<0.01$, and ***$p<0.001$ as determined by comparing CCI to sham condition using one-way ANOVA followed by Dunnett's multiple comparisons test except for the use of Student's t-test followed by Welch's correction for 2 hours post-mild injury. Error bars = S.E.M.

*3.3.4 Knockdown of PSD-95 does not protect neurons after stretch-induced injury*

We previously reported that knockdown of PSD-95 protects neurons from NMDA-induced excitotoxicity[43]; however, it is not known whether PSD-95 knockdown protects neurons from mechanical injury. Since PSD-95 expression and interaction with APC and EB3 increase after injury, we asked whether downregulation of PSD-95 has any effect on neuronal viability after stretch injury. We created viruses containing scramble control shRNA and shRNA targeting PSD-95. Scrambled shRNA has no effect on PSD-95 levels while PSD-95 shRNA decreased levels by 50% in cultured neurons transduced with virus (**Fig. 3.4**).

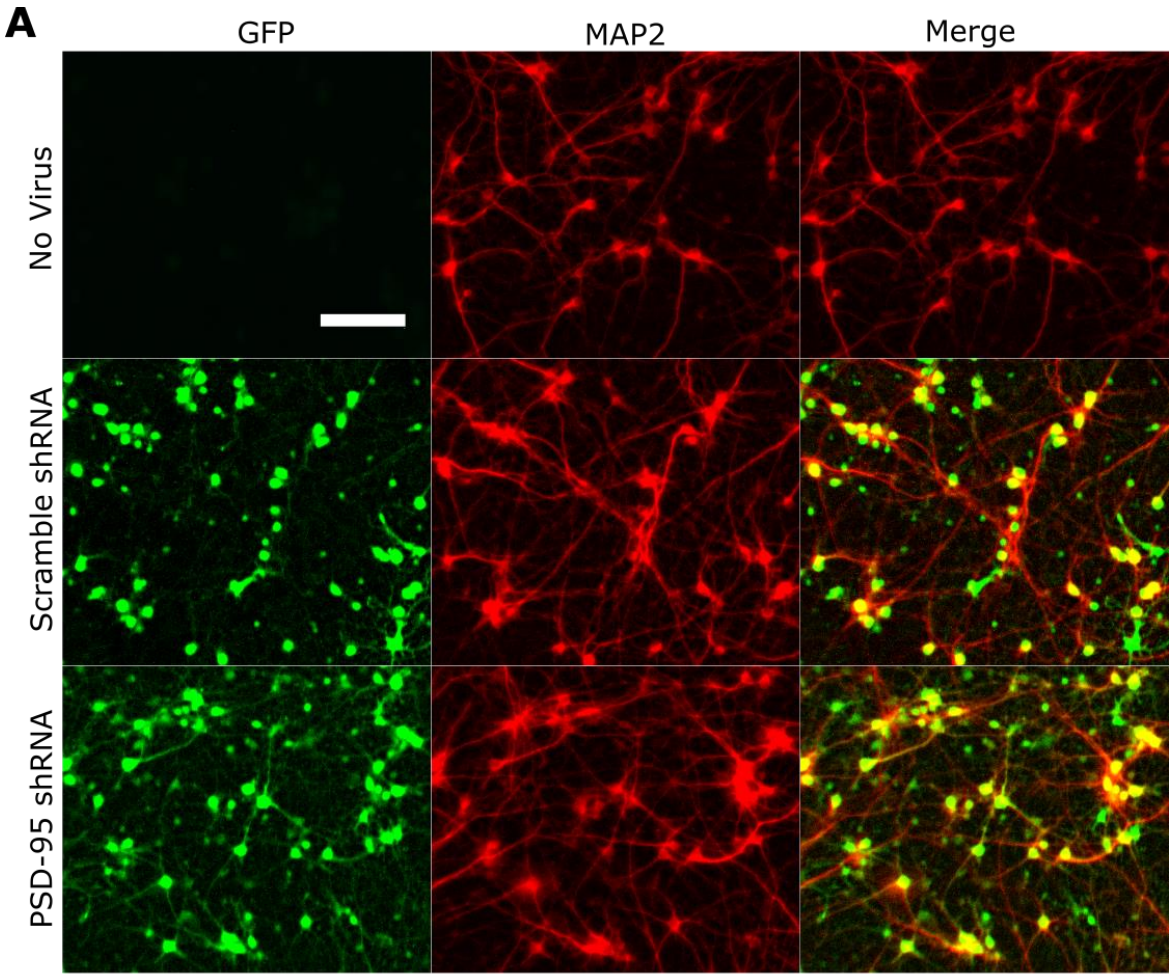
A
GFP
MAP2
Merge
No Virus
Scramble shRNA
PSD-95 shRNA

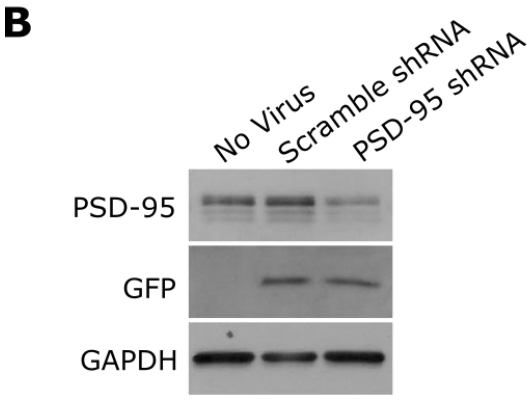
B
No Virus
Scramble shRNA
PSD-95 shRNA
PSD-95
GFP
GAPDH

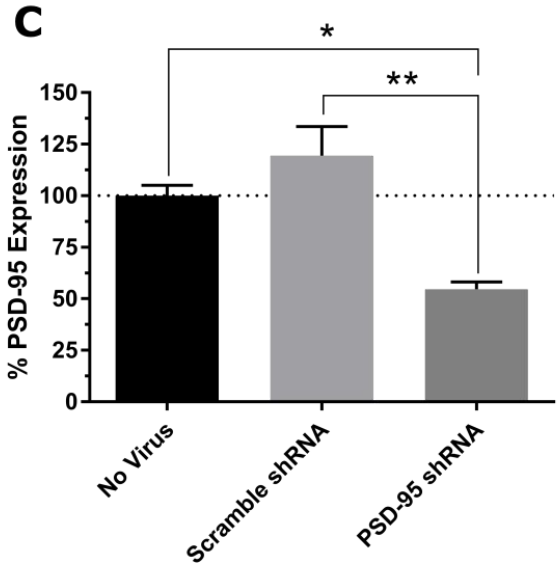
C
*
**
% PSD-95 Expression
150
125
100
75
50
25
0
No Virus
Scramble shRNA
PSD-95 shRNA

**Fig. 3.4. PSD-95 shRNA decreases PSD-95 protein levels by 50%. (A)** Representative images of neurons transduced with lentivirus encoding scramble shRNA (control) and GFP or PSD-95 shRNA on DIV 11 and fixed on DIV 17. Neurons were immunostained for GFP (green) and MAP2 (red). Transduction efficiency is almost 100%. **(B)** Western blot showing GFP and PSD-95 expression in cortical neurons transduced with scramble shRNA or PSD-95 shRNA. **(C)** Quantification of PSD-95 knockdown. *$p<0.05$; **$p<0.01$ as determined by one-way ANOVA followed by Tukey's multiple comparisons test. n=3. Error bars = S.E.M. Scale bar = 100 μm.

We then assessed neuronal survival after stretch. In control (scramble shRNA) cultures, stretch induced approximately 40% neuronal death as determined by counts of MAP2-positive neurons (**Fig. 3.5**). Knockdown of PSD-95 had no effect on neuronal viability, and unlike the NMDA-mediated injury paradigm, PSD-95 knockdown did not protect neurons from stretch-induced injury (**Fig. 3.5**). These data suggest that the mechanisms that mediate injury due to stretch and NMDA exposure differ.

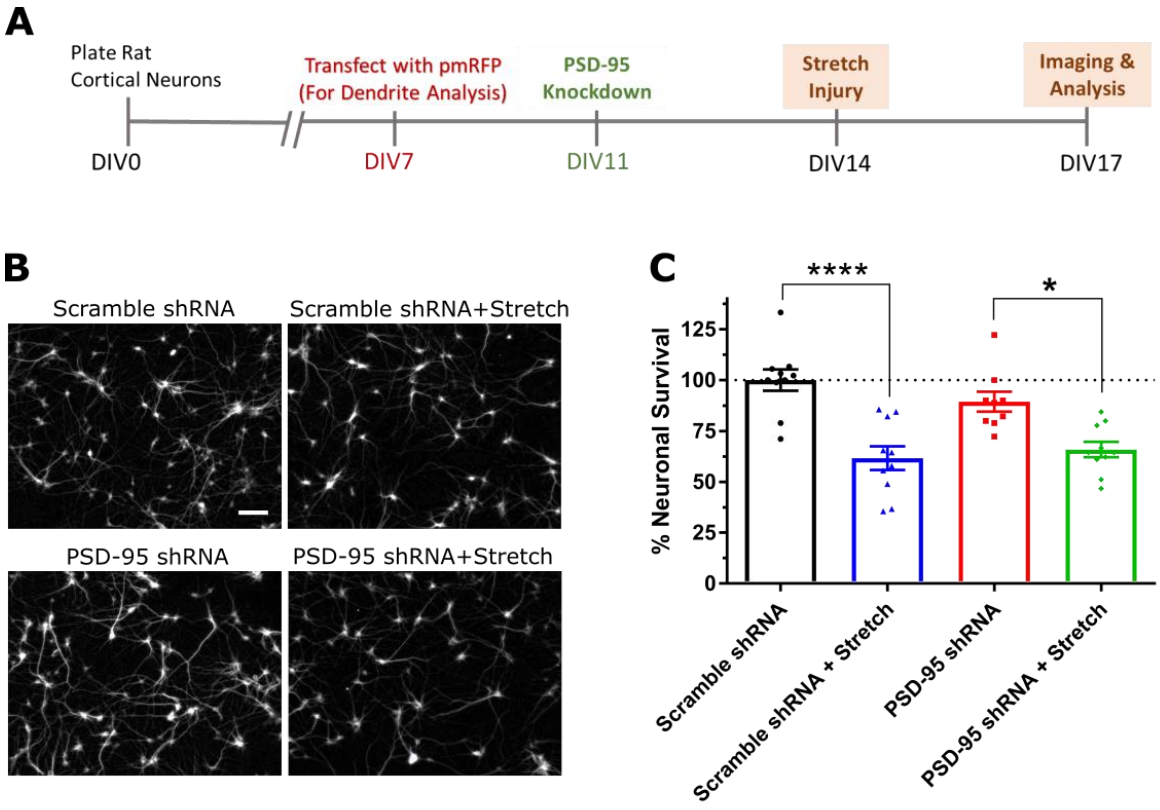


**Fig. 3.5. PSD-95 knockdown does not prevent stretch injury-induced neuronal death. (A)** Experimental timeline for neuronal survival and dendrite branching analysis after stretch injury. **(B)** Representative images of MAP2-positive neurons for each condition. **(C)** Percentage of surviving neurons at three days after injury. *$p<0.05$; ****$p<0.0001$ as determined by one-way ANOVA followed by Tukey's multiple comparisons test. n=10 regions of interest (ROI) per condition of single independent experiment. Experiment was repeated three times. Error bars = S.E.M. Scale bar = 100 µm.

### *3.3.5 Downregulation of PSD-95 prevents stretch-mediated decreases in dendrite branching*

It is not known how stretch-induced injury affects the dendritic arbor. As such, we performed Sholl analysis and simple dendrite assessment on cultured dissociated cortical neurons subjected to stretch injury. Stretch injury decreased Sholl curves and secondary and higher order dendrites as well as total dendrite length, number of branch points, and number of terminal points (**Fig. 3.6**). Since PSD-95 is involved in regulation of dendrite branching by binding to the microtubule +TIP binding proteins EB3[28, 31] and APC[33], we asked whether downregulation of PSD-95 can prevent these stretch injury-mediated decreases in dendrite branching. PSD-95 knockdown partially prevented stretch-mediated decreases in secondary dendrite number and total dendrite length post-injury (**Fig. 3.6D,G**). However, it did not reverse decreases seen in the Sholl curve (**Fig. 3.6B**). Although PSD-95 knockdown resulted in decreases in the number of higher order dendrites, total dendrite number, number of branch points, and terminal points (**Fig. 3.6E,F,H,I**), stretch injury does not further induce decreases, suggesting that PSD-95 must be present for stretch injury to mediate insult to the arbor. Thus, targeting PSD-95 knockdown after TBI may be a therapeutic strategy for restoring the dendritic arbor.

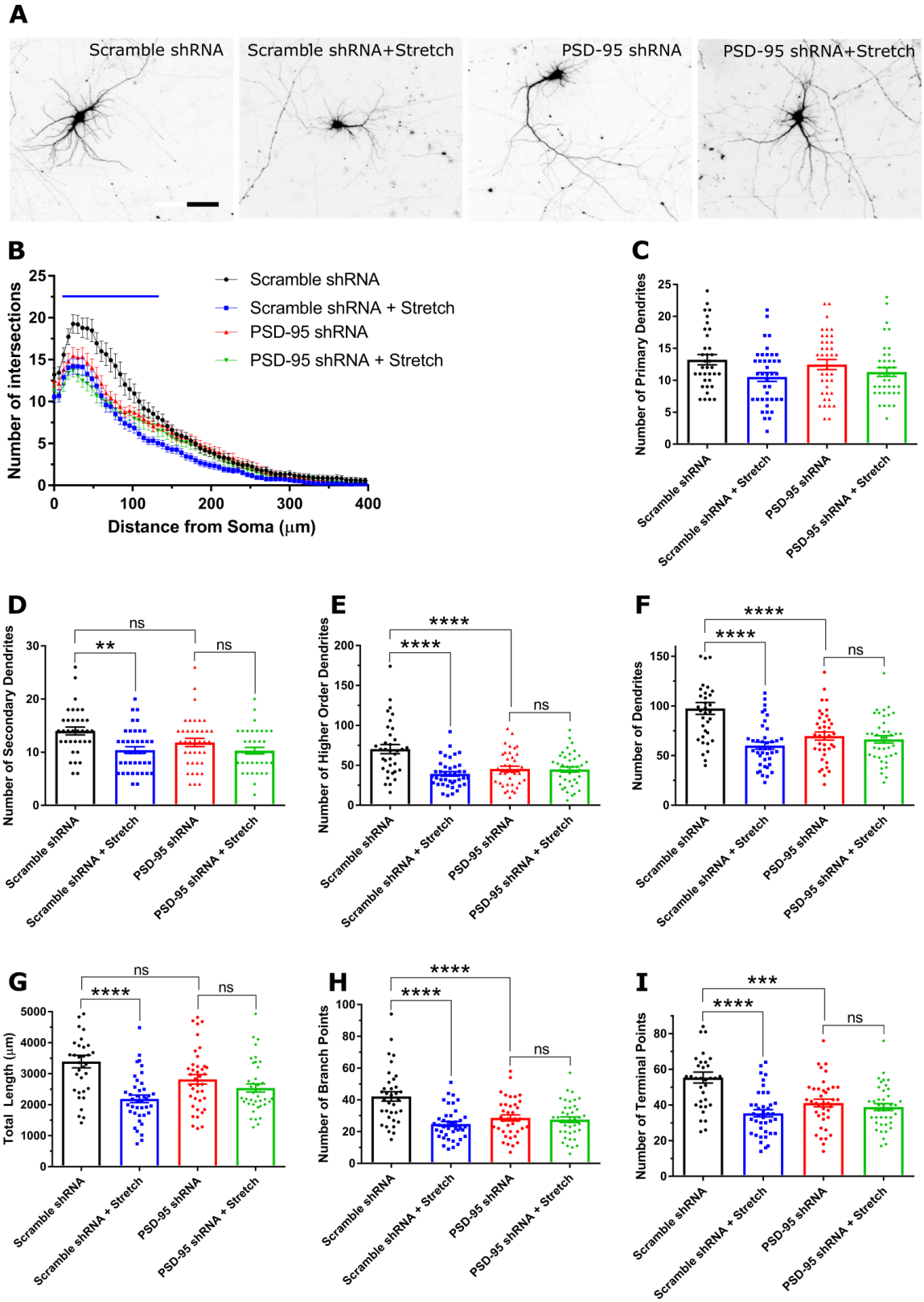
A
Scramble shRNA
Scramble shRNA+Stretch
PSD-95 shRNA
PSD-95 shRNA+Stretch
B
Number of intersections
Distance from Soma (μm)
Scramble shRNA
Scramble shRNA + Stretch
PSD-95 shRNA
PSD-95 shRNA + Stretch
C
Number of Primary Dendrites
D
Number of Secondary Dendrites
E
Number of Higher Order Dendrites
F
Number of Dendrites
G
Total Length (μm)
H
Number of Branch Points
I
Number of Terminal Points
ns
**
****
***

**Fig. 3.6. PSD-95 knockdown prevents stretch injury-mediated decreases in dendrite branching. (A)** Representative images of neurons expressing mRFP and transduced with virus encoding scramble or PSD-95 shRNA. Shown is the mRFP channel for single neuron dendrite analysis. **(B)** Sholl analysis of transfected neurons. Blue line indicates *$p<0.05$ for control versus stretch injury for neurons transduced with virus for scrambled shRNA at distances 18 µm – 132 µm away from soma as determined by two-way ANOVA followed by Tukey's multiple comparisons test. **(C)** Neither stretch injury nor PSD-95 knockdown decrease primary dendrites. **(D)** PSD-95 knockdown prevents stretch-mediated decreases in secondary dendrite number. **(E)** PSD-95 knockdown decreases higher order dendrites, and stretch does not cause a further decrease. **(F)** PSD-95 knockdown decreases total dendrite number, and stretch does not cause a further decrease. **(G)** PSD-95 knockdown prevents stretch-mediated decreases in total dendrite length. **(H)** PSD-95 knockdown decreases number of dendrite branch points, and stretch does not cause a further decrease. **(I)** PSD-95 knockdown decreases number of dendrite terminal points, and stretch does not cause a further decrease. **$p<0.01$, ***$p<0.001$, and ****$p<0.0001$ as determined by one-way ANOVA followed by Tukey's multiple comparisons test. n=35-41 neurons. Error bars = S.E.M. Scale bar =100 µm.

## 3.4 Discussion

In this study, we assessed how changes to PSD-95 and interaction with binding partners change after injury using both *in* vitro and *in vivo* models of TBI. Our *in vitro* data suggest that 1 hour after primary injury induced by mechanical stretch, interaction of PSD-95 with its binding partner EB3 increases with no change in the total levels of these proteins. These results are consistent with those seen after moderate CCI. Furthermore, our *in vivo* data suggest that mild and moderate injury induce distinct pathways. At 2 hours post-mild injury, EB3 levels increase but its interaction with PSD-95 decreases. In contrast, total levels of PSD-95 and its interaction with EB3 increase at 1 and 7 days post-moderate CCI and that of APC increases at 1 day. We also report that knockdown of PSD-95 does not promote neuronal survival but prevents changes to dendrites after stretch-induced injury *in vitro*. Taken together, our data suggest a role for PSD-95 and binding partners post-injury.

How the interaction between PSD-95 and its binding partners may regulate the dendritic arbor after injury can been gleaned from past work from our group and that of others. We previously reported that PSD-95 binds to EB3 and sequesters EB3 from the +*TIPs* of microtubules, altering microtubule polarity, thus resulting in decreased dendrite branching.[28, 31] This suggests that early after mild injury, when higher levels of EB3 remain unbound to PSD-95, remodeling of dendrites can occur. In contrast, moderate injury promotes mechanisms that reduce dendrite branching and remodeling as EB3 is sequestered from microtubules. Furthermore, there are reports that binding of PSD-95 to APC enhances microtubule bundling in COS-7 cells,[34] and this microtubule bundling

with PSD-95 overexpression correlates with decreased dendrites.[28] Thus, the transient increase in the interaction between APC and PSD-95 at 1 day post-moderate injury is also consistent with mechanisms that reduce dendrite branching and remodeling. Collectively, moderate, but not mild, injury induces mechanisms that are detrimental to dendrite regrowth after injury. A model depicting these mechanisms is presented in **Fig. 3.7**.

**A**

| Injury | Total Levels | | | PSD-95 Interaction | |
|---|---|---|---|---|---|
| | PSD-95 | APC | EB3 | APC | EB3 |
| 1 hr post-Stretch Injury | - | - | - | - | ↑ |
| 2 hr post-CCI (Mild) | - | - | ↑ | - | ↓ |
| 1 day post-CCI (Moderate) | ↑ | - | - | ↑ | ↑ |
| 7 days post-CCI (Moderate) | ↑ | - | - | - | ↑ |
| 14 days post-CCI (Moderate) | - | - | - | - | - |

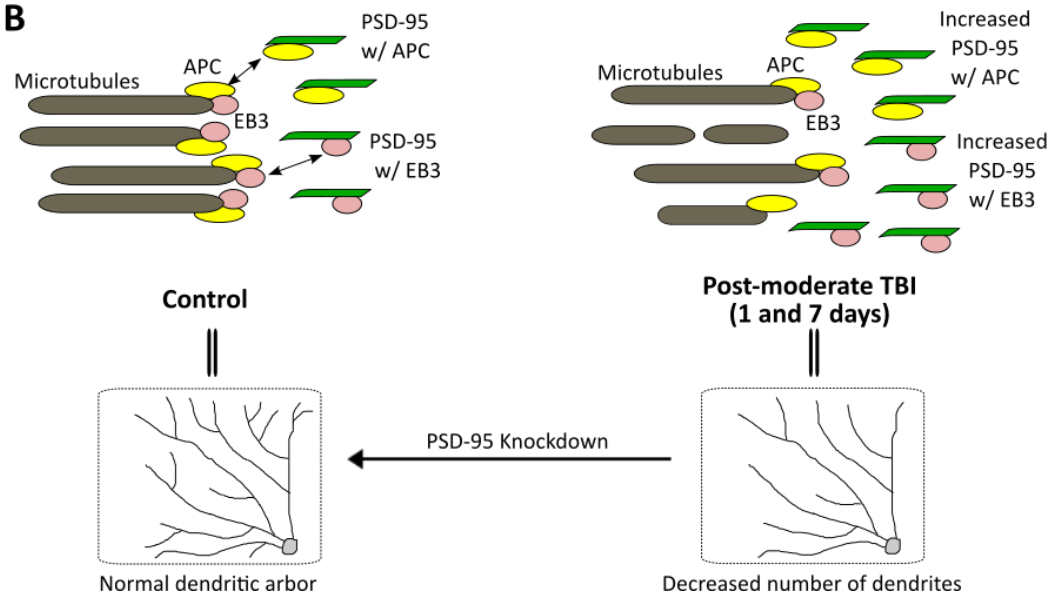


**Fig. 3.7. Model of role of PSD-95 and interactors post-moderate CCI. (A)** Summary of findings. **(B)** Model showing increases in PSD-95 and interaction with APC and EB3 post-moderate CCI. Increased PSD-95 level results in decreased dendrite number, and

increased PSD-95 interaction with APC and EB3 decreases APC and EB3 binding to *+TIPs*. This results in decreased dendrite dynamics and increased microtubule bundling, leading to decreased dendrite number. Knockdown of PSD-95 prevents changes to dendrites after stretch-induced injury by increasing free EB3 and APC, allowing them to bind to *+TIPs* of microtubules.

We observed high variability in co-immunoprecipitation with PSD-95 after moderate injury (**Fig. 3.4**). This may be due to the fact that both APC[33] and EB3[28] bind to PSD-95 and that APC and EB3 also directly bind to each other.[115] Thus, co-immunoprecipitates of PSD-95 include the combination of the direct APC-PSD-95 and the indirect APC-EB3-PSD-95 interaction, each of which may be altered distinctly after injury.

Our data are in contrast to those presented in previous studies showing reduction of PSD-95 expression in the hippocampus[55-58] and the cortex[58] 1-7 days after CCI. The differences in data may be due to a number of parameters. First, our study includes cortical tissue whereas the majority of previous reports studied the hippocampus. Second, we examined tissue after mild or moderate CCI while the previous studies used a severe CCI model.[58] This difference in models is important as differential effects of mild and moderate CCI on post-injury protein levels are observed here (**Fig. 3.3**) and in published work.[117, 118] Furthermore, different models, including rats[55, 57] and mice,[56, 58] were used in studies.

We have previously reported that knockdown of PSD-95 is neuroprotective against NMDA-induced excitotoxicity (secondary injury).[43] However, here we report that PSD-

95 knockdown does not prevent mechanical stretch-induced injury (primary injury)-mediated neuronal death. These data suggest distinct mechanisms for primary versus secondary injury. Although both types of injury are mediated by the NMDA receptor, mechanotransduction, which occurs during primary injury, is mediated by NR1/NR2B NMDA receptors[119, 120] while overstimulation of multiple subunit-containing NMDA receptors can mediate neuronal death.[121, 122] Similarly, we reported that knockdown of PSD-95 increases the number of secondary dendrites in immature neurons.[28] Here, we do not report an increase in proximal dendrites when PSD-95 is knocked down. This may be due to the fact that in our previous study[28], PSD-95 was knocked down and dendrites were assessed during the active branching period (by DIV 12) while in the current study, we knocked down and assessed dendrite numbers after the dendritic arbors had stabilized (DIV 17). Here, knockdown of PSD-95 decreased the number of higher order dendrites, total dendrite number, number of branch points, and terminal points. This is consistent with our previous report that PSD-95 knockdown results in decreased total dendrites and lengths due to a limiting reagent in the neuron.[28] Taken together, our published and current results suggest distinct roles of PSD-95 at different developmental time points, i.e. when active dendritic branching occurs and when the arbor is stabilized, having implications for restoration of dendrites after injury.

Our study shows for the first time that stretch injury decreases dendritic arborization of surviving cortical neurons. Because TBI leads to acute dendritic degeneration,[49, 58] stretch-induced injury can be used as an *in vitro* TBI model to study the effect of trauma on dendrite branching. Our PSD-95 knock down studies show that PSD-95 is required for the stretch injury-mediated insult to the dendritic arborization and that knocking down

PSD-95 is a therapeutic strategy for restoration of neural circuitry after TBI. However, since PSD-95 is an essential mediator of spinogenesis,[123] the timing of PSD-95 knockdown after injury is crucial for restoration of the dendritic arbor and allowance of spine reemergence and synapse stability.

## 3.5 Methods and Materials

All animal experiments were carried out in accordance with the National Institutes of Health guide for the care and use of Laboratory animals (NIH Publication No. 8023, revised 1978).

### *3.5.1 Neuronal culture*

Hippocampal and cortical neuronal cultures were prepared from rat embryos at 18-19 days gestation as we have previously described.[28, 30, 31, 95, 124-126] Neurons were cultured in Neurobasal medium supplemented with B27 and GlutaMax (ThermoFisher Scientific). Hippocampal neurons plated on glass coverslips coated with poly-D-Lysine (PDL; 0.1mg/ml, Sigma) were used to study the role of PDZ domains of PSD-95 in the regulation of dendrite branching. Cortical neurons were plated at a density of 105 cells/cm$^2$ on stretchable elastomeric silicon membranes (SMI Inc.; Gloss 0.01" thick, 40 Durometer) that were coated overnight PDL (0.1mg/ml, Sigma) and laminin (0.002mg/ml, Sigma) in a 37°C incubator with 5 % $CO_2$ for stretch-mediated injury

experiments. Silastic membranes were pre-stretched to 142.8% of their original width.[127-129]

*3.5.2 Brain slices*

In brief, adult male mouse brains (C57BL/6J; #000664; 23-29g; Jackson Laboratory) were carefully removed and placed into ice-cold, Gey's Balanced Salt Solution (GBSS; G9779; Sigma) supplemented with 4 mg/ml Dextrose. Coronal slices (400 μm) from each hemisphere were prepared using the McIlwain Tissue Chopper (10180; Ted Pella, Inc.) and transferred to a recovery chamber containing GBSS (27.8 mM Dextrose) for >30 min at room temperature. These slices either contained cortex alone or cortex and hippocampus. Results for both types of slices were identical, and data were pooled.

*3.5.3 Mechanical Stretch Injury*

Cultured cortical neurons grown on flexible membranes were placed into a sealed stretch injury chamber.[127-129] Pressurized air was applied at 20 psi (consistent output pressure of 12 psi) for 50 ms. The membrane in the injured region was stretched uniaxially, where the width was extended to 60% beyond the initial width before returning to the original dimensions. Naive non-stretched neurons were used as uninjured controls. Brain slices were placed onto silastic membranes in full Neurobasal medium, and membrane wells were placed into the stretch injury chamber and injured as described above. Immediately after stretch, slices were incubated in a 37°C, 5% $CO_2$ chamber for 1 hour followed by tissue lysate preparation.

*3.5.4 Controlled Cortical Impact*

Animals were injured using the controlled cortical impact model.[130, 131] Adult male mice (C57BL/6J; #000664; 23-29g; Jackson Laboratory) were anesthetized with isoflurane (5% induction, 1-2% maintenance) and placed into a stereotactic frame. A 1.0 cm midline rostral-to-caudal incision was made, and a craniotomy was performed over the left parietotemporal cortex midway between bregma and lambda sutures 2.5 mm lateral to the sagittal suture. The dura was kept intact. One hour after induction of anesthesia, a spherical 2 mm diameter indentor tip was brought slowly down until it contacted the cortical brain surface and retracted into a pull-type solenoid. The indentation depth (1 mm) was adjusted using a micrometer, and the solenoid was energized to deliver an impact at the desired velocity (mild: 0.4-0.5 m/s; moderate: 2.4-5.0 m/s). Sham injury included craniotomy only.

*3.5.5 Western Blot Analysis*

Western blot analysis was performed as previously described.[54] Rat brain, cortical tissue or cultured cortical neurons were homogenized in RIPA buffer (50 mM Tris-HCl, pH 7.4, 150 mM NaCl, 0.5% deoxycholate, 1% NP-40, 0.1% SDS, 1 mM EDTA, pH 7.4). Protein concentrations were determined using the Pierce BCA protein assay kit (Thermo Scientific) following the manufacturer's protocol. Proteins (15 μg) were resolved on a 10% SDS-polyacrylamide gel and transferred to PVDF membrane. The membrane was blocked with 5% bovine serum albumin (BSA) in TBST (20 mM Tris pH 7.5, 150 mM

NaCl, 0.1% Tween-20) for 1 hour. The blot was probed with indicated antibodies in TBST containing 3% BSA: mouse anti-PSD-95 (1:1000; K28/43, UC Davis/NIH NeuroMab Facility), rabbit anti-APC (1:250; SC-20, Santa Cruz Biotech.; 1:100; Ab15270, Abcam), mouse anti-GAPDH (1:1000; MAB374, Millipore), and rabbit anti-EB3 (BF4 as described in [31]). Blots were scanned, and the intensities of bands were quantified using ImageJ software (NIH). The number of pixels of absolute intensity of bands was normalized to the intensity of those for GAPDH (internal control) and was compared to that of the control condition.

*3.5.6 Co-immunoprecipitation*

For co-immunoprecipitation (co-IP) experiments, total protein extract from 0.9 mg of slice or cortical tissue was used for each IP. Mouse anti-PSD-95 (K28/43, UC Davis/NIH NeuroMab Facility) or normal mouse IgG (5 µg) was added to the extracts, and the extracts were incubated overnight at 4°C. Protein A Sepharose beads (30 µl; GE Healthcare) were added, and the extracts were incubated for 1 hour at 4°C. Beads were washed three times with TEE buffer (20 mM Tris-HCl, pH 7.4, 1mM EDTA, 1 mM EGTA, pH 7.4), and immunoprecipitated proteins were eluted into 25µl 2x SDS-PAGE sample buffer (0.02 M Tris-HCl, pH 6.8, 40% glycerol, 20% β-mercaptoethanol, 4.6% SDS, 0.01% bromophenol blue) and boiled for 5 min followed by centrifugation. The supernatant, containing immunoprecipitated proteins, and the initial extract (load) were resolved and Western blot performed as described above in the section for *Western Blot Analysis*. The band intensities of immunoprecipitated PSD-95 and co-immunoprecipitated APC and EB3 were normalized to their respective band intensities in the load. The ratio of normalized intensities of PSD-95 and APC or EB3 from CCI or

stretch-mediated injury was compared to that of sham control. Band intensities of all three proteins were normalized to those of GAPDH and compared to those of sham control. Statistical differences ($p<0.5$) were evaluated by ANOVA followed by Tukey's multiple comparisons test using GraphPad Prism7 software. For immunoprecipitation of APC, 1mg of whole rat brain lysate was used to pulldown APC (C-20, Santa Cruz Biotech.) followed by Western Blot analysis and probing for APC and PSD-95 as discussed previously.

*3.5.7 shRNA and Lentivirus Production*

Lentivirus was produced as previously described.[54, 94] Scramble (Target sequence - CCTAAGGTTAAGTCGCCCTCG; VB170329-1128paq; VectorBuilder) and PSD-95 shRNA (Target sequence in ORF - ACGATCATCGCTCAGTATAAA; VB170328-1088ner; VectorBuilder) lentivirus were used in this study. In brief, on day 1, HEK293T cells were plated at a density of $6.5 \times 10^6$ cells/T75 flask. On day 2, cells were transfected with lentiviral plasmid and PAX2 and VSV packaging vectors using Lipofectamine 2000 reagent (Invitrogen) following the manufacturer's protocol. On day 5, supernatant was collected and centrifuged at 1500x*g* for 5 min to remove dead cells and debris. The supernatant was transferred into a new tube containing 5x PEG-it virus precipitation solution (System Biosciences; 1:4 dilution), followed by incubation at 4°C for 2 days to concentrate the virus. On day 7, the mixture was centrifuged at 1500x*g* for 30 min at 4°C to pellet the virus. The supernatant was carefully removed, and the pellet was resuspended in 150–200µl sterile phosphate-buffered saline (PBS) and aliquoted into 10µl fractions, which were stored at − 80°C until further use.

*3.5.8 Neuronal Survival Assay*

Neurons were transduced on DIV 11 with scramble or PSD-95 shRNA lentivirus. Neurons were mechanically injured on DIV 14, followed by fixation on DIV 17 with 4% paraformaldehyde (PFA) in phosphate-buffered saline and immunostaining with mouse anti-MAP2 (1:250; BD PharMingen). MAP2-positive neurons were counted to determine neuronal viability. Ten random regions observed under 10x objective were selected and imaged, and the average number of MAP2-positive neurons was counted for each condition.

*3.5.9 Sholl Analysis*

Hippocampal neurons were co-transfected with mRFP and cDNA encoding GFP or GFP-tagged PSD-95, PSD-95ΔPDZ1, PSD-95ΔPDZ2 or PSD-95ΔPDZ3 on DIV 7 to analyze on DIV 12 to study the role of PDZ regions of PSD-95 on dendrite branching.

To study the effect of stretch injury on dendrite branching, cultured cortical neurons were transfected with pGW1-mRFP on DIV 7 using Lipofectamine LTX+PLUS reagent (Invitrogen) following the manufacturer's protocol. Neurons were then transduced on DIV 11 with scramble or PSD-95 shRNA lentivirus. Neurons were mechanically injured on DIV 14 and fixed on DIV 17 with PFA. Cells were then immunostained with chicken anti-GFP (1:250; ThermoFisher) and mouse anti-MAP2 (1:250; BD PharMingen). Immunostaining was visualized with Alexa Fluor 488 and 647 conjugated secondary

antibodies (ThermoFisher Sci.). Imaging was performed using an EVOS-FL fluorescence imaging system (ThermoFisher Sci.). All images were analyzed using ImageJ software (NIH) and MATLAB (MathWorks). Sholl analysis was performed using the Bonfire program developed by the Firestein laboratory.[63, 132] In brief, concentric circles were drawn around the soma at every 6 μm, and intersections with MAP-2-positive dendrite branches were counted. All data were exported from MATLAB to Excel for quantification. Statistical differences ($p<0.5$) were determined by two-way ANOVA followed by Tukey's multiple comparisons test using GraphPad Prism7 software. The experimenter was blinded to conditions during all Sholl and data analyses.

## 3.6 Acknowledgements

This work was funded by the New Jersey Commission on Brain Injury Research grant # CBIR14IRG019 (to B.L.F. and D.F.M.). M.P. was supported in part by a Predoctoral Fellowship from the New Jersey Commission on Brain Injury Research # CBIR15FEL009.

**Author contributions**

M.V.P., E.S., S.D., and H.K. carried out the experimental work. M.V.P., D.F.M., and B.L.F. analyzed the data and wrote the manuscript. All authors were involved in planning the experiments.

# Chapter 4: To elucidate a role for cypin in dendritogenesis and neurobehavior *in vivo.*

## 4.1 Introduction

As discussed in Chapter 1.3.3 & Chapter 2, products of the *GDA* gene, cypin and cypinS, are involved in the regulation of neuronal morphology. We generated knockout (KO) mice to further investigate the detailed *in vivo* role of cypin. KO-first strategy provides high flexibility for gene manipulation by combining FLP/FRT and Cre/loxP systems.

Here, we show that cypin KO-first mice retain 15-20% of total cypin expression and are hypomorphic. Although hypomorphic Gda mice do not show changes in behavior and levels of synaptic proteins, dendritic arborization is decreased in neurons cultured from hypomorphic embryos. In addition, hypomorphic females show decreased motor function and increased learning compared to wildtype females. Due to the fact that the low expression of cypin may fulfill essential roles for cypin in brain tissue, conditional KO mice will be used in the future to further study the function of the *GDA* gene in the brain.

## 4.2 Results

### *4.2.1 Generation of Cypin KO-first mice*

The *GDA* gene consists of 14 exons. ES cell clone (EPD0770_5_B01; EUCOMM) containing Gda tm1a KO-first allele (**Fig. 4.1A**) was purchased from KOMP and used to generate a chimera. The chimera was crossed with B6J mice expressing FRT recombinase driven by the β-actin promoter to remove the FRT-lacZ-neo-FRT cassette, restoring gene activity, to produce a tm1c or loxP allele. The resultant female progeny (carrying tm1c or loxP allele) were mated with CamKIIα-Cre males (R1ag#5; with B6J background)[133] to generate brain-specific KO mice by excision of exon 4, resulting in a frameshift mutation that causes nonsense decay of the transcript. (**Fig. 4.1A, Fig. 4.2**) Nomenclature of mice line is shown in **Fig. 4.1A,B**. For genotyping, the strategy of primer selection and expected size of the PCR products are shown in **Fig. 4.3A-C.**

A

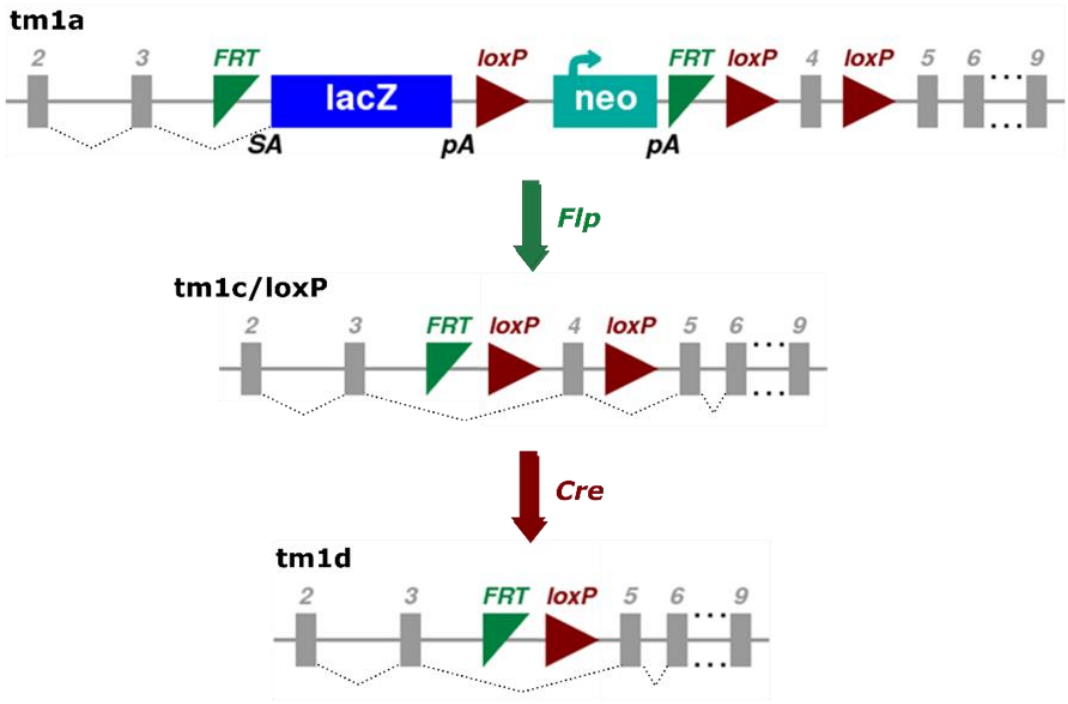


B

| Mice | Heterozygous | Homozygous |
|---|---|---|
| WT | - | $Gda^{+/+}$ |
| KO-first | $Gda^{tm1a/+}$ | $Gda^{tm1a/tm1a}$ |
| Post FLP | $Gda^{loxP/+}$ | $Gda^{loxP/loxP}$ |
| Post Cre | $Gda^{-/+}$ | $Gda^{-/-}$ |

**Fig. 4.1. Schematic diagram of the targeting strategy for the *GDA* (cypin) gene. (A)** The *GDA* gene consists of 14 exons. ES cell clone (EPD0770_5_B01; EUCOMM) containing tm1a KO-first allele was used to generate chimeras. After removing FRT-lacZ-neo-FRT cassette the KO-first mice were crossed with B6J mice expressing FRT recombinase, and the resultant female progeny (carrying tm1c or loxP allele) can be mated with specific cre-mice lines to generate tissue-specific KO mice via excision of exon 4. **(B)** Nomenclature and genotypes of mice. **tm1a**: KO-first allele (reporter-tagged insertion allele); **tm1c**: Conditional allele (post-Flp; loxP); **tm1d**: Deletion allele (post-

Flp and Cre with no reporter). tm= targeted mutation, #=for serial number, a= knockout-first allele, c=allele suitable for conditional mutagenesis, d= deletion of critical exon (exon4).

Image modified from KOMP:

http://www.mousephenotype.org/data/alleles/MGI:95678/tm1a(KOMP)Wtsi

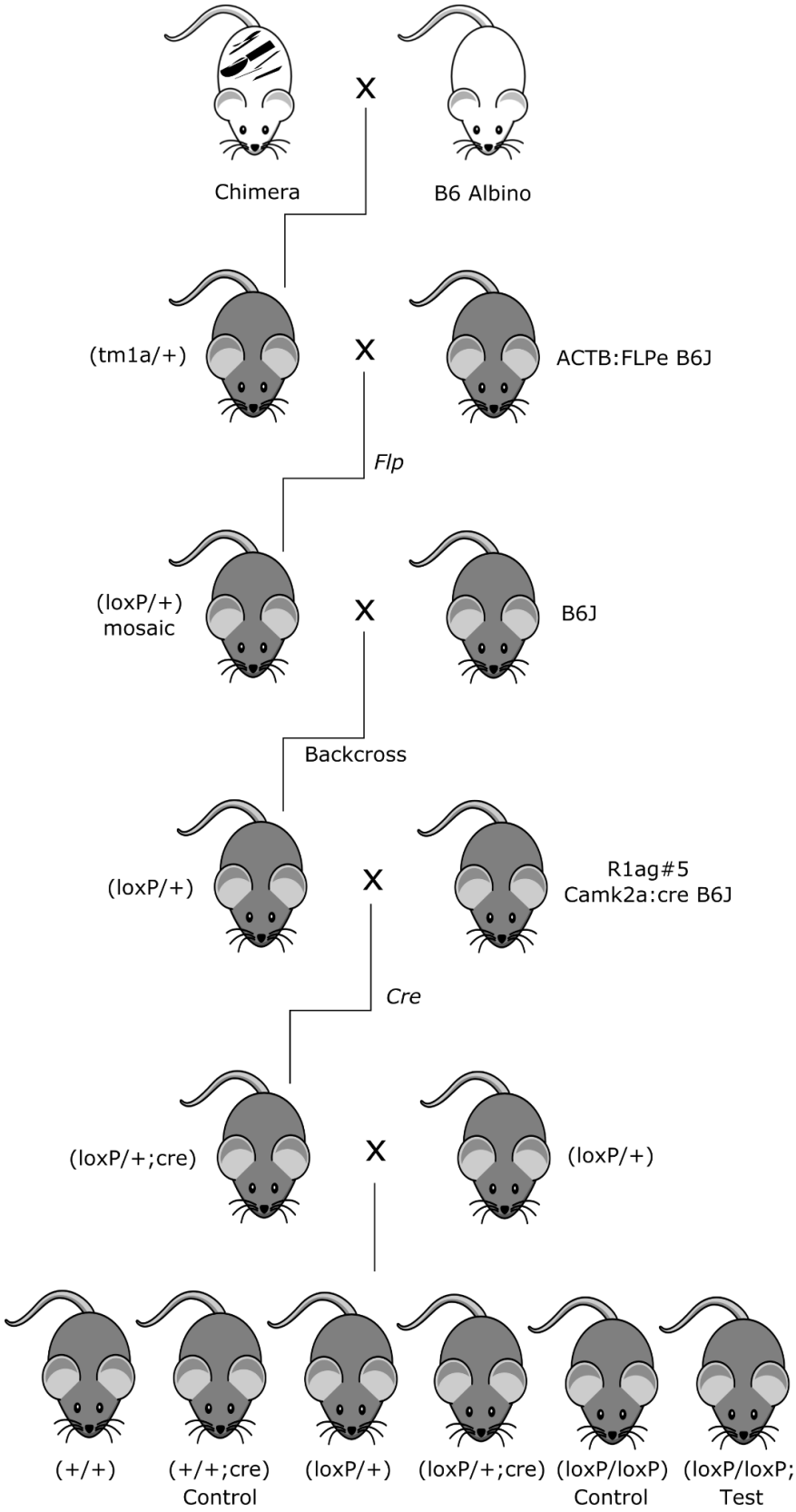
Chimera
X
B6 Albino
(tm1a/+)
X
ACTB:FLPe B6J
Flp
(loxP/+)
mosaic
X
B6J
Backcross
(loxP/+)
X
R1ag#5
Camk2a:cre B6J
Cre
(loxP/+;cre)
X
(loxP/+)
(+/+)
(+/+;cre)
Control
(loxP/+)
(loxP/+;cre)
(loxP/loxP)
Control
(loxP/loxP;cre)
Test

**Fig. 4.2. Breeding scheme for the generation of conditional Gda KO mice.** Embryonic stem cells (ESC) carrying black coat color were used to generate a chimera. Chimeric mice were back-crossed with B6 Albino mice to generate offspring carrying the KO-first allele tm1a, and these offspring were identified by their black coat color. $Gda^{tm1a/+}$ mice were crossed with B6J mice expressing flipase (*Flp*) under the β-actin promoter to generate $Gda^{loxp/+}$ mice. The expression of the *Flp* transgene is mosaic, and resultant mice ($Gda^{loxP/+}$) were back-crossed with B6J wildtype (WT) mice to remove the mosaicism. $Gda^{loxp/+}$ mice can be crossed with $Gda^{loxp/+;Cre}$ mice carrying brain-specific Cre expression[133] to generate brain-specific Gda KO mice.

**A**

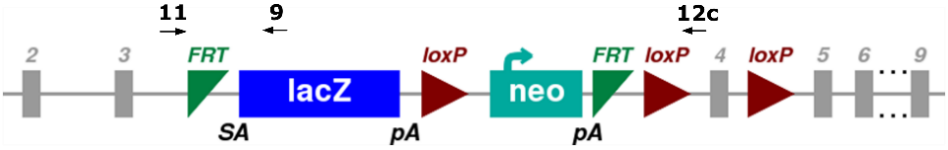


primer en2-Rev (referred to as 9) CCAACTGACCTTGGGCAAGAACAT
primer 3'arm (referred to as 12c) GCCAGTTCTTTGGGATTGCG
primer 5' (referred to as 11) GAACTCCGGAGGGAGCGAAC
Cre-F: CTGCCACGACCAAGTGACAGC
Cre-R: CTTCTCTACACCTGCGGTGCT

**B**

Size of PCR product expected:

| **Primers pair** | **WT (+)** | **tm1a** | **tm1c (loxP)** | **Cre** |
|---|---|---|---|---|
| 11 + 12c | 599bp | - | 811bp | - |
| 11 + 9 | - | 435bp | - | - |
| Cre F + Cre R | - | - | - | 325bp |

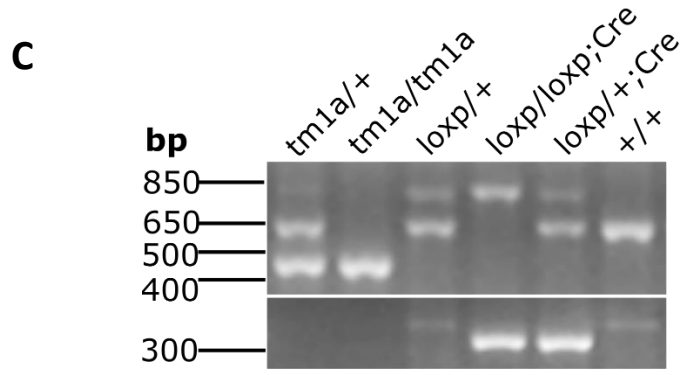


**Fig. 4.3. Primer design and genotyping strategy for Gda transgenic lines. (A)** Primer design and sequence to check the presence of WT, tm1a, or loxP (tm1c) alleles. **(B)** Expected size of PCR products using primer pairs 11 and 12c or 11 and 9. **(C)** Representative gel image showing DNA bands from PCR products generated from tail lysate of transgenic mice carrying different genotypes.

Since our Gda KO-first ($Gda^{tm1a/tm1a}$) transgenic line expresses 15-20% of wildtype cypin (**Fig. 4.4**), it is a hypomorph. We used this line to study the effect of decreased cypin expression (**Fig. 4.2**). Future studies will focus on tissue-specific KO of Gda.

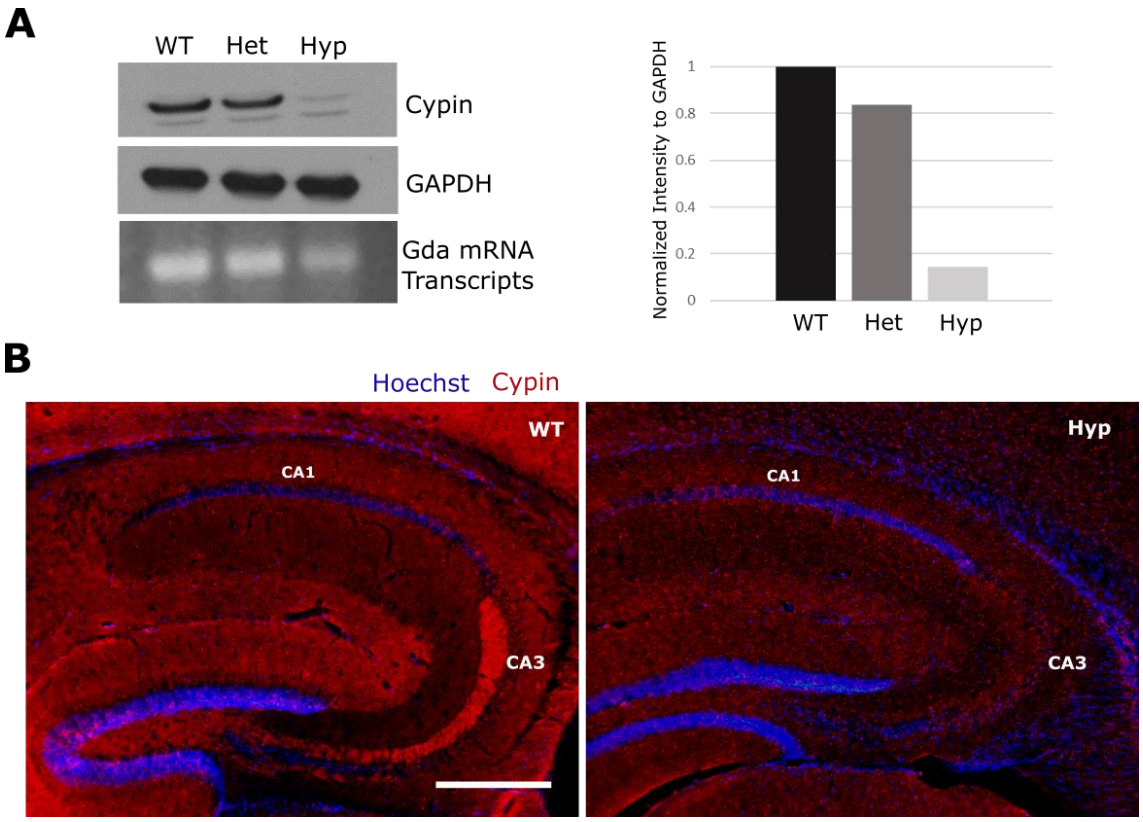


**Fig. 4.4. Cypin expression in the Gda hypomorphic mouse. (A) Representative** Western blot and quantitation showing cypin expression in WT, heterozygous (Het) and hypomorphic (Hypo) mice. **(B)** Immunohistostaining of brain sections from WT and Hypo mice. Hoechst and cypin immunostaining are shown in blue and red, respectively. WT brain There is high expression of cypin in the CA3 region of hippocampus of WT mice while there is low expression of cypin in CA3 region of Hypo mice. Scalebar=400µm.

*4.2.2 Decreased dendritic arborization occurs in neurons cultured from Gda hypomorphic (Gda$^{tm1a/tm1a}$) mice*

To study the effect of decreased cypin expression on dendritic arborization, hippocampal neurons were cultured from E16 embryos from timed-pregnant heterozygous female mice (Gda$^{tm1a/+}$) mated with heterozygous male mice (Gda$^{tm1a/+}$). As shown in **Fig. 4.5**, neurons cultured from hypomorphic (tm1a/tm1a) mice have significantly decreased dendritic arborization compared to neurons cultured from WT mice. These data complement our previously published *in vitro* data supporting a role for cypin in the regulation of dendrite arborization.

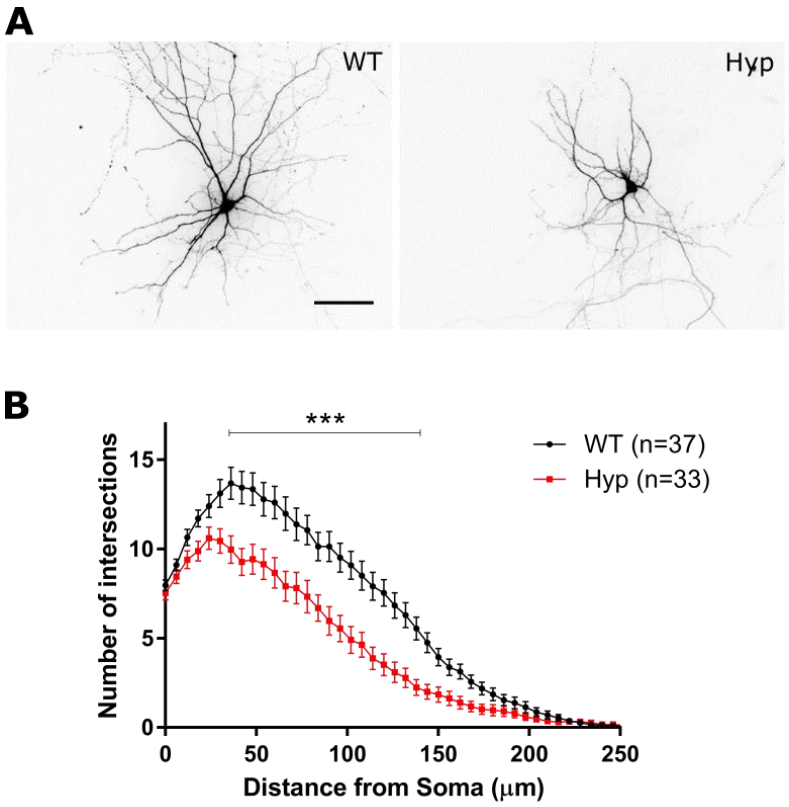

**Fig. 4.5. Decreased dendritic arborization in hippocampal neurons cultured from hypomorph ($Gda^{tm1a/tm1a}$) mice. (A)** Representative images of neurons cultured from E16 embryos resulting from mating between female (tm1a/+) and male mice (tm1a/+) to produce all genotypes in littermates. Neurons were transfected at DIV 7 with cDNA encoding mRFP to identify dendrites for analysis. **(B)** Sholl analysis of neurons at DIV12. Neurons cultured from hypomorphic mice show decreased dendritic arborization. n=33 for WT and n=37 for hypomorph, from three independent experiments. ***$p<0.001$ determined by two-way ANOVA followed by Sidak's multiple comparisons test. Scalebar=50µm.

*4.2.3 Behavioral screening of Cypin KO-first mice*

We performed behavioral screening of cypin hypomorphic mice (**Fig. 4.6, 4.7**). Since cypin regulates dendrite morphology and is involved in maternal autoantibody-related autism (MAR),[39] we screened hypomorphic mice using neurobehavioral tests generally employed to detect autistic phenotypes. There was no change in self-grooming (repetitive behavior) observed (**Fig. 4.6D**). There is a relationship between anxiety and autism; [134] thus, anxiety was measured by open-field task (for 15 min) and marble burying task. There was no significant difference in anxiety levels between genotypes (**Fig. 4.6E,F**). Female hypomorphic mice showed decreased motor function as determined by rotarod test (**Fig. 4.6C**). In contrast, no change in motor function was observed in males. As some autistic patients show deficits in learning and memory,[135] we also tested cypin

hypomorphic mice using the Morris Water Maze (MWM) learning and memory task. Female hypomorphic mice showed increased learning (**Fig. 4.7C**); however, there was no change in memory (probe trial, **Fig. 4.7D**) and reversal memory (reverse probe trial, **Fig. 4.7E**). Importantly, there was no difference in visibility between genotypes (**Figure 4.7F**). In summary, female hypomorphic mice showed faster learning and decreased motor function. These data suggest a role for cypin in learning and balance.

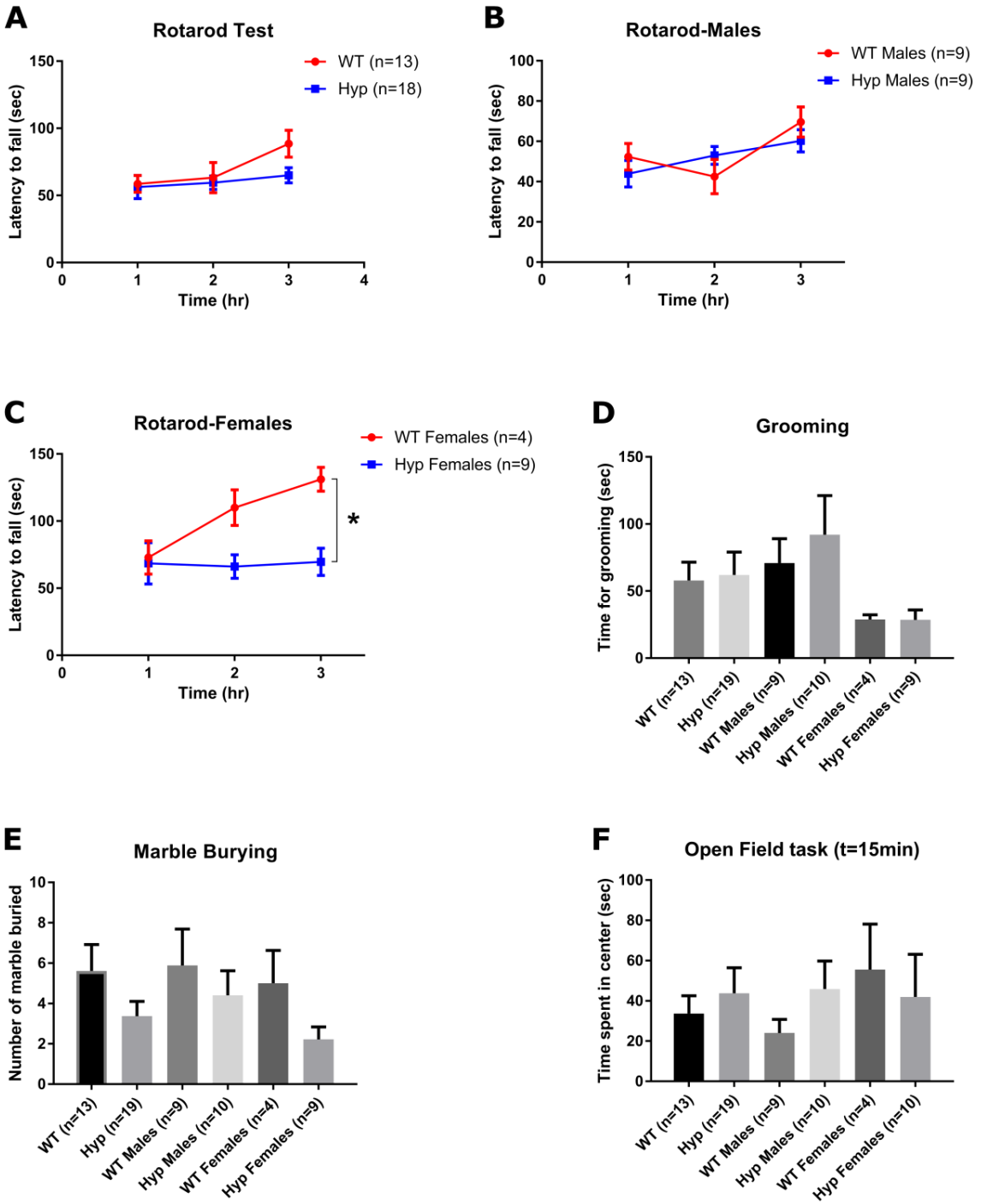


**Fig. 4.6. Female cypin hypomorphic mice have lower time to fall than do WT mice.** **(A**, **B**, **C)** Rotorod test was performed for three consecutive hours to measure motor function. There was a significant effect of genotype on latency to fall, and hypomorphic

female mice showed a decrease in latency to fall. *p<0.05 determined by repeated measures ANOVA. **(D)** Grooming on face, head, or body was measured manually for 10 min. No significant effect of genotype was observed. **(E, F)** Marble burying and open field tasks were performed to measure anxiety levels. Higher number of buried marbles and lower time spent in center (OFT) represents higher levels of anxiety. No significant changes in anxiety measures were observed.

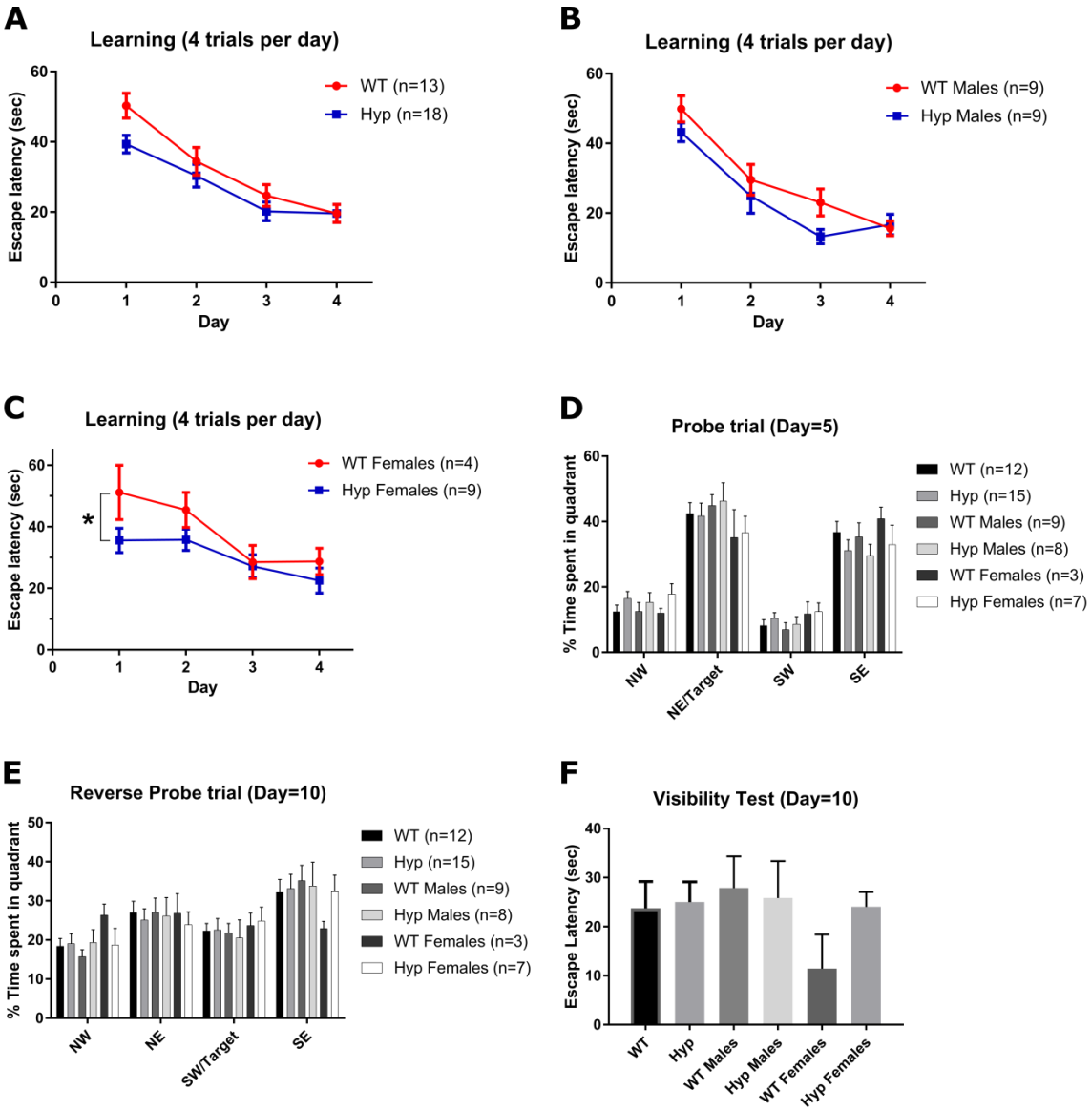

**Fig. 4.7. Female cypin hypomorphic mice show increased learning in the Morris Water Maze (MWM) test. (A)** Escape latency for Morris Water Maze (MWM) learning for four consecutive days. No significant difference was observed between cypin hypomorphic and WT mice. p=0.0738 for genotype determined by repeated measures ANOVA. **(B)** MWM learning curve for males only. No significant effect of genotype was observed. **(C)** MWM learning curve for females only; *p<0.05 for genotype determined by repeated measures ANOVA. **(D)** MWM probe trial on day 5. No significant effect of genotype on time spent in target quadrant was observed. **(E)** Reverse learning was performed on day 9, followed by a probe trial 24hr post-learning. No significant effect of genotype was observed in reverse learning. **(F)** Motor function and visibility were assessed by swimming speed in the visibility test in which a visible flag was attached to the platform. Swim speed: WT (sexes combined)= 17.20 ± 0.87 cm/s; hypomorph (sexes combined)= 17.52 ± 0.97 cm/s; WT (males) = 16.64 ± 0.91 cm/s; Hypomorph (males) = 16.67 ± 1.44 cm/s: WT (females) = 18.89 ± 2.16 cm/s; Hypomorph (females) = 18.71 ± 1.49 cm/s. No significant effect of genotype was observed. All data are shown as mean ± SEM.

*4.2.4 No change in trafficking of PSD-95 family proteins (MAGUKs) to the PSD (postsynaptic density) in male cypin hypomorphic mice*

Cypin is involved in the regulation of synaptic trafficking of PSD-95 family proteins.[29] As shown above, female hypomorphic mice show increased learning. To analyze changes

in the levels of MAGUKs at postsynaptic sites, synaptoneurosomes were prepared from male mice from both genotypes to isolate the postsynaptic density and synaptic cytosol.[93] Proteins were separated by SDS-PAGE, analyzed by Western blotting, and quantitated using ImageJ (NIH). The intensities of protein bands were normalized to that of GAPDH or synaptophysin (internal controls). There was no significant change in total levels or trafficking of any of the proteins studied (**Fig. 6.8**). As we did not observe changes to learning and memory in male hypomorphic mice, these data are consistent with our neurobehavioral data. Interestingly, we did observe a significant increase in the α-amino-3-hydroxy-5-methyl-4-isoxazolepropionic acid (AMPA) glutamate receptor subunit GluR2 (full length) in the synaptic cytosol but not at the synapse (**Fig. 6.8A,B**). Unfortunately, our mating did not yield enough female mice to perform these experiments, and thus, these studies are included in future experiments. Moreover, in hypomorphic male mice, the cypin-Short isoform is expressed at levels similar to those observed in WT mice, suggesting that this isoform may compensate for some of the lost functions of cypin, although this isoform lacks guanine deaminase activity.

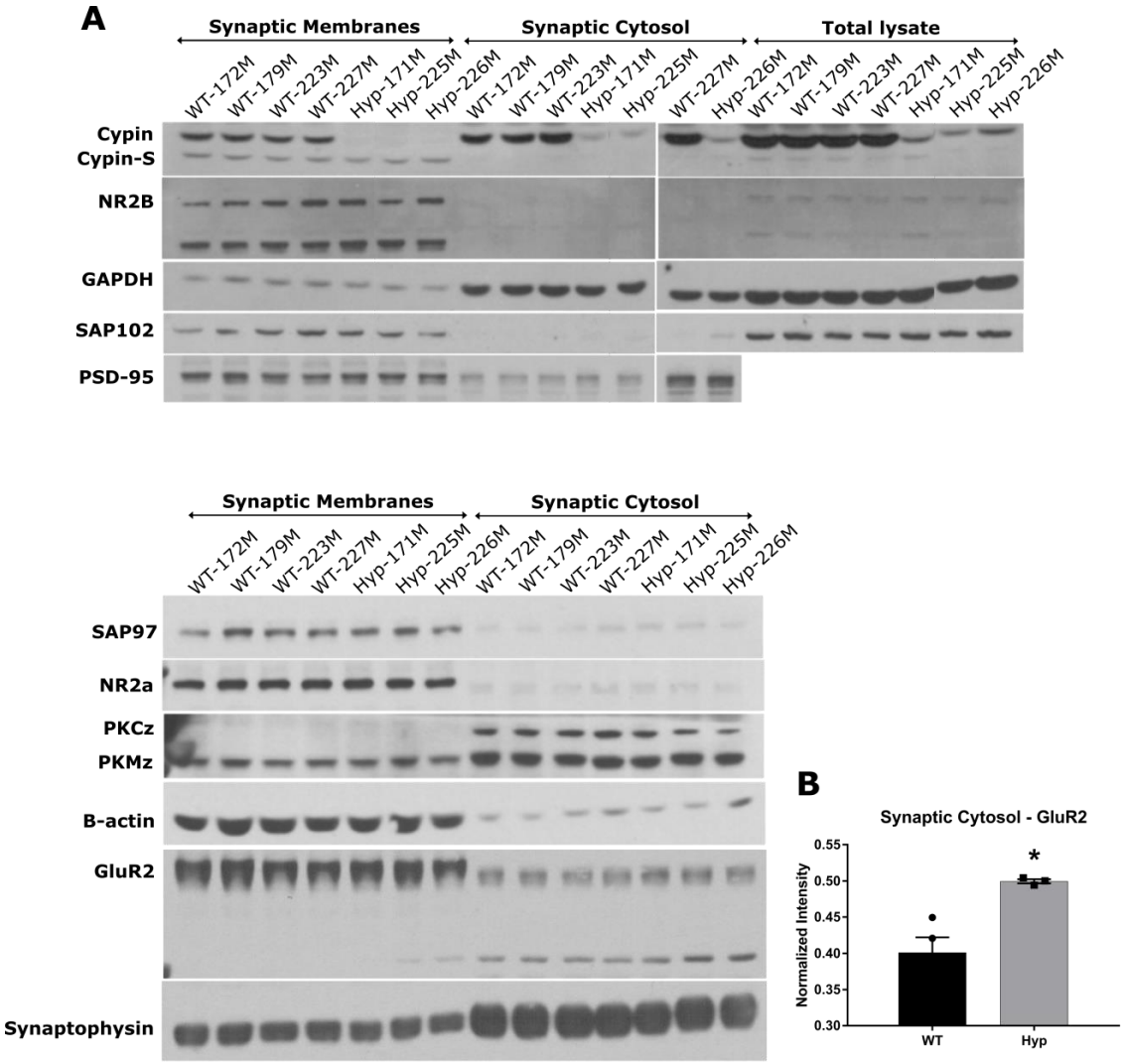


**Fig. 6.8. Biochemical analysis of protein levels in the postsynaptic density and synaptic cytosol of WT, heterozygous (Het), and cypin hypomorphic (Hypo) mice.** Synaptoneurosomes were prepared from hippocampi of WT and cypin hypomorphic male mice. **(A)** Representative images of Western blots showing expression of indicated proteins in synaptic membranes, synaptic cytosol, and total lysate. **(B)** Quantitation of full length GluR2 in synaptic. There is a significant increase in hypomorphic mice. *$p<0.05$ determined by Student's t-test.

## 4.3 Discussion

In this study, we attempted to construct a cypin KO mouse using a KO-first strategy. The KO-first allele may produce hypomorphic rather than complete KO if RNA processing is partially bypassed like that previously observed in the Pannexin1 transgenic line.[136] In fact, this appears to be the case in our Gda transgenic mouse line, where the mice express 15-20% of WT cypin levels. However, studies on our cypin hypomorphic mice give insight into sex-specific cypin function in the brain. Cypin is involved in regulation of dendrite branching,[28, 30, 36-38, 54, 59] hippocampal neurons cultured from cypin hypomorphic embryos have significantly decreased dendritic arborization, supporting previous reports. Furthermore, cypin hypomorphic females, but not males, show decreases in motor function. This suggests a sex-specific required role of cypin in maintaining normal motor function.

We also show for the first time that cypin is highly expressed in CA3 and dentate gyrus regions of hippocampus. We observed a decrease in cypin protein levels in hypomorphic mice. Since overexpression of cypin decreases localization of PSD-95 and other family members at the synapse,[29] we would expect an increase in the trafficking of PSD-95 binding partners, such as NMDA and AMPA glutamate receptor subunits,[137-142] at the synapse. Interestingly, there were no changes in synaptic levels for any of the proteins studied except for increased GluR2 in the cytosol. We do not yet know the significance of this change. Furthermore, it is possible that changes in total levels and/or postsynaptic trafficking of proteins in hypomorphic mice may not be detectable using Western blot analysis if the changes to expression of cypin is not uniform throughout the hippocampus.

This possibility is supported by guanine deaminase activity assays on brain sections, showing higher GDA activity in the CA3 and DG regions of hippocampus than in other brain regions.[61]

Biochemical analysis of synaptoneurosome preparations from hippocampi from male hypomorphic mice shows that there are increased levels of full length glutamate receptor 2 (GluR2) in synaptic cytosol compared to that of WT males. GluR2 receptors are excitatory receptors[143] and are involved in mediating glutamate-induced excitotoxicity.[144] Moreover, cypin level increases in the hippocampus after oxidative stress,[40] and in the striatum in a rat model of Parkinson's disease.[41] In addition, overexpression of cypin is protective against and knockdown of cypin increases glutamate-induced toxicity in neurons.[42, 43] and activation of cypin with small molecule compounds protects neurons from changes in basal electrophysiology and from neurocognitive deficits after traumatic brain injury.[118] Thus, the increase of GluR2 in synaptic cytosol as a consequence of decreased cypin levels may have relevance to disease and injury states.

It is interesting that female, but not male, hypomorphic mice show increased learning compared to WT females in the MWM learning and memory task. Furthermore, it was surprising that female hypomorphic mice have reduced motor function. We and others previously reported that cypin/guanine deaminase is absent from/expressed at low levels in the cerebellum in adult rodents.[29, 54, 61] Furthermore, cypin is expressed in the developing cerebellum (Kwon and Firestein, unpublished results). Thus, our work may

have uncovered a previously unknown function for cypin in cerebellum in females. Previous studies show that there are sex differences in learning and memory. Females use landmarks to learn while males use geometry,[145-148] representing a difference in strategy selection but not in learning capacity.[149] In addition, spatial memory in mice declines earlier in females than males with aging.[150] These data suggest that cypin may play an important role in motor function and CA3- and DG-mediated learning and memory in a sex-specific manner.

As shown in **Chapter 2**, although cypinS does not have guanine deaminase activity, it also increases dendrite branching, but at distances more distal from the cell body than the increases promoted by cypin. Overexpression of either cypin and cypinS increases mEPSC frequency. Moreover, cypinS also binds to PSD-95 and may regulate synaptic targeting of PSD-95 and PSD-95 family members. As cypinS is present at WT levels in hypomorphic mice, we cannot rule out the possibility that cypinS may compensate and act to function in the absence of cypin, and therefore, the hypomorphic mice do not exhibit many neurobehavioral phenotypes. Therefore, future study of Gda conditional KO mice is required to identify the detailed function of the *GDA* gene in the brain.

## 4.4 Methods & Materials

### *4.4.1 Generation of Gda (cypin) knockout mice*

The mouse *GDA* (cypin) gene contains 14 exons. As shown in **Fig. 4.1 and 4.2**, ES cell clones (EPD0770_5_B01; strain: C57BL/6N-A/a; Cell line: JM8A3.N1; EUCOMM) containing the tm1a (KO-first) allele were injected into blastocysts (B6J-albino) for chimera production. The chimera was test crossed with C57Bl/6J-Albino mice to detect ESC-derived germline based on coat color. This line was further crossed as Het x Het to generate homozygous KO-first mice ($Gda^{tm1a/tm1a}$). Female mice carrying the tm1a (KO-first) allele ($Gda^{tm1a/+}$) were crossed with B6J male mice expressing FRT recombinase (FLP) driven by the β-actin promoter (#005703; The Jackson Lab) to remove the FRT-lacZ-neo-FRT cassette, restoring gene activity. The resultant line (post-FLP) carrying the tm1c (loxP) allele can be crossed with the CamKIIα-Cre B6J transgenic lines[133] to derive brain-specific KO mice ($Gda^{-/-}$).

### *4.4.2 Genotyping*

Tail snips (<2 mm), were lysed in 100µl of 1X lysis buffer – 50 mM KCl, 10 mM Tris HCl pH8.3, 2.5 mM MgCl2.6H2O, 0.5 mM Gelatin, 0.5% Igepal/NP-40, 0.5% Tween 20 and 0.04 µg/ml Proteinase K. The extract was incubated at 56-60°C 3h-6h with shaking every 1-2h or overnight to allow lysis. The lysate was centrifuged at 10,000x*g* for 5 min at room temperature to pellet insoluble debris. The supernatant was then incubated at 95°C for 10min to heat inactivate the Proteinase K.[151] The lysate was used for PCR

reactions using following primers. Primer en2-Rev (referred to as primer 9; CCAACTGACCTTGGGCAAGAACAT); primer 3'arm (referred to as primer 12c; GCCAGTTCTTTGGGATTGCG) and primer 5' arm (referred to as primer 11; GAACTCCGGAGGGAGCGAAC). The PCR reaction (total volume 12.5µl) was prepared using 2x Green PCR Mix (Promega), 0.4µM primer 9, 0.4µM primer 12c, 0.8µM primer 11, and 4.25µl of tail lysate. PCR performed with a 95°C deannealing step for 5 min, followed by 35 cycles of deannealing, annealing, and extension (94°C for 30 sec, 55°C for 1 min, and 72°C for 1 min) with a final elongation step of 72°C for 5 minutes. PCR reactions were kept at 4°C until further use. The sizes of expected PCR products are shown in **Fig. 4.3.**

*4.4.3 Mice colony*

$Gda^{tm1a/+}$ x $Gda^{tm1a/+}$ mating was set up to produce all possible littermates. Littermates with genotypes $Gda^{+/+}$ and $Gda^{tm1a/tm1a}$ were used for all neurobehavioral and biochemical experiments. At least 10 mice per genotype per gender were used for the tests. Mice were acclimated to an environment for at least 15 min before the tests.

*4.4.4 Sholl Analysis*

Hippocampal neurons were cultured from E16 embryos from timed-pregnant heterozygous female mice ($Gda^{tm1a/+}$) mated with heterozygous male mice ($Gda^{tm1a/+}$) and plated at 200,000 cells/well in 24 well plates containing Neurobasal medium supplemented with B27 and GlutaMAX (ThermoFisher). Neurons from each embryo

were plated separately. Neurons were transfected on DIV 7 with pmRFP using Lipofectamine LTX with PLUS (ThermoFisher) following the manufacturer's directions to visualize neuronal morphology. Neurons were fixed on DIV 12, and dendrites were traced. Sholl analysis was performed using the Bonfire program as described in **Chapter 2.5.7** & **3.5.9** and in our previous studies.[63, 64, 132] The experimenter was unblinded to genotypes after analysis.

*4.4.5 Repetitive behaviors test*

Repetitive self-grooming was analyzed by measuring time spent grooming face, head, or body for 10 min.

*4.4.6 Morris water maze*

The visible maze was placed in a large circular pool (4 ft diameter) containing white, opaque, and non-toxic water. The pool was divided into four quadrants. The maze was submerged by 1 cm in one of the quadrants. Mice were allowed to swim from a fixed quadrant to find the maze. If the mice could not find the maze, they were guided toward the maze and allowed to sit on the platform for 15s followed by placing the mice into the home cage. Latency to reach the platform or maze, total distance traveled, and time spent in each quadrant were measured. Mice were trained in the same way for 4 trials per day for 4-6 consecutive days. The probe trial was performed after 24 hr at the termination of learning by removing the platform from the pool to evaluate memory formation. Comparison of latency times during learning and probe trials was used to evaluate

learning and memory in cypin hypomorphic mice. Reversal learning (3 days after probe) and reversal probe trial (24hr after reversal learning) were performed. Mice were tested for visibility by analyzing swimming speed in a cued version of the Morris water maze test.

*4.4.7 Open field test*

Mice were placed into a square test chamber for 5 min for new environment analysis and 30 min for familiar environment analysis to measure movement by photocell coupled with cameras. WT mice spend more time near the periphery or near the wall and will try to avoid a central open field. Mice that spend more time in the central open field are considered to have anxiolytic-like behavior. The total time spent in the center or near the periphery and total distance traveled were measured.

*4.4.8 Marble burying task*

Rat cages with 4-5cm of corn cob bedding were used. Twenty autoclaved marbles were arranged in a four by five pattern. Mice were dropped in corner of the cage and allowed to stay in the cage for 30min. The number of marbles buried (at least 2/3$^{rd}$ of volume submerged) were counted. A higher number of marbles buried correlates with higher anxiety.

*4.4.9 Rotarod*

A rotating rod was used with a velocity that increases from 4 to 40 rpm over a maximum of a 180 sec interval. Each trial ended when the mouse falls off of the Rotarod. Each mouse underwent 3 trials per day with a 1 hr inter-trial interval on the Rotarod device. The average latency to fall off was recorded using the Rod program.

*4.4.10 Synaptoneurosome preparation*

Brain tissue was homogenized in sucrose buffer (10mM HEPES, pH7.5, 1.5mM MgCl2, 320mM sucrose, 5mM EDTA, 5mM DTT, 0.1mM PMSF, 10μM MG132 and protease inhibitor). One ml of buffer was used for every 100mg of tissue. The homogenate was centrifuged at 700x*g* at 4ºC for 10 min to remove nuclei and debris. The supernatant was centrifuged at 9250x*g* at 4ºC for 15min to pellet the crude synaptosome. The pellet was resuspended in sucrose buffer containing 1% Triton X-100 for 60min at 4ºC. The resultant suspension was centrifuged at 40,000x*g* for 30 min at 4ºC to pellet synaptic membranes with synaptic cytosol as supernatant.

*4.4.11 Western Blot Analysis*

All protein extracts were evaluated for protein concentration using Pierce BCA protein assay kit (Thermo Scientific) following the manufacturer's protocol. Protein from tissue and synaptoneurosomes (15 μg) was resolved on a 10% SDS-polyacrylamide gel and transferred to PVDF membrane. The membrane was blocked with 5% bovine serum albumin (BSA) in TBST (20mM Tris pH 7.5, 150mM NaCl, 0.1% Tween-20) for 1 hr at

room temperature. The blots were probed with the indicated antibodies in TBST containing 3% BSA and incubated with secondary antibodies coupled to horse radish peroxidase. Blots were developed with HyGLO chemiluminescent reagent (Denville Sci.) and scanned, and the intensities of the bands were quantified using ImageJ software from NIH. The number of pixels of absolute intensity of bands was normalized to the intensity of those for GAPDH or synaptophysin (internal controls) and were compared to those of the control (WT) condition. The following antibodies were used: rabbit anti-cypin (1:500; BF6) [38, 54, 60], mouse anti-PSD-95 (1:1000; K28/43, UC Davis/NIH NeuroMab Facility), mouse anti-SAP97 (1:1000; K64-15, UC Davis/NIH NeuroMab Facility), mouse anti-NR2B (1:1000; 59/20, UC Davis/NIH NeuroMab Facility), rabbit anti-PKMzeta/PKCzeta (1:250; 38-1400, ThermoFisher), guinea pig anti-SAP102 (1:1000; BLF29838), polyclonal rabbit anti-NR2A (1:1000; 07-632, Upstate), mouse anti-β-actin (1:1000; A4700, Sigma), rabbit anti-synaptophysin (1:2000, 04-1019, EMD Millipore), mouse anti-GluR2 (1:1000; MAB397, EMD Millipore), and mouse anti-GAPDH (1:1000; MAB374, Millipore).

*4.4.12 Immunohistochemistry*

Mice were anesthetized, perfused, and brains were dissected, cryopreserved in OCT medium (Tissue-Tek), and sectioned at 30 μm using a cryostat. Sections were mounted on charged slides (Globe Sci., cat#1354W). Sections were washed in PBS three times to remove extra OCT medium, followed by incubation in block solution (2% normal goat serum, 0.2% Triton-X, 0.02% sodium azide in PBS) for 1hr at room temperature. Sections were incubated with primary antibody (rabbit anti-cypin, BF6, 1:50) in block

solution for 1hr to overnight at 4ºC. Then, sections were washed with PBS three times to remove unbound antibodies, followed by incubation with secondary antibody in block solution for 1hr to visualize staining. Sections were washed with PBS three times, air dried, and coverslips were mounted onto the sections using ProLong Gold Antifade reagent (Life Technologies, Inc.). Images were captured using EVOS FL microscope (ThermoFisher) with 2x objective.

# Chapter 5: Conclusion and Future Directions

## 5.1 A new isoform of cypin, cypinS, regulates neuronal development

This dissertation work identifies a new short isoform of cypin and studies its role in neuronal development. Cypin is involved in the regulation of dendrite branching by promoting microtubule polymerization.[30] A novel short isoform of cypin, termed cypinS, is expressed in mouse and human tissues but not in rat tissues. Like cypin, cypinS binds to PSD-95. As mRNA and protein levels of cypin and cypinS peak at P7 and P14, these isoforms may have important but distinct roles in neuronal development. In addition, cypinS does not have guanine deaminase activity, and its overexpression increases dendrite branching further away from soma than does overexpression of cypin. Overexpression of cypin, but not cypinS decreases spine density. This suggests that changes to spines, but not to dendrites, are dependent on guanine deaminase activity. Overexpression of cypin or cypinS increases mEPSC frequency, which may suggest new roles for both isoforms in the regulation of pre-synaptic vesicle pool release, as cypin also binds the SNARE-associated protein, snapin.[36] The increase observed in mEPSC frequency with cypinS overexpression was significantly higher than that of cypin, suggesting distinct roles for cypin and cypinS in neuronal development.

**Future Directions:** Zinc is involved in regulation of dendrite branching[77-83] and neurotransmitter release.[87-91] Cypin binds zinc,[59] and cypinS retains all sites required for zinc binding. These data suggest that cypin and cypinS may act as zinc sensors to mediate

changes to the dendritic arbor and vesicular release of neurotransmitters. This motivates to further investigate the role of cypin and cypinS as a zinc sensor in regulation of neuronal development. Dendritic branching and mEPSCs experiments will be performed in presence of zinc chelators and up- or downregulation of cypin or cypinS. In addition, cypin or cypinS mutants that lack zinc-binding sites can be overexpressed to study dependence of zinc on cypin-promoted dendrite branching and vesicular release of neurotransmitters.

## 5.2 A Role for PSD-95 and its Binding Partners in Models of TBI

Here, we identify a novel mechanism by which PSD-95 regulates dendrite branching post-TBI. PSD-95 levels increase post-moderate CCI and sequester APC and EB3 from +TIPs of microtubules. This destabilizes microtubules and causes decreases in the number of secondary dendrites and total dendrite length post-injury. These findings were validated with our *in vitro* model of mechanical stretch injury and *in vivo* model of controlled cortical impact (CCI). Using our stretch model to mimic moderate injury, we show that PSD-95 plays no role in the regulation of neuronal survival post-stretch injury, which is in contrast to our previous report in an NMDA-mediated injury system[43]. This suggests that mechanical stretch injury, and hence mechanotransduction, activates different mechanisms than does NMDA-mediated injury. Thus, PSD-95 plays a role in secondary or NMDA-mediated injury, but not primary or mechanical injury, to protect neurons from cell death.

**Future Directions:** PSD-95 is involved in the maturation of excitatory synapses, and its overexpression leads to an increase in the number and size of dendritic spines.[25] Moreover, cognitive deficits after TBI, and in specific, the CCI model, are associated with a delayed reduction in PSD-95 levels in the hippocampal postsynaptic density.[56] As overexpression of PSD-95 decreases dendritogenesis[28] and has detrimental effects on neurons after NMDA treatment,[43] normal synaptogenesis after injury cannot be rescued solely by upregulating PSD-95. Normal dendritogenesis concurrent with normal synaptogenesis is also required for proper neuronal function. Further study includes downregulation of PSD-95 in the early phase (0-3 days) after injury to repair dendritogenesis, followed by up-regulation of PSD-95 in the late phase (3-7 days) after injury to facilitate synaptogenesis should be performed. We will also move into an *in vivo* mouse system to alter PSD-95 levels after TBI to repair dendritogenesis. These experiments will allow us to generate therapies for functional recovery after TBI.

## 5.3 Characterization of Cypin KO-first (Hypomorphic) Mice

This dissertation work characterizes the cypin (Gda) KO-first mice for their behavior and biochemistry. We discovered that our Gda KO-first mouse retains 15-20% of the total cypin expression and is a cypin hypomorphic mouse. Behavioral screening suggests that cypin is required for normal motor function and learning in female mice. Moreover, cypin is highly expressed in the CA3 and dentate gyrus regions of the hippocampus, and thus, may play an important role in CA3- and DG-mediated learning and memory.

Additionally, the fact that there is increased GluR2 in the synaptic cytosol of hippocampi from hypomorphic mice suggests that cypin plays an important role in the regulation of GluR2 levels in spines. Thus, increased levels of cypin in the hippocampus after oxidative stress,[40] and in the striatum in a rat model of Parkinson's disease,[41] suggests a neuroprotective role of cypin, possibly by downregulating GluR2 in spines, in line with the fact that overexpression of cypin is protective against glutamate-induced toxicity in neurons.[42, 43]

**Future Directions:** Cypin hypomorphic mice have 15-20% of WT cypin levels, but they maintain WT levels of cypinS. It is possible that the expression of cypinS may compensate an perform cypin function in the absence of cypin. Thus, future study of Gda conditional KO mice with tissue-specific deletion is required to identify the detailed function of the *GDA* gene in the brain. CA3/DG-specific Gda conditional KO mice may be studied to explore the detailed role of cypin in hippocampal function. Since cypin is involved in the regulation of the synaptic targeting of PSD-95 and related MAUGKs, synaptoneurosome and immunohistochemical experiments in these mice will yield further insight into role of cypin in regulation of synaptic trafficking and the NMDA/AMPA ratio *in vivo*. A gross anatomy study of conditional KO mice may explore changes in brain regions due to cypin's role in the regulation of dendrite branching.[30] As cypin affects spine density,[43] Golgi impregnation experiments will yield further insight into dendrite arborization and spine density changes. As explained in **Chapter 2**, cypin and cypinS may regulate presynaptic vesicle pools of neurotransmitters, and hypomorphic and conditional KO mice should be tested for changes to electrophysiology. Conditional KO mice will be screened for different neurobehaviors as maternal auto-

antibody related autism (MAR) has been linked to cypin.[39] Gda conditional KO mice should be tested to study recovery post-TBI as cypin has recently been identified as novel target for the TBI recovery.[118]

# References

1. Craig, A.M. and Banker, G. (1994). Neuronal polarity. Annual review of neuroscience 17, 267-310.
2. Georges, P.C., Hadzimichalis, N.M., Sweet, E.S. and Firestein, B.L. (2008). The yin–yang of dendrite morphology: unity of actin and microtubules. Molecular neurobiology 38, 270-284.
3. Dailey, M.E. and Smith, S.J. (1996). The dynamics of dendritic structure in developing hippocampal slices. Journal of Neuroscience 16, 2983-2994.
4. Rajan, I. and Cline, H.T. (1998). Glutamate receptor activity is required for normal development of tectal cell dendrites in vivo. Journal of Neuroscience 18, 7836-7846.
5. Kaufmann, W.E. and Moser, H.W. (2000). Dendritic anomalies in disorders associated with mental retardation. Cerebral cortex 10, 981-991.
6. Kulkarni, V.A. and Firestein, B.L. (2012). The dendritic tree and brain disorders. Molecular and Cellular Neuroscience 50, 10-20.
7. McAllister, A.K. (2000). Cellular and molecular mechanisms of dendrite growth. Cerebral cortex 10, 963-973.
8. Schaefer, A.W., Kabir, N. and Forscher, P. (2002). Filopodia and actin arcs guide the assembly and transport of two populations of microtubules with unique dynamic parameters in neuronal growth cones. The Journal of cell biology 158, 139-152.
9. Goode, B.L., Drubin, D.G. and Barnes, G. (2000). Functional cooperation between the microtubule and actin cytoskeletons. Current opinion in cell biology 12, 63-71.
10. Cingolani, L.A. and Goda, Y. (2008). Actin in action: the interplay between the actin cytoskeleton and synaptic efficacy. Nature Reviews Neuroscience 9, 344.
11. Munemitsu, S., Souza, B., Müller, O., Albert, I., Rubinfeld, B. and Polakis, P. (1994). The APC gene product associates with microtubules in vivo and promotes their assembly in vitro. Cancer research 54, 3676-3681.
12. Moseley, J.B., Bartolini, F., Okada, K., Wen, Y., Gundersen, G.G. and Goode, B.L. (2007). Regulated binding of adenomatous polyposis coli protein to actin. Journal of Biological Chemistry 282, 12661-12668.
13. Vitre, B., Coquelle, F.M., Heichette, C., Garnier, C., Chrétien, D. and Arnal, I. (2008). EB1 regulates microtubule dynamics and tubulin sheet closure in vitro. Nature cell biology 10, 415.
14. Nakagawa, H., Koyama, K., Murata, Y., Morito, M., Akiyama, T. and Nakamura, Y. (2000). EB3, a novel member of the EB1 family preferentially expressed in the central nervous system, binds to a CNS-specific APC homologue. Oncogene 19, 210.

15. Yamanaka, H., Hashimoto, N., Koyama, K., Nakagawa, H., Nakamura, Y. and Noguchi, K. (2002). Expression of Apc2 during mouse development. Gene Expression Patterns 1, 107-114.
16. Imura, T., Wang, X., Noda, T., Sofroniew, M.V. and Fushiki, S. (2010). Adenomatous polyposis coli is essential for both neuronal differentiation and maintenance of adult neural stem cells in subventricular zone and hippocampus. Stem Cells 28, 2053-2064.
17. Shintani, T., Takeuchi, Y., Fujikawa, A. and Noda, M. (2012). Directional neuronal migration is impaired in mice lacking adenomatous polyposis coli 2. Journal of Neuroscience 32, 6468-6484.
18. Cho, K.O., Hunt, C.A. and Kennedy, M.B. (1992). The rat brain postsynaptic density fraction contains a homolog of the Drosophila discs-large tumor suppressor protein. Neuron 9, 929-942.
19. Kistner, U., Wenzel, B.M., Veh, R.W., Cases-Langhoff, C., Garner, A.M., Appeltauer, U., Voss, B., Gundelfinger, E.D. and Garner, C.C. (1993). SAP90, a rat presynaptic protein related to the product of the Drosophila tumor suppressor gene dlg-A. J Biol Chem 268, 4580-4583.
20. Kim, E., Naisbitt, S., Hsueh, Y.-P., Rao, A., Rothschild, A., Craig, A.M. and Sheng, M. (1997). GKAP, a novel synaptic protein that interacts with the guanylate kinase-like domain of the PSD-95/SAP90 family of channel clustering molecules. The Journal of cell biology 136, 669-678.
21. Brenman, J.E., Chao, D.S., Gee, S.H., McGee, A.W., Craven, S.E., Santillano, D.R., Wu, Z., Huang, F., Xia, H., Peters, M.F., Froehner, S.C. and Bredt, D.S. (1996). Interaction of nitric oxide synthase with the postsynaptic density protein PSD-95 and alpha1-syntrophin mediated by PDZ domains. Cell 84, 757-767.
22. Naisbitt, S., Kim, E., Tu, J.C., Xiao, B., Sala, C., Valtschanoff, J., Weinberg, R.J., Worley, P.F. and Sheng, M. (1999). Shank, a novel family of postsynaptic density proteins that binds to the NMDA receptor/PSD-95/GKAP complex and cortactin. Neuron 23, 569-582.
23. Passafaro, M., Sala, C., Niethammer, M. and Sheng, M. (1999). Microtubule binding by CRIPT and its potential role in the synaptic clustering of PSD-95. Nature neuroscience 2, 1063.
24. El-Husseini, A.E.-D., Schnell, E., Dakoji, S., Sweeney, N., Zhou, Q., Prange, O., Gauthier-Campbell, C., Aguilera-Moreno, A., Nicoll, R.A. and Bredt, D.S. (2002). Synaptic strength regulated by palmitate cycling on PSD-95. Cell 108, 849-863.
25. El-Husseini, A.E.-D., Schnell, E., Chetkovich, D.M., Nicoll, R.A. and Bredt, D.S. (2000). PSD-95 involvement in maturation of excitatory synapses. Science 290, 1364-1368.
26. Okabe, S., Miwa, A. and Okado, H. (2001). Spine formation and correlated assembly of presynaptic and postsynaptic molecules. Journal of Neuroscience 21, 6105-6114.
27. Prange, O. and Murphy, T.H. (2001). Modular transport of postsynaptic density-95 clusters and association with stable spine precursors during early development of cortical neurons. Journal of Neuroscience 21, 9325-9333.
28. Charych, E.I., Akum, B.F., Goldberg, J.S., Jornsten, R.J., Rongo, C., Zheng, J.Q. and Firestein, B.L. (2006). Activity-independent regulation of dendrite patterning by postsynaptic density protein PSD-95. J Neurosci 26, 10164-10176.

29. Firestein, B.L., Brenman, J.E., Aoki, C., Sanchez-Perez, A.M., El-Husseini, A.E. and Bredt, D.S. (1999). Cypin: a cytosolic regulator of PSD-95 postsynaptic targeting. Neuron 24, 659-672.
30. Akum, B.F., Chen, M., Gunderson, S.I., Riefler, G.M., Scerri-Hansen, M.M. and Firestein, B.L. (2004). Cypin regulates dendrite patterning in hippocampal neurons by promoting microtubule assembly. Nat Neurosci 7, 145-152.
31. Sweet, E.S., Previtera, M.L., Fernandez, J.R., Charych, E.I., Tseng, C.Y., Kwon, M., Starovoytov, V., Zheng, J.Q. and Firestein, B.L. (2011). PSD-95 alters microtubule dynamics via an association with EB3. J Neurosci 31, 1038-1047.
32. Sweet, E.S., Tseng, C.Y. and Firestein, B.L. (2011). To branch or not to branch: How PSD-95 regulates dendrites and spines. Bioarchitecture 1, 69-73.
33. Yanai, H., Satoh, K., Matsumine, A. and Akiyama, T. (2000). The colorectal tumour suppressor APC is present in the NMDA-receptor-PSD-95 complex in the brain. Genes Cells 5, 815-822.
34. Takamori, N., Shimomura, A. and Senda, T. (2006). Microtubule-bundling activity of APC is stimulated by interaction with PSD-95. Neurosci Lett 403, 68-72.
35. Kuwahara, H., Araki, N., Makino, K., Masuko, N., Honda, S., Kaibuchi, K., Fukunaga, K., Miyamoto, E., Ogawa, M. and Saya, H. (1999). A Novel NE-dlg/SAP102-associated Protein, p51-nedasin, Related to the Amidohydrolase Superfamily, Interferes with the Association between NE-dlg/SAP102 and N-Methyl-D-aspartate Receptor. Journal of Biological Chemistry 274, 32204-32214.
36. Chen, M., Lucas, K.G., Akum, B.F., Balasingam, G., Stawicki, T.M., Provost, J.M., Riefler, G.M., Jornsten, R.J. and Firestein, B.L. (2005). A novel role for snapin in dendrite patterning: interaction with cypin. Mol Biol Cell 16, 5103-5114.
37. Chen, H. and Firestein, B.L. (2007). RhoA regulates dendrite branching in hippocampal neurons by decreasing cypin protein levels. J Neurosci 27, 8378-8386.
38. Kwon, M., Fernandez, J.R., Zegarek, G.F., Lo, S.B. and Firestein, B.L. (2011). BDNF-promoted increases in proximal dendrites occur via CREB-dependent transcriptional regulation of cypin. J Neurosci 31, 9735-9745.
39. Braunschweig, D., Krakowiak, P., Duncanson, P., Boyce, R., Hansen, R.L., Ashwood, P., Hertz-Picciotto, I., Pessah, I.N. and Van de Water, J. (2013). Autism-specific maternal autoantibodies recognize critical proteins in developing brain. Transl Psychiatry 3, e277.
40. Wang, X., Pal, R., Chen, X.W., Kumar, K.N., Kim, O.J. and Michaelis, E.K. (2007). Genome-wide transcriptome profiling of region-specific vulnerability to oxidative stress in the hippocampus. Genomics 90, 201-212.
41. Fuller, H.R., Hurtado, M.L., Wishart, T.M. and Gates, M.A. (2014). The rat striatum responds to nigro-striatal degeneration via the increased expression of proteins associated with growth and regeneration of neuronal circuitry. Proteome Sci 12, 20.
42. Hedlund, E., Karlsson, M., Osborn, T., Ludwig, W. and Isacson, O. (2010). Global gene expression profiling of somatic motor neuron populations with different vulnerability identify molecules and pathways of degeneration and protection. Brain 133, 2313-2330.
43. Tseng, C.-Y. and Firestein, B.L. (2011). The role of PSD-95 and cypin in morphological changes in dendrites following sublethal NMDA exposure. Journal of Neuroscience 31, 15468-15480.

44. Ray, S., Dixon, C. and Banik, N. (2002). Molecular mechanisms in the pathogenesis of traumatic brain injury. Histology and histopathology 17, 1137-1152.
45. Mark, L.P., Prost, R.W., Ulmer, J.L., Smith, M.M., Daniels, D.L., Strottmann, J.M., Brown, W.D. and Hacein-Bey, L. (2001). Pictorial review of glutamate excitotoxicity: fundamental concepts for neuroimaging. American journal of neuroradiology 22, 1813-1824.
46. Walker, K.R. and Tesco, G. (2013). Molecular mechanisms of cognitive dysfunction following traumatic brain injury. Frontiers in aging neuroscience 5, 29.
47. Levin, H.S. and Robertson, C.S. (2013). Mild traumatic brain injury in translation. Journal of neurotrauma 30, 610-617.
48. Dikmen, S.S., Corrigan, J.D., Levin, H.S., Machamer, J., Stiers, W. and Weisskopf, M.G. (2009). Cognitive outcome following traumatic brain injury. The Journal of head trauma rehabilitation 24, 430-438.
49. Gao, X., Deng, P., Xu, Z.C. and Chen, J. (2011). Moderate traumatic brain injury causes acute dendritic and synaptic degeneration in the hippocampal dentate gyrus. PloS one 6, e24566.
50. Greenwood, S.M., Mizielinska, S.M., Frenguelli, B.G., Harvey, J. and Connolly, C.N. (2007). Mitochondrial dysfunction and dendritic beading during neuronal toxicity. Journal of Biological Chemistry 282, 26235-26244.
51. Hasbani, M.J., Schlief, M.L., Fisher, D.A. and Goldberg, M.P. (2001). Dendritic spines lost during glutamate receptor activation reemerge at original sites of synaptic contact. Journal of Neuroscience 21, 2393-2403.
52. Yamamoto, K., Morimoto, K. and Yanagihara, T. (1986). Cerebral ischemia in the gerbil: transmission electron microscopic and immunoelectron microscopic investigation. Brain research 384, 1-10.
53. Tomimoto, H. and Yanagihara, T. (1992). Electron microscopic investigation of the cerebral cortex after cerebral ischemia and reperfusion in the gerbil. Brain research 598, 87-97.
54. Patel, M.V., Swiatkowski, P., Kwon, M., Rodriguez, A.R., Campagno, K. and Firestein, B.L. (2018). A Novel Short Isoform of Cytosolic PSD-95 Interactor (Cypin) Regulates Neuronal Development. Mol Neurobiol.
55. Ansari, M.A., Roberts, K.N. and Scheff, S.W. (2008). A time course of contusion-induced oxidative stress and synaptic proteins in cortex in a rat model of TBI. J Neurotrauma 25, 513-526.
56. Wakade, C., Sukumari-Ramesh, S., Laird, M.D., Dhandapani, K.M. and Vender, J.R. (2010). Delayed reduction in hippocampal postsynaptic density protein-95 expression temporally correlates with cognitive dysfunction following controlled cortical impact in mice. J Neurosurg 113, 1195-1201.
57. Ansari, M.A., Roberts, K.N. and Scheff, S.W. (2008). Oxidative stress and modification of synaptic proteins in hippocampus after traumatic brain injury. Free Radic Biol Med 45, 443-452.
58. Wang, C.F., Zhao, C.C., Jiang, G., Gu, X., Feng, J.F. and Jiang, J.Y. (2016). The Role of Posttraumatic Hypothermia in Preventing Dendrite Degeneration and Spine Loss after Severe Traumatic Brain Injury. Sci Rep 6, 37063.

59. Fernandez, J.R., Welsh, W.J. and Firestein, B.L. (2008). Structural characterization of the zinc binding domain in cytosolic PSD-95 interactor (cypin): Role of zinc binding in guanine deamination and dendrite branching. Proteins 70, 873-881.
60. Tseng, C.Y. and Firestein, B.L. (2011). The role of PSD-95 and cypin in morphological changes in dendrites following sublethal NMDA exposure. J Neurosci 31, 15468-15480.
61. Paletzki, R.F. (2002). Cloning and characterization of guanine deaminase from mouse and rat brain. Neuroscience 109, 15-26.
62. Fernandez, J.R., Sweet, E.S., Welsh, W.J. and Firestein, B.L. (2010). Identification of small molecule compounds with higher binding affinity to guanine deaminase (cypin) than guanine. Bioorg Med Chem 18, 6748-6755.
63. Kutzing, M.K., Langhammer, C.G., Luo, V., Lakdawala, H. and Firestein, B.L. (2010). Automated Sholl analysis of digitized neuronal morphology at multiple scales. J Vis Exp.
64. Langhammer, C.G., Previtera, M.L., Sweet, E.S., Sran, S.S., Chen, M. and Firestein, B.L. (2010). Automated Sholl analysis of digitized neuronal morphology at multiple scales: Whole cell Sholl analysis versus Sholl analysis of arbor subregions. Cytometry A 77, 1160-1168.
65. Sweet, E.S., Langhammer, C.L., Kutzing, M.K. and Firestein, B.L. (2013). Semiautomated analysis of dendrite morphology in cell culture. Methods Mol Biol 1018, 261-268.
66. Gu, Y. and Ihara, Y. (2000). Evidence that collapsin response mediator protein-2 is involved in the dynamics of microtubules. J Biol Chem 275, 17917-17920.
67. Fukata, Y., Itoh, T.J., Kimura, T., Menager, C., Nishimura, T., Shiromizu, T., Watanabe, H., Inagaki, N., Iwamatsu, A., Hotani, H. and Kaibuchi, K. (2002). CRMP-2 binds to tubulin heterodimers to promote microtubule assembly. Nat Cell Biol 4, 583-591.
68. Mural, R.J., Adams, M.D., Myers, E.W., Smith, H.O., Miklos, G.L.G., Wides, R., Halpern, A., Li, P.W., Sutton, G.G., Nadeau, J., Salzberg, S.L., Holt, R.A., Kodira, C.D., Lu, F., Chen, L., Deng, Z., Evangelista, C.C., Gan, W., Heiman, T.J., Li, J., Li, Z., Merkulov, G.V., Milshina, N.V., Naik, A.K., Qi, R., Shue, B.C., Wang, A., Wang, J., Wang, X., Yan, X., Ye, J., Yooseph, S., Zhao, Q., Zheng, L., Zhu, S.C., Biddick, K., Bolanos, R., Delcher, A.L., Dew, I.M., Fasulo, D., Flanigan, M.J., Huson, D.H., Kravitz, S.A., Miller, J.R., Mobarry, C.M., Reinert, K., Remington, K.A., Zhang, Q., Zheng, X.H., Nusskern, D.R., Lai, Z., Lei, Y., Zhong, W., Yao, A., Guan, P., Ji, R.-R., Gu, Z., Wang, Z.-Y., Zhong, F., Xiao, C., Chiang, C.-C., Yandell, M., Wortman, J.R., Amanatides, P.G., Hladun, S.L., Pratts, E.C., Johnson, J.E., Dodson, K.L., Woodford, K.J., Evans, C.A., Gropman, B., Rusch, D.B., Venter, E., Wang, M., Smith, T.J., Houck, J.T., Tompkins, D.E., Haynes, C., Jacob, D., Chin, S.H., Allen, D.R., Dahlke, C.E., Sanders, R., Li, K., Liu, X., Levitsky, A.A., Majoros, W.H., Chen, Q., Xia, A.C., Lopez, J.R., Donnelly, M.T., Newman, M.H., Glodek, A., Kraft, C.L., Nodell, M., Ali, F., An, H.-J., Baldwin-Pitts, D., Beeson, K.Y., Cai, S., Carnes, M., Carver, A., Caulk, P.M., Center, A., Chen, Y.-H., Cheng, M.-L., Coyne, M.D., Crowder, M., Danaher, S., Davenport, L.B., Desilets, R., Dietz, S.M., Doup, L., Dullaghan, P., Ferriera, S., Fosler, C.R., Gire, H.C., Gluecksmann, A., Gocayne, J.D., Gray, J., Hart, B., Haynes, J., Hoover, J., Howland, T., Ibegwam, C., Jalali, M., Johns, D., Kline, L., Ma, D.S., MacCawley, S., Magoon, A.,

Mann, F., May, D., McIntosh, T.C., Mehta, S., Moy, L., Moy, M.C., Murphy, B.J., Murphy, S.D., Nelson, K.A., Nuri, Z., Parker, K.A., Prudhomme, A.C., Puri, V.N., Qureshi, H., Raley, J.C., Reardon, M.S., Regier, M.A., Rogers, Y.-H.C., Romblad, D.L., Schutz, J., Scott, J.L., Scott, R., Sitter, C.D., Smallwood, M., Sprague, A.C., Stewart, E., Strong, R.V., Suh, E., Sylvester, K., Thomas, R., Tint, N.N., Tsonis, C., Wang, G., Wang, G., Williams, M.S., Williams, S.M., Windsor, S.M., Wolfe, K., Wu, M.M., Zaveri, J., Chaturvedi, K., Gabrielian, A.E., Ke, Z., Sun, J., Subramanian, G., Venter, J.C., Pfannkoch, C.M., Barnstead, M. and Stephenson, L.D. (2002). A comparison of whole-genome shotgun-derived mouse chromosome 16 and the human genome. Science 296, 1661-1671.

69. Gibbs, R.A., Weinstock, G.M., Metzker, M.L., Muzny, D.M., Sodergren, E.J., Scherer, S., Scott, G., Steffen, D., Worley, K.C., Burch, P.E., Okwuonu, G., Hines, S., Lewis, L., DeRamo, C., Delgado, O., Dugan-Rocha, S., Miner, G., Morgan, M., Hawes, A., Gill, R., Celera, Holt, R.A., Adams, M.D., Amanatides, P.G., Baden-Tillson, H., Barnstead, M., Chin, S., Evans, C.A., Ferriera, S., Fosler, C., Glodek, A., Gu, Z., Jennings, D., Kraft, C.L., Nguyen, T., Pfannkoch, C.M., Sitter, C., Sutton, G.G., Venter, J.C., Woodage, T., Smith, D., Lee, H.-M., Gustafson, E., Cahill, P., Kana, A., Doucette-Stamm, L., Weinstock, K., Fechtel, K., Weiss, R.B., Dunn, D.M., Green, E.D., Blakesley, R.W., Bouffard, G.G., De Jong, P.J., Osoegawa, K., Zhu, B., Marra, M., Schein, J., Bosdet, I., Fjell, C., Jones, S., Krzywinski, M., Mathewson, C., Siddiqui, A., Wye, N., McPherson, J., Zhao, S., Fraser, C.M., Shetty, J., Shatsman, S., Geer, K., Chen, Y., Abramzon, S., Nierman, W.C., Havlak, P.H., Chen, R., Durbin, K.J., Egan, A., Ren, Y., Song, X.-Z., Li, B., Liu, Y., Qin, X., Cawley, S., Worley, K.C., Cooney, A.J., D'Souza, L.M., Martin, K., Wu, J.Q., Gonzalez-Garay, M.L., Jackson, A.R., Kalafus, K.J., McLeod, M.P., Milosavljevic, A., Virk, D., Volkov, A., Wheeler, D.A., Zhang, Z., Bailey, J.A., Eichler, E.E., Tuzun, E., Birney, E., Mongin, E., Ureta-Vidal, A., Woodwark, C., Zdobnov, E., Bork, P., Suyama, M., Torrents, D., Alexandersson, M., Trask, B.J., Young, J.M., Huang, H., Wang, H., Xing, H., Daniels, S., Gietzen, D., Schmidt, J., Stevens, K., Vitt, U., Wingrove, J., Camara, F., Mar Alba, M., Abril, J.F., Guigo, R., Smit, A., Dubchak, I., Rubin, E.M., Couronne, O., Poliakov, A., Hubner, N., Ganten, D., Goesele, C., Hummel, O., Kreitler, T., Lee, Y.-A., Monti, J., Schulz, H., Zimdahl, H., Himmelbauer, H., Lehrach, H., Jacob, H.J., Bromberg, S., Gullings-Handley, J., Jensen-Seaman, M.I., Kwitek, A.E., Lazar, J., Pasko, D., Tonellato, P.J., Twigger, S., Ponting, C.P., Duarte, J.M., Rice, S., Goodstadt, L., Beatson, S.A., Emes, R.D., Winter, E.E., Webber, C., Brandt, P., Nyakatura, G., Adetobi, M., Chiaromonte, F., Elnitski, L., Eswara, P., Hardison, R.C., Hou, M., Kolbe, D., Makova, K., Miller, W., Nekrutenko, A., Riemer, C., Schwartz, S., Taylor, J., Yang, S., Zhang, Y., Lindpaintner, K., Andrews, T.D., Caccamo, M., Clamp, M., Clarke, L., Curwen, V., Durbin, R., Eyras, E., Searle, S.M., Cooper, G.M., Batzoglou, S., Brudno, M., Sidow, A., Stone, E.A., Venter, J.C., Payseur, B.A., Bourque, G., Lopez-Otin, C., Puente, X.S., Chakrabarti, K., Chatterji, S., Dewey, C., Pachter, L., Bray, N., Yap, V.B., Caspi, A., Tesler, G., Pevzner, P.A., Haussler, D., Roskin, K.M., Baertsch, R., Clawson, H., Furey, T.S., Hinrichs, A.S., Karolchik, D., Kent, W.J., Rosenbloom, K.R., Trumbower, H., Weirauch, M., Cooper, D.N., Stenson, P.D., Ma, B., Brent, M., Arumugam, M., Shteynberg, D., Copley, R.R., Taylor, M.S., Riethman, H., Mudunuri, U., Peterson, J., Guyer, M., Felsenfeld, A., Old, S., Mockrin, S., Collins, F. and Rat Genome Sequencing Project, C. (2004). Genome

sequence of the Brown Norway rat yields insights into mammalian evolution. Nature 428, 493-521.
70. Futcher, B., Latter, G.I., Monardo, P., McLaughlin, C.S. and Garrels, J.I. (1999). A sampling of the yeast proteome. Mol Cell Biol 19, 7357-7368.
71. Greenbaum, D., Colangelo, C., Williams, K. and Gerstein, M. (2003). Comparing protein abundance and mRNA expression levels on a genomic scale. Genome Biol 4, 117.
72. Gygi, S.P., Rochon, Y., Franza, B.R. and Aebersold, R. (1999). Correlation between protein and mRNA abundance in yeast. Mol Cell Biol 19, 1720-1730.
73. Barrett, L.W., Fletcher, S. and Wilton, S.D. (2012). Regulation of eukaryotic gene expression by the untranslated gene regions and other non-coding elements. Cell Mol Life Sci 69, 3613-3634.
74. Barreau, C., Paillard, L. and Osborne, H.B. (2005). AU-rich elements and associated factors: are there unifying principles? Nucleic Acids Res 33, 7138-7150.
75. Chen, C.Y. and Shyu, A.B. (1995). AU-rich elements: characterization and importance in mRNA degradation. Trends Biochem Sci 20, 465-470.
76. Gruber, A.R., Fallmann, J., Kratochvill, F., Kovarik, P. and Hofacker, I.L. (2011). AREsite: a database for the comprehensive investigation of AU-rich elements. Nucleic Acids Res 39, D66-69.
77. Perrin, L., Roudeau, S., Carmona, A., Domart, F., Petersen, J.D., Bohic, S., Yang, Y., Cloetens, P. and Ortega, R. (2017). Zinc and Copper Effects on Stability of Tubulin and Actin Networks in Dendrites and Spines of Hippocampal Neurons. ACS Chem Neurosci 8, 1490-1499.
78. Dvergsten, C.L., Johnson, L.A. and Sandstead, H.H. (1984). Alterations in the postnatal development of the cerebellar cortex due to zinc deficiency. III. Impaired dendritic differentiation of basket and stellate cells. Brain Res 318, 21-26.
79. Shi, L., Lin, S., Grinberg, Y., Beck, Y., Grozinger, C.M., Robinson, G.E. and Lee, T. (2007). Roles of Drosophila Kruppel-homolog 1 in neuronal morphogenesis. Dev Neurobiol 67, 1614-1626.
80. Clark, S.G. and Chiu, C. (2003). C. elegans ZAG-1, a Zn-finger-homeodomain protein, regulates axonal development and neuronal differentiation. Development 130, 3781-3794.
81. Li, W., Wang, F., Menut, L. and Gao, F.B. (2004). BTB/POZ-zinc finger protein abrupt suppresses dendritic branching in a neuronal subtype-specific and dosage-dependent manner. Neuron 43, 823-834.
82. Kuo, T.Y., Chen, C.Y. and Hsueh, Y.P. (2010). Bcl11A/CTIP1 mediates the effect of the glutamate receptor on axon branching and dendrite outgrowth. J Neurochem 114, 1381-1392.
83. Koyama, Y., Hattori, T., Nishida, T., Hori, O. and Tohyama, M. (2015). Alterations in dendrite and spine morphology of cortical pyramidal neurons in DISC1-binding zinc finger protein (DBZ) knockout mice. Front Neuroanat 9, 52.
84. Prakash, A., Bharti, K. and Majeed, A.B.A. (2015). Zinc: indications in brain disorders. Fundam Clin Pharmacol 29, 131-149.
85. Turrigiano, G.G., Leslie, K.R., Desai, N.S., Rutherford, L.C. and Nelson, S.B. (1998). Activity-dependent scaling of quantal amplitude in neocortical neurons. Nature 391, 892-896.

86. Ilardi, J.M., Mochida, S. and Sheng, Z.H. (1999). Snapin: a SNARE-associated protein implicated in synaptic transmission. Nat Neurosci 2, 119-124.
87. Arons, M.H., Lee, K., Thynne, C.J., Kim, S.A., Schob, C., Kindler, S., Montgomery, J.M. and Garner, C.C. (2016). Shank3 Is Part of a Zinc-Sensitive Signaling System That Regulates Excitatory Synaptic Strength. The Journal of neuroscience : the official journal of the Society for Neuroscience 36, 9124-9134.
88. Westbrook, G.L. and Mayer, M.L. (1987). Micromolar concentrations of Zn2+ antagonize NMDA and GABA responses of hippocampal neurons. Nature 328, 640-643.
89. Mayer, M.L. and Vyklicky, L., Jr. (1989). The action of zinc on synaptic transmission and neuronal excitability in cultures of mouse hippocampus. J Physiol 415, 351-365.
90. Lu, Y.M., Taverna, F.A., Tu, R., Ackerley, C.A., Wang, Y.T. and Roder, J. (2000). Endogenous Zn(2+) is required for the induction of long-term potentiation at rat hippocampal mossy fiber-CA3 synapses. Synapse 38, 187-197.
91. Li, Y., Hough, C.J., Suh, S.W., Sarvey, J.M. and Frederickson, C.J. (2001). Rapid translocation of Zn(2+) from presynaptic terminals into postsynaptic hippocampal neurons after physiological stimulation. J Neurophysiol 86, 2597-2604.
92. Kwon, M. and Firestein, B.L. (2013). DNA transfection: calcium phosphate method. Methods Mol Biol 1018, 107-110.
93. Chao, H.W., Tsai, L.Y., Lu, Y.L., Lin, P.Y., Huang, W.H., Chou, H.J., Lu, W.H., Lin, H.C., Lee, P.T. and Huang, Y.S. (2013). Deletion of CPEB3 enhances hippocampus-dependent memory via increasing expressions of PSD95 and NMDA receptors. J Neurosci 33, 17008-17022.
94. Mendenhall, A., Lesnik, J., Mukherjee, C., Antes, T. and Sengupta, R. (2012). Packaging HIV- or FIV-based lentivector expression constructs and transduction of VSV-G pseudotyped viral particles. J Vis Exp, e3171.
95. Hernandez, K., Swiatkowski, P., Patel, M.V., Liang, C., Dudzinski, N.R., Brzustowicz, L.M. and Firestein, B.L. (2016). Overexpression of Isoforms of Nitric Oxide Synthase 1 Adaptor Protein, Encoded by a Risk Gene for Schizophrenia, Alters Actin Dynamics and Synaptic Function. Front Cell Neurosci 10, 6.
96. Taylor, C.A., Bell, J.M., Breiding, M.J. and Xu, L. (2017). Traumatic Brain Injury-Related Emergency Department Visits, Hospitalizations, and Deaths - United States, 2007 and 2013. MMWR Surveill Summ 66, 1-16.
97. Cohen, J.S., Gioia, G., Atabaki, S. and Teach, S.J. (2009). Sports-related concussions in pediatrics. Current opinion in pediatrics 21, 288-293.
98. Elder, G.A. and Cristian, A. (2009). Blast-related mild traumatic brain injury: mechanisms of injury and impact on clinical care. Mount Sinai Journal of Medicine: A Journal of Translational and Personalized Medicine 76, 111-118.
99. Monnerie, H., Tang-Schomer, M.D., Iwata, A., Smith, D.H., Kim, H.A. and Le Roux, P.D. (2010). Dendritic alterations after dynamic axonal stretch injury in vitro. Experimental neurology 224, 415-423.
100. Marshall, L.F. (2000). Head injury: recent past, present, and future. Oxford University Press.
101. Prins, M., Greco, T., Alexander, D. and Giza, C.C. (2013). The pathophysiology of traumatic brain injury at a glance. Disease models & mechanisms 6, 1307-1315.
102. Hill, C.S., Coleman, M.P. and Menon, D.K. (2016). Traumatic Axonal Injury: Mechanisms and Translational Opportunities. Trends Neurosci 39, 311-324.

103. Siedler, D.G., Chuah, M.I., Kirkcaldie, M.T., Vickers, J.C. and King, A.E. (2014). Diffuse axonal injury in brain trauma: insights from alterations in neurofilaments. Front Cell Neurosci 8, 429.
104. Johnson, V.E., Stewart, W. and Smith, D.H. (2013). Axonal pathology in traumatic brain injury. Exp Neurol 246, 35-43.
105. Kim, E., Niethammer, M., Rothschild, A., Jan, Y.N. and Sheng, M. (1995). Clustering of Shaker-type K+ channels by interaction with a family of membrane-associated guanylate kinases. Nature 378, 85-88.
106. Kornau, H.C., Schenker, L.T., Kennedy, M.B. and Seeburg, P.H. (1995). Domain interaction between NMDA receptor subunits and the postsynaptic density protein PSD-95. Science 269, 1737-1740.
107. Kim, E., Cho, K.O., Rothschild, A. and Sheng, M. (1996). Heteromultimerization and NMDA receptor-clustering activity of Chapsyn-110, a member of the PSD-95 family of proteins. Neuron 17, 103-113.
108. Sattler, R., Xiong, Z., Lu, W.Y., Hafner, M., MacDonald, J.F. and Tymianski, M. (1999). Specific coupling of NMDA receptor activation to nitric oxide neurotoxicity by PSD-95 protein. Science 284, 1845-1848.
109. Yamada, Y., Chochi, Y., Takamiya, K., Sobue, K. and Inui, M. (1999). Modulation of the channel activity of the epsilon2/zeta1-subtype N-methyl D-aspartate receptor by PSD-95. J Biol Chem 274, 6647-6652.
110. Weiner, A.T., Lanz, M.C., Goetschius, D.J., Hancock, W.O. and Rolls, M.M. (2016). Kinesin-2 and Apc function at dendrite branch points to resolve microtubule collisions. Cytoskeleton (Hoboken) 73, 35-44.
111. Votin, V., Nelson, W.J. and Barth, A.I. (2005). Neurite outgrowth involves adenomatous polyposis coli protein and beta-catenin. J Cell Sci 118, 5699-5708.
112. Koester, M.P., Muller, O. and Pollerberg, G.E. (2007). Adenomatous polyposis coli is differentially distributed in growth cones and modulates their steering. J Neurosci 27, 12590-12600.
113. Gartner, A., Huang, X. and Hall, A. (2006). Neuronal polarity is regulated by glycogen synthase kinase-3 (GSK-3beta) independently of Akt/PKB serine phosphorylation. J Cell Sci 119, 3927-3934.
114. Luo, P., Fei, F., Zhang, L., Qu, Y. and Fei, Z. (2011). The role of glutamate receptors in traumatic brain injury: implications for postsynaptic density in pathophysiology. Brain Res Bull 85, 313-320.
115. Nakagawa, H., Koyama, K., Murata, Y., Morito, M., Akiyama, T. and Nakamura, Y. (2000). EB3, a novel member of the EB1 family preferentially expressed in the central nervous system, binds to a CNS-specific APC homologue. Oncogene 19, 210-216.
116. Nortje, J. and Menon, D.K. (2004). Traumatic brain injury: physiology, mechanisms, and outcome. Curr Opin Neurol 17, 711-718.
117. Yu, S., Kaneko, Y., Bae, E., Stahl, C.E., Wang, Y., van Loveren, H., Sanberg, P.R. and Borlongan, C.V. (2009). Severity of controlled cortical impact traumatic brain injury in rats and mice dictates degree of behavioral deficits. Brain Res 1287, 157-163.
118. Swiatkowski, P., Sewell, E., Sweet, E.S., Dickson, S., Swanson, R.A., McEwan, S.A., Cuccolo, N., McDonnell, M.E., Patel, M.V., Varghese, N., Morrison, B., Reitz, A.B., Meaney, D.F. and Firestein, B.L. (2018). Cypin: A novel target for traumatic brain injury. Neurobiology of Disease.

119. Singh, P., Doshi, S., Spaethling, J.M., Hockenberry, A.J., Patel, T.P., Geddes-Klein, D.M., Lynch, D.R. and Meaney, D.F. (2012). N-methyl-D-aspartate receptor mechanosensitivity is governed by C terminus of NR2B subunit. J Biol Chem 287, 4348-4359.
120. Spaethling, J., Le, L. and Meaney, D.F. (2012). NMDA receptor mediated phosphorylation of GluR1 subunits contributes to the appearance of calcium-permeable AMPA receptors after mechanical stretch injury. Neurobiol Dis 46, 646-654.
121. Rameau, G.A., Akaneya, Y., Chiu, L. and Ziff, E.B. (2000). Role of NMDA receptor functional domains in excitatory cell death. Neuropharmacology 39, 2255-2266.
122. Sattler, R. and Tymianski, M. (2001). Molecular mechanisms of glutamate receptor-mediated excitotoxic neuronal cell death. Mol Neurobiol 24, 107-129.
123. El-Husseini, A.E., Schnell, E., Chetkovich, D.M., Nicoll, R.A. and Bredt, D.S. (2000). PSD-95 involvement in maturation of excitatory synapses. Science 290, 1364-1368.
124. Kutzing, M.K., Luo, V. and Firestein, B.L. (2011). Measurement of synchronous activity by microelectrode arrays uncovers differential effects of sublethal and lethal glutamate concentrations on cortical neurons. Ann Biomed Eng 39, 2252-2262.
125. Kutzing, M.K., Luo, V. and Firestein, B.L. (2012). Protection from glutamate-induced excitotoxicity by memantine. Ann Biomed Eng 40, 1170-1181.
126. Svane, K.C., Asis, E.K., Omelchenko, A., Kunnath, A.J., Brzustowicz, L.M., Silverstein, S.M. and Firestein, B.L. (2018). d-Serine administration affects nitric oxide synthase 1 adaptor protein and DISC1 expression in sex-specific manner. Mol Cell Neurosci 89, 20-32.
127. Lusardi, T.A., Wolf, J.A., Putt, M.E., Smith, D.H. and Meaney, D.F. (2004). Effect of acute calcium influx after mechanical stretch injury in vitro on the viability of hippocampal neurons. Journal of neurotrauma 21, 61-72.
128. Mesfin, M.N., von Reyn, C.R., Mott, R.E., Putt, M.E. and Meaney, D.F. (2012). In vitro stretch injury induces time-and severity-dependent alterations of STEP phosphorylation and proteolysis in neurons. Journal of neurotrauma 29, 1982-1998.
129. Spaethling, J., Le, L. and Meaney, D.F. (2012). NMDA receptor mediated phosphorylation of GluR1 subunits contributes to the appearance of calcium-permeable AMPA receptors after mechanical stretch injury. Neurobiology of disease 46, 646-654.
130. Choo, A.M., Miller, W.J., Chen, Y.-C., Nibley, P., Patel, T.P., Goletiani, C., Morrison III, B., Kutzing, M.K., Firestein, B.L. and Sul, J.-Y. (2013). Antagonism of purinergic signalling improves recovery from traumatic brain injury. Brain 136, 65-80.
131. Chen, Y., Mao, H., Yang, K.H., Abel, T. and Meaney, D.F. (2014). A modified controlled cortical impact technique to model mild traumatic brain injury mechanics in mice. Frontiers in neurology 5, 100.
132. O'Neill, K.M., Akum, B.F., Dhawan, S.T., Kwon, M., Langhammer, C.G. and Firestein, B.L. (2015). Assessing effects on dendritic arborization using novel Sholl analyses. Front Cell Neurosci 9, 285.
133. Dragatsis, I. and Zeitlin, S. (2000). CaMKIIα-cre transgene expression and recombination patterns in the mouse brain. genesis 26, 133-135.
134. Fairless, A.H., Dow, H.C., Kreibich, A.S., Torre, M., Kuruvilla, M., Gordon, E., Morton, E.A., Tan, J., Berrettini, W.H. and Li, H. (2012). Sociability and brain development in BALB/cJ and C57BL/6J mice. Behavioural brain research 228, 299-310.

135. Blundell, J., Blaiss, C.A., Etherton, M.R., Espinosa, F., Tabuchi, K., Walz, C., Bolliger, M.F., Südhof, T.C. and Powell, C.M. (2010). Neuroligin-1 deletion results in impaired spatial memory and increased repetitive behavior. Journal of Neuroscience 30, 2115-2129.
136. Hanstein, R., Negoro, H., Patel, N.K., Charollais, A., Meda, P., Spray, D.C., Suadicani, S.O. and Scemes, E. (2013). Promises and pitfalls of a Pannexin1 transgenic mouse line. Frontiers in pharmacology 4, 61.
137. Schnell, E., Sizemore, M., Karimzadegan, S., Chen, L., Bredt, D.S. and Nicoll, R.A. (2002). Direct interactions between PSD-95 and stargazin control synaptic AMPA receptor number. Proceedings of the National Academy of Sciences 99, 13902-13907.
138. Schlüter, O.M., Xu, W. and Malenka, R.C. (2006). Alternative N-terminal domains of PSD-95 and SAP97 govern activity-dependent regulation of synaptic AMPA receptor function. Neuron 51, 99-111.
139. Elias, G.M., Funke, L., Stein, V., Grant, S.G., Bredt, D.S. and Nicoll, R.A. (2006). Synapse-specific and developmentally regulated targeting of AMPA receptors by a family of MAGUK scaffolding proteins. Neuron 52, 307-320.
140. Béïque, J.-C., Lin, D.-T., Kang, M.-G., Aizawa, H., Takamiya, K. and Huganir, R.L. (2006). Synapse-specific regulation of AMPA receptor function by PSD-95. Proceedings of the National Academy of Sciences 103, 19535-19540.
141. Losi, G., Prybylowski, K., Fu, Z., Luo, J., Wenthold, R.J. and Vicini, S. (2003). PSD-95 regulates NMDA receptors in developing cerebellar granule neurons of the rat. The Journal of physiology 548, 21-29.
142. Elias, G., Apostolides, P., Kriegstein, A. and Nicoll, R. (2008). Differential trafficking of AMPA and NMDA receptors by SAP102 and PSD-95 underlies synapse development. Proceedings of the National Academy of Sciences 105, 20953-20958.
143. Boulter, J., Hollmann, M., O'Shea-Greenfield, A., Hartley, M., Deneris, E., Maron, C. and Heinemann, S. (1990). Molecular cloning and functional expression of glutamate receptor subunit genes. Science 249, 1033-1037.
144. Manev, H., Favaron, M., Guidotti, A. and Costa, E. (1989). Delayed increase of Ca2+ influx elicited by glutamate: role in neuronal death. Molecular pharmacology 36, 106-112.
145. Saucier, D.M., Green, S.M., Leason, J., MacFadden, A., Bell, S. and Elias, L.J. (2002). Are sex differences in navigation caused by sexually dimorphic strategies or by differences in the ability to use the strategies? Behavioral neuroscience 116, 403.
146. Kanit, L., Taskiran, D., Yilmaz, Ö.A., Balkan, B., Demirgören, S., Furedy, J. and Pögün, S. (2000). Sexually dimorphic cognitive style in rats emerges after puberty. Brain Research Bulletin 52, 243-248.
147. Kanit, L., Taşkıran, D., Furedy, J.J., Kulali, B., McDonald, R. and Pöğün, Ş. (1998). Nicotine interacts with sex in affecting rat choice between “look-out” and “navigational” cognitive styles in the Morris water maze place learning task. Brain Research Bulletin 46, 441-445.
148. Sandstrom, N.J., Kaufman, J. and Huettel, S.A. (1998). Males and females use different distal cues in a virtual environment navigation task1. Cognitive brain research 6, 351-360.

149. Whishaw, I.Q., Cassel, J.-C. and Jarrad, L. (1995). Rats with fimbria-fornix lesions display a place response in a swimming pool: a dissociation between getting there and knowing where. Journal of Neuroscience 15, 5779-5788.
150. Frick, K., Burlingame, L., Arters, J. and Berger-Sweeney, J. (1999). Reference memory, anxiety and estrous cyclicity in C57BL/6NIA mice are affected by age and sex. Neuroscience 95, 293-307.
151. Granier, C.J., Wang, W., Tsang, T., Steward, R., Sabaawy, H.E., Bhaumik, M. and Rabson, A.B. (2014). Conditional inactivation of PDCD2 induces p53 activation and cell cycle arrest. Biology open 3, 821-831.